230 AD

CEAC-TR-96-0102

LEAKAGE FAILURE OF THREADED FIBER-COMPOSITE JOINTS UNDER COMBINED INTERNAL PRESSURE, AXIAL AND MAKEUP LOADING: EXPERIMENTS AND ANALYSES

By

S. S. Wang* and X. Lu**

Composites Engineering and Applications Center, and
Department of Mechanical Engineering
University of Houston
4800 Calhoun Road
Houston, TX 77204-0900

December, 1996

*Professor and Director, CEAC and Mechanical Engineering Department
**Research Associate, CEAC; Formerly, Graduate Research Assistant, Department of Mechanical Engineering

CEAC-TR-96-0102

(Report #2 of the Final Report Series to American Petroleum Institute and Amoco Corporation for the Project on Long-Term Multiaxial Strength of Fiberglass Tubing)

LEAKAGE FAILURE OF THREADED FIBER-COMPOSITE JOINTS UNDER COMBINED INTERNAL PRESSURE, AXIAL AND MAKEUP LOADING: EXPERIMENTS AND ANALYSES

by

S. S. Wang* and X. Lu**

Composites Engineering and Applications Center, and
Department of Mechanical Engineering
University of Houston
4800 Calhoun Road
Houston, TX 77204-0900

December, 1996

---

* Professor and Director, CEAC and Mechanical Engineering Department
**Research Associate, CEAC; Formerly, Graduate Research Assistants, Department of Mechanical Engineering

FORWARD

This report is the first part in the final report series for the project on long-term multiaxial strength of fiberglass tubing, conducted during the period of 1994-96 by researchers of the Composites Engineering and Applications Center (CEAC) for Petroleum Exploration and Production at the University of Houston, Houston, TX. The research was funded mainly by a contract from the American Petroleum Institute (API), Washington D. C. Owing to the broad scope of work and the depth of the investigation, supplementary support was also provided by a grant from the Amoco Corporation, Chicago, IL and by CEAC internal funds.

The overall objectives of the research program, as requested by API, were to:
(1). Examine the validity of the assumptions and hypotheses of the proposed API rating methodology for long-term strength of fiberglass composite tubing under multiaxial loading;
(2). Provide rigorous understanding of progressive leakage failure mechanisms and mechanics of FRP tubing subjected to combined internal pressure and axial loading, and
(3). Identify the limitations of the proposed API rating methodology.

The current study has been directed to focus on the following critical issues of the leakage failure in fiberglass composite tubing used in oil and gas exploration and production operations:
(1). Progressive leakage failure modes;
(2). Long-term and short-term leakage failure envelopes;
(3). Safety (or service) factors in composite tubing design, and
(4). Load sequence effects.
Both composite tube bodies and threaded fiber-composite joints are studied. Two types of composite tubing were considered; one for downhole applications and the other for typical line pipe applications. The effect of different multiaxial loading modes, including short-term loading, long-term creep and cyclic fatigue, on the composite tubing leakage was investigated.

This first report addresses the aforementioned critical issues of leakage failure in a fiberglass *composite tube body*. In the second report, the complicated leakage failure of *threaded fiber-composite tubular joints* is investigated. The third report covers the important problem of long-term composite tubing leakage under *multiaxial cyclic fatigue loading*. In all these reports, the analytical and experimental methods developed for the studies are described in detail to ensure a clear understanding of the advanced level of the approach used in the investigation.

ABSTRACT

A combined experimental and analytical study has been conducted to investigate leakage failure of threaded fiber-composite tubular joints subjected to combined internal pressure, axial loading and make-up interference. Owing to material, geometric and loading complexities, nonlinear composite constitutive equations, local thread contact and material damage in the composite joints have been included in the analytical part of the study. Based on experimental observations, and contact and failure mechanics considerations, leakage failure modes are identified and proper mechanism-based failure criteria are established. To predict the leakage failure of threaded composite joints, several rigorous mathematical models are introduced. Computational mechanics analyses of the composite joint failure under various multiaxial loading modes are conducted. With the current development of quasi three-dimensional finite elements and the mechanism-based failure criteria, both direct full-field modeling and coupled global-local modeling of the threaded composite joints are performed. In the experimental part of the study, threaded integral composite joints were used in a joint make-up study and in leakage failure experiments. The leakage failure experiments were conducted on the integral composite joints with prescribed make-up interferences subjected to combined internal pressure and axial loading with various biaxial loading ratios. A rigorous analytical method for defining the make-up interference in a threaded composite joint has been introduced. To provide a clear insight into the experimental results, fundamental leakage failure maps have been constructed from the experimental and analytical results, and relate different leakage failure modes to the critical pressure, axial load and makeup turns. Analytical predictions of the threaded composite tubular joint failure, based on the proposed mechanical models, mechanism-based leakage failure criteria and local contact analyses, are compared well with the experimental results. Effects of the make-up interference, hoop-to-axial loading ratio, geometric imperfection and thread surface friction on the joint leakage failure are studied in details. The probabilistic nature of the threaded composite joint leakage failure is also addressed in conjunction with the thread tightening safety factor introduced in the study.

TABLE OF CONTENTS

LIST OF ABBREVIATIONS AND SYMBOLS

$\bar{C}_{ij}$	Elastic stiffness in material coordinates
$\tilde{C}_{ij}$	Elastic stiffness in interfacial coordinates
D_L	Leakage threshold
DSC	Differential Scanning Calorimetry
E	Elastic modulus of isotropic material
E_{ij}	Elastic moduli of composite lamina
f	Coefficient of friction
$\{\mathbf{f}\}$	Equivalent nodal force
FRP	Fiber reinforced plastic material
G_{ij}	Shear moduli of composite lamina
GPIB	General purpose interface bus
IJ	Integral Joint
$[\mathbf{K}]$	Finite element stiffness matrix
LVDT	Linear variable displacement transducer
MUX	Multiplexer
N_i	Shape functions
P_a	Axial loading
P_B	Bearing pressure
P_i	Internal pressure
$\{\mathbf{q}\}$	Nodal displacement vector
$\bar{S}_{6666}$	High order shear compliance
$\bar{S}_{ij}$	Elastic compliance in material coordinates
SSR	Solid state relay
T	Make-up turn
T&C	Threaded and Coupled
U, V, W	Displacements
U_i, V_i, W_i	Nodal displacements
X	Tightening safety factor
$\tilde{X}$	Leakage tightening factor
XRD	X-ray diffraction
δ	Radial interference
ε_{ij}	Strain
$\varepsilon_{ijf}^{(T)}$	Ply tensile failure strain
$\varepsilon_{ijf}^{(C)}$	Ply compressive failure strain
γ_{ijf}	Ply shear failure strain
σ_{ij}	Stress
υ	Poisson's ratio of isotropic material
υ_{ij}	Poisson's ratios of composite lamina

1. INTRODUCTION

The demand of alternative and/or better materials to meet stringent performance and cost-effectiveness requirements in petroleum exploration and production operations has led to consideration of light-weight, fiber composites for a variety of aggressive, load-bearing applications. Joining of composite tubing, especially the threaded composite joints, has been a major concern because of the complexities involved. It is recognized that design and analysis methodologies for monolithic metallic joints have been practiced for a long time and well established. However, the mechanics and failure behavior of threaded composite tubular joints for load-bearing applications has not been well understood. Rigorous analytical and experimental methods to study the mechanical response of a threaded composite joint simply do not exist, mainly because the following difficulties and complexities:

1) Complexities in fiber composite joint materials. Composite materials have inherently inhomogeneous microstructures and anisotropic properties. An accurate leakage failure study of composite joints requires knowledge of nonlinear anisotropic material properties, complicated failure criteria, and nonlinear thread contact mechanics.

2) Lack of understanding of threaded joint contact mechanics: Complexities of the local joint geometry and lack understanding of the thread contact pose a fundamental problem for evaluation and prediction of joint failure. The connection threads are recognized to be the weakest link in a composite joint system. A detailed study of a threaded composite joint made of different kinds of composite materials is generally tedious, difficult and very complex.

3) Complexities in leakage failure modes: The three-dimensional states of stress and deformation in a threaded region of a fiber composite joint are known to be very complex. Various leakage failure modes may be developed under a combined internal pressure, axial loading and make-up interference. Very little is understood about the failure modes and the effect of the combined loading modes on the joint failure.

4) Unknown long-term deformation and leakage failure resistance: Compared to monolithic metallic joints, the threaded composite joints exhibit more complicated stress states and failure modes, in addition to the issue of material degradation. Long-term deformation and failure behavior of threaded composite joints are not fully known at present.

5) Lack of accurate methods for analysis and design: The complexities of the joint materials, geometry, and loading and difficulties in handling the contact mechanics and failure modes in a threaded composite joint have laid serious barriers in the development of sound analysis and design methodologies. The analysis and design methodologies for traditional threaded metallic joints are not able to nor suitable for

the threaded fiber composite joint problem. In-depth knowledge of leakage-failure mechanics of a threaded composite joint is needed to develop proper design and analysis methodologies.

It is obvious that the materials, geometry and functions of the threads used in a composite tubular joint are significantly different from a joint made of mechanical fasteners, such as a bolt-nut joint. Various thread configurations have been used for connecting tubular components; they all have two common functions: structural load-transfer and resisting leakage. While a threaded joint is generally used for convenience in joining tubular composite structures, several unique features are critical in their performance and failure evaluation:

1) Thread taper. The thread taper along the axis of a composite joint is important to provide a proper radial interference between the two connected components after a mechanical made-up.

2) Thread sealing. The contact force developed between thread surface under external loading prevents leakage failure of the joint. Leakage failure through the thread contact surface is a complex nonlinear mechanics problem, which has not been fully investigated and understood.

3) Three-dimensional characteristics of threads. Localized stress concentrations in the threads are inherently three-dimensional and very complicated. Therefore, the existing one-dimensional theories, such as those used in analyzing a bolt-nut joint, is incapable of addressing the threaded composite joint failure problem.

Given these aforementioned complexities, one may recognize that a combined analytical and experimental approach may be the only viable way to understand the leakage failure behavior and to provide quantitative relationships to relate the joint leakage failure to various geometric, lamination, material and loading variables in a threaded composite joint.

The objectives of the research are to: (1) establish fundamental fiber and particulate composite material constitutive equations, especially in the nonlinear regime, through micromechanics and experiments for the composites used in the joints, (2) determine leakage failure modes and associated failure criteria by multiaxial loading experiments and failure/contact mechanics, and (3) develop mechanics models and nonlinear numerical methods to analyze and predict deformations and leakage in threaded composite joints under various combinations of internal pressure, axial loading, and make-up interference.

In the next section, a comprehensive review of the literature is conducted on analytical and experimental studies of various tubular joint systems, including both metallic and fiber-composite joints. Critical studies on composite thread and joint geometry, microstructures, and materials used are presented in Section 4 to establish a basis for subsequent investigation of the composite joint leakage failure. Unique

multiaxial-loading and leakage-detection facilities developed for this research, and the composite joint leakage experiments conducted are described in Section 5. The boundary-value problem of a threaded composite joint under combined multiaxial external loading is formulated in Section 6. To solve the leakage failure problem (with complex local and global geometry, unknown thread surface contact and nonlinear constitutive equations), mechanical models of different levels of complexities are introduced in Section 7. Failure criteria associated with individual leakage failure modes are introduced in Section 8 and subsequently used in conjunction with the mechanical models. With the aid of a Lagrangian multiplier technique (to account for thread surface contact) and a progressive material degradation scheme (for composite damage during increasing loading), an incremental-iterative numerical method is developed in Section 9 to simulate the composite joint leakage failure. The analytical and experimental methods developed are applied to threaded integral composite joints made of filament-wound, glass-fiber reinforced epoxy laminate tube bodies molded with particulate-filled composite threads, subjected to various combinations of internal pressure, axial loading and make-up interference. Experimental results and numerical predictions are given in Section 10. Leakage failure maps with different failure modes are constructed and compared with the experimental data obtained from the integral composite joint tests. The important effects of multiaxial loading modes, make-up interference, geometric imperfection, thread surface friction, thread tightening and others on the joint failure are discussed. Also, based on the experimental and numerical results, the probabilistic nature of the joint leakage failure is determined, and predictions of the statistical leakage occurrence can be properly made. Several important conclusions are drawn in Section 11.

2. LITERATURE REVIEW

To study the leakage failure of a threaded composite joint under multiaxial loading, a major issue is the stress transfer between threads of a pin[1] and box[2]. Of equal importance are the sealing mechanisms and contact mechanics involved in the joint. Since current development of threaded composite joints is mainly based on the knowledge of conventional metallic tubular joints, a review of threaded metallic joints and other related threaded connectors, such as bolt-nut connections, is included.

2.1 Analyses of Tubular Joint Systems

2.1.1 Stress Analyses and Failure of Composite Tubulars

The analysis of a filament-wound composite tubular (or cylindrical shell) under multiaxial loading has been an important research subject for decades. The early study by Whitney and Halpin [4] has demonstrated that a multilayer fiber-composite cylindrical shell may exhibit highly anisotropic behavior under general loading. Failure envelopes for cylindrical glass/polyester composite shells under multiaxial loading have been constructed by many researches, for example, Eckold, et al. [5]. A ply-by-ply progressive failure study has been conducted in [5], based on the well-known maximum-stress failure criterion, coupled with instantaneous unloading of a damaged ply. In the construction of failure envelopes, failure initiation and final structural failure are identified.

The effect of nonlinear material constitutive equations on leakage of a glass-fiber/epoxy composite tube under combined internal pressure and axial loading has been studied by Wang, et al. [6]. The study is focused on leakage failure, and onset of the leakage is identified as formation of a through-thickness microcrack. The results indicate that a linear composite laminate analysis with stress-based failure criteria may grossly under-estimate the critical load of composite leakage failure and that composite material nonlinearity significantly affects deformations and failure.

It has been well known that winding angles of reinforcing fibers influence the performance of composite tubulars. Mistry [3] has conducted a theoretical investigation on the effect of fiber winding angles on the strength of GRP (graphite-fiber reinforced plastic) tubes subjected to combined external pressure and axial compression. In the study, a finite element analysis has been conducted to determine buckling loads and the first-ply failure of composite cylinders with different winding angles. The results demonstrate that, in a composite tube under a simple hydrostatic external pressure, preferred fiber winding angles are close to $\pm 80^{o}$, instead of $\pm 55^{o}$ for a closed end case.

---

[1] A pin is a tubular section with male threads.

[2] A box is a tubular section with female threads.

2.1.2 Analyses of Threaded Bolt-Nut Joints

Before examining a threaded tubular composite joint, it is appropriate to review the commonly used threaded metallic joints with a bolt-nut connection. Investigation of load bearing capacity of threaded metallic fasteners has been conducted by many researchers since Den Hartog [7] first examined the subject of bolts holding a stack of plate rotors in a turbo-generator. Local deformations and stresses are of particular interest because the majority of reported failures initiate at the root of the first loaded thread. Den Hartog has found that, for the particular threaded joint studied, the stresses along the thread follows an exponential distribution with a peak at the seat of the nut, reaching nine times the "average stress" and taking 45% of the load with the first two turns of the thread.

Goodier [8] has used a semi-analytical method to determine the load distribution in a thread of a metallic bolt. The detailed stress in the thread is obtained from radial expansion and axial deformation of a nut measured by an extensometer. The results show that the load distribution along a thread in a bolt is governed by tension in the bolt, compression in the nut, bending of the thread, and circumferential deformation of the nut. The stretching in the bolt and the axial contraction of the nut are primarily responsible for local stress concentrations. Sopwith [9] has conducted a detailed analysis of a bolt-nut joint subjected to axial loading. Sopwith's approach is based on the fact that axial extension of a bolt and compression of a nut, which cause stress concentrations at a loaded end of the joint, are relieved to some extent by other deformations. These may include (1) bending deflection on threads, (2) axial recession due to radial compression of the nut and the bolt thread, and (3) axial recession due to radial contraction of the bolt and expansion of the nut. Expressions describing the recessions have been derived, and the results are compared favorably with experimental data. Sopwith's theory has been modified by Patterson and Kenny [10] to evaluate thread deflection of an incomplete thread form. Good correlations are obtained between theoretical and experimental results by incorporating a thread runout.

Numerical methods, such as finite elements, have been extensively used to analyze threaded metallic bolt-nut connections because of the convenience. Dragoni [11] has studied effects of thread pitch and friction on stress concentrations in a metallic bolt-nut connection. The exact contour of a thread is modeled and, consequently, an extremely fine element mesh is needed to determine accurately local stresses. The results show that, for a given nominal diameter with a total bolt load, the maximum elastic stress in a bolt increases appreciably as the pitch decreases. The analysis also reveals that stresses in the bolt increase linearly with the coefficient of friction up to about 0.6. In an alternative model, Bretl and Cook [12] have replaced all the threads with an equivalent load-transfer layer of orthotropic properties. Principal directions of the orthotropy depend upon local thread geometry and the load transfer direction which is not known a priori. With this approach, a thread joint may be modeled by relatively coarse finite elements with a high computational efficiency. The results obtained correlate well with Goodier's semi-analytical study [8], Sopwith's theoretical analysis [9] and Patterson and Kenny's experimental work [10].

Instead of treating a threaded bolt-nut joint as an axisymmetric problem, Rhee [13] has studied three-dimensional deformations of a threaded connection, using 3-D solid modeling with a combination of 20-node 3-D elements and interface elements. The results indicate that a 2-D model may underestimate the critical stress in a metallic thread bolt-nut joint by approximately 20%, when compared with a 3-D model for a joint with a helix thread angle of 5^{o}.

Since dimensions of a thread are generally much smaller than those of a joint, Andrieux and Leger [14] have proposed a multiple-scaling method for analyzing a threaded joint. The method is based on the concept of decomposition of the original problem into two problems of two different scales. The local problem, involving only the detailed geometry of threads, is studied with a standard numerical (finite element) model to address the nonlinear, thread contact mechanics, whereas the global one is solved by a 1-D approach, which allows a comprehensive parametric study of joint variables.

2.1.3 Analyses of Threaded Metallic Tubular Joints

When used in connecting metallic tubulars, a threaded joint is usually subjected to complex multiaxial loading, such as a combination of internal pressure, axial loading, and bending. Threads in the tubular joint are different from those in a bolt-nut joint in both geometry and load transfer. Threads in a tubular joint not only transfer loads between a pin and a box in a more complicated manner but also provide sealing to prevent the joint from leaking. Of particular interest are the make-up interference and its effects on leakage failure of threaded connections, because of their extensive use and safety concerns.

Weiner and Sewell [15] have examined sealing mechanisms of threaded metallic tubular joints and concluded that a leakage failure criterion, involving only torque in make-up, is not reliable. The make-up torque depends primarily on friction between a mating pin and the box thread and, for clean connections, is largely a function of the type of a thread compound employed. Different types of thread compound can cause make-up torque variations up to 500%. Therefore, based upon observations of different sealing mechanisms, an alternative make-up (i.e., torque-turn) criterion is introduced. Although the torque-turn criterion has been successfully used for many years for threaded metallic joints, the smooth finish introduced by current machining techniques along with variations in thread tolerance, has created problems in counting the make-up turn[1]. Day, Moyer, and Hirshberg [16] have developed a method to establish a proper torque-position criterion. For an API eight-round connection make-up, the method accounts for variations in thread tolerance, coupling coating or plating and the thread compound. A finite element simulation has also been conducted to establish key make-

[1] With the torque-turn criterion, the turn counter starts counting turns once a reference torque is reached during the make-up. This reference torque varies from 50 to 300 ft-lb for various tubing sizes to 10% of the minimum make-up torque value for a normal casing. Furthermore, changes in thread surface coefficients of friction, thread manufacturing methods, thread compounds, and variation in the coating or plating coefficient of friction, may cause the turn counter to start recording turns at different positions of the pin and the coupling engagement, and give erratic results.

up parameters.

In recent years, a quantum leap in problem-solving capabilities has been realized due to the introduction of supercomputers and workstations; solving a large computational problem has become feasible at a low cost. Hilbert and Kalil [17] have evaluated a premium threaded metallic connection by a combined approach of finite element modeling and full-scale testing. In the modeling, the connection has been discretized by axisymmetric elements with a total of 10,000 degrees of freedom. Nonlinearity caused by thread surface contact has also been investigated. In the full-scale test, the gas sealing capacity, failure loads and modes have been investigated. Nonlinear finite element models have been used by Assanelli and Dvorkin [18] to study standard API eight-round metallic connections, buttress connections, and other connections.

When an excessively large tensile load, significantly exceeding the design allowable, is applied to a threaded tubular connection, the pin body may be pulled apart from the coupling, called jump-out. Morita, et al. [19] have investigated this phenomenon with a finite element method, which includes large deformations, surface sliding, and material nonlinearity. To obtain a reference, the jump-out of a one-ring thread has been numerically and experimentally studied, and jump-out tests also conducted on an 18-5/8-inch joint. Based on the results, a criterion has been proposed for the slide out of threads in the FEM simulation. Bahai, et al. [20] have introduced a hybrid model to calculate the load transfer in a threaded metallic connection subjected to combined axial and bending loads. In the model, a tubular joint is approximated by a set of spring elements with stiffness and stress concentration of the threads determined by a 2-D finite element method. The results are comparable with those from a fully 3-D finite element analysis. The approach may be suitable for parametric studies of local thread stresses and global joint deformations.

While analyzing a threaded tubular joint with a finite element method is technically straightforward feasible, the direct brutal force numerical approach is generally costly, time-consuming, and not without difficulties. Accurate and efficient methodologies are needed. Kwon, et al. [21] have developed a joint-service-life-analysis model, based on the beam-on-elastic-foundation approximation with the aid of bolt/nut equations and Lamé's equation. The model gives reasonable results when compared with detailed numerical solutions and strain gage measurements.

It is well recognized that geometric details of a joint affect its local stress/strain concentrations and failure. Based on field measurements of actual geometry of a threaded metallic joint, Beghini, et al. [22] have conducted a detailed stress analysis on a threaded connection. A nonlinear finite element analysis has been employed to evaluate the influence of the geometric variation on local stresses in the joint. The results show that the stress distribution along a thread may differ significantly from that predicted in the joint with a nominal geometry. In conjunction with a Monte Carlo simulation, a probability density function of a conventional stress parameter (i.e., the stress at a thread fillet root) has been determined for cases of different external loading.

2.1.4 Analyses of Threaded Composite Tubular Joints

While many studies have been conducted on fiber composite tubulars, very limited work, e.g., see [23,24], has focused on mechanical reliability of threaded composite tubular connections. The study conducted by Dilintas [23] addresses relationships among different loading modes (i.e., make-up, axial tension, and internal pressure) and the joint response. Frictionless surface contact and linear material properties are assumed in the study. The results show that the frictionless contact assumption between thread surfaces gives good results for the cases under service loading. Also applied axial tension reduces contact pressure on a thread surface and consequently, reduces the sealing capacity of the joint. The influence of filament winding angle on performance of a threaded composite joint has also been studied by Dilintas [24]. A reduction in the longitudinal stiffness of the box with a predominantly circumferential winding angle results in a slight decrease in stress concentrations in male threads and an improvement in sealing performance of the joint.

It is noted here that, owing to the complications introduced by the threads and the multiaxial loading applied, no analytical solution has been found in the literature on deformation and thread contact in a threaded composite joint. Nor any information is available on the failure analysis methodology for a threaded composite joint leakage.

2.1.5 Failure Theories for Composite Lamina and Composite Laminate

For a fiber composite laminate, failure prediction is generally difficult because of the inherent material anisotropy, discontinuity through the thickness direction and the complicated ply stress state. A recent survey of existing failure theories for fiber composite laminae has been given by Nahas [25]. Among the theories, the well-known Tsai-Wu's tensorial polynomial has been widely used. However, the polynomial failure criterion [26], cannot identify the complex composite laminate failure modes. A simple mechanism-based failure theory is the maximum stress (or strain) criterion, which does not account for interactions of stress components on failure. The failure theory introduced by Hashin [27] is a mechanism-based failure criterion. The theory is based on the stress invariants with individual fiber and matrix-dominated failure modes being distinguished. The strain-based failure theory by Christensen [28] also accounts for composite failure modes with proper assumptions.

Unlike a monolithic material, failure of individual plies in a composite laminate does not necessarily results in the complete loss of load-bearing capability of the composite laminate. A number of progressive failure theories have been used to examined the ply-by-ply failure progression in a composite laminate [25]. A common feature of the progressive failure theories is that ply unloading would take place after a ply is failed. The instantaneous unloading model proposed by Chiu [29] assumes that a composite ply loses its entire load-carrying capacity immediately after the ply fails. The Hahn-Tsai method [30] suggests that a failed ply may still partially support the load it carries, until the final laminate failure occurs. The model proposed by Petit and Waddoups [31] takes an unloading path lying between those of Chiu and Hahn-Tsai.

2.2 Experimental Studies of Threaded Joints

2.2.1 Threaded Bolt-Nut Joints

It is well known that the detailed geometry of a joint may have a significant influence on local stresses at the thread root. Several experimental studies have been conducted to examine this effect. A photoelastic stress-freezing technique has been performed by Hetenyi [32] on the stress distribution in nuts with different geometry. The nut with a tapered lip is found to give the most uniform stress state. Patterson and Kenny [33] have studied detailed stress distributions in threads of an ISO metric nut and bolt by a frozen-stress photoelastic method, employing a fringe-multiplying polarscope with a recording micro-densitometer. The experimental results have a good correlation with the solution obtained by Sopwith [9].

2.2.2 Threaded Metal Tubular Joints

A full-scale test may provide a useful means to evaluate the behavior of a threaded tubular joint. Ishikawa, et al. [34] have measured structural deformations in a threaded tubular connector under severe stresses. Deformations in a threaded joint under make-up, tension and bending have been gaged, and a finite element analysis has also been carried out to calculate detailed stresses and joint sealing capacity. Good correlations are obtained between the finite-element results and experimental data in different loading conditions.

An experimental investigation has also been conducted by Traweek, et al. [35] on internally coated tubular connections. Plastic deformations are found to occur during joint make-up and additional plastic strains result from pressurization of the joint. The results indicate that the API eight-round connection may not be the optimal choice for the case when the joint is subjected to repetitive make-up and breakout[1], such as in a work string. Since the joint is permanently deformed during each make-up, it could be continually made-up with greater penetration until worn out.

Broodbent and Fessler [36] have employed a photoelastic stress-freezing method to determine the stress distribution in a threaded tubular joint. The study focuses on stresses at a thread fillet in the joint. The maximum stress in a tubular connection occurs in the fillet nearest to the loaded contacts. An axisymmetric finite element analysis has also been conducted. Empirical equations have been developed to determine the commonly used thread geometry. The position and magnitude of the critical stress are predicted and compared well with photoelastic models in different loading modes.

2.2.3 Threaded Composite Tubular Joints

The only experimental study in the literature on mechanical behavior of a threaded composite joint is conducted by Yamagata, et al. [37]. The study focuses on joining methods of graphite/epoxy composite tubulars, commonly used to construct truss assembles for space structures. Issues on design, fabrication, and performance evaluation of a graphite/epoxy cylinder with threads on its inner wall have been

[1] Breakout is a procedure of disconnecting the threaded tubular joint.

addressed. Three types of composite tubulars containing different fiber arrangements for integrated joints have been developed. The results show that composite tubular joints with fibers along the longitudinal direction have the highest load-bearing capacity.

3. SCOPE OF THE RESEARCH

It is important to recognize that at present rigorous experimental and analytical methodologies for understanding and prediction of leakage failure in threaded fiber composite tubular joints under combined internal pressure, axial loading and make-up interference do not exist. Leakage failure modes and associated failure criteria, which relate joint material damage and sealing reliability to the thread geometry, composite lamination parameters, joint configuration and multiaxial loading, are not known. The leakage failure behavior of a threaded composite joint is simply not well understood in both short term and long-term loading conditions.

The scope of this research include:

1) Thorough understanding of the leakage failure behavior of threaded fiber-composite tubular joints under external multiaxial loading;

2) Development of rigorous experimental and analytical modeling methods to quantitatively define and determine the leakage failure envelope(s) for a threaded joint subjected to various combinations of internal pressure, axial loading and make-up interference;

3) Determination of the effects of joint geometric variables, material parameters, tread contact conditions, and loading modes on the composite-joint leakage failure resistance.

To accomplish these goals, the following specific technical tasks, involving several different disciplinary areas, such as composite materials, damage and failure theories of solids, contact mechanics, advanced material testing and experimental methods, and nonlinear computational mechanics, are conducted.

1) Critical study on composite joint geometry, thread configurations, and material microstructures and constitutive properties. Emphases are placed on detailed characteristics of the threads and nonlinear composite constitutive equations, which are critical for subsequent local (microscale) modeling and analyses.

2) Development of unique experimental facilities for conducting properly designed leakage failure experiments to understand the joint leakage failure phenomena and later validate the analytical models developed. The facilities contain unique capabilities, including multiaxial (axial, pressure and torsional) loading with digital and analog controllers, make-up interference application and measurement, real-time multiaxial deformation measurement, high-sensitivity leakage detection, and computer-controlled on-line data acquisition and analysis.

3) Identifying the leakage failure modes in threaded composite joints by conducting

carefully designed experiments and detailed microscopic observations. The failure mode identification should include considerations of composite tube-body damage, tube-body/thread interface debonding, thread material failure, and the loss of bearing pressure in the thread surface contact region.

4) Establishing proper mathematical failure criteria (functions) for each individual failure mode identified in the multiaxial leakage failure experiments. The failure criteria are constructed, based on the most recent developments of failure theories for fiber- and particulate-reinforced composites, and interface and contact mechanics of dissimilar media.

5) Formulating governing differential equations and associated boundary, interface and loading conditions for the threaded composite joint problem. The formulation should include the unique features of the joint failure problem, including nonlinear contact mechanics along the thread surface, composite material nonlinear constitutive equations, damage and associated ply property degradation during loading, and failure criteria for individual leakage failure modes.

6) Constructing proper mechanical models for modeling the threaded joint leakage failure problem and evaluating the suitability and validity of the individual models based on comparisons between experimental results and analytical solutions. Formulations of individual models are made at both global and local levels so that information on global joint deformations and local thread contact stresses can be properly extracted for further use.

7) Development of advanced numerical simulation methods and associated computational algorithms for analysis and prediction of leakage failure in threaded composite tubular joints. The computer-aided simulation methods should have the capability of addressing complex local and global joint geometry, material and (contact) geometric nonlinearities, degradation and damage evolution, and various combinations of axial loading, internal pressure and make-up interference.

8) Based on the multiaxial-loading experiments, analytical modeling and simulation methods developed, defining and establishing leakage failure envelopes (maps) for threaded composite tubular joints.

9) Investigating the effects of thread make-up interference, geometric tolerance/imperfections, thread contact surface friction, and multiaxial loading modes on the thread joint leakage failure envelopes. Also included in the study is the fundamental statistical nature of the threaded joint leakage failure, due to the inherent material and geometric variabilities.

10) Based on the experimental observations and test results and the analytical solutions obtained from the modeling and prediction, evaluating the assumptions and the recommended procedure in the API proposed ranking methodology for threaded FRP composite tubing joints.

4. THREADED COMPOSITE JOINT GEOMETRY AND MATERIAL CONSTITUTIVE PROPERTIES

To ensure the leakage failure mechanics analysis mathematically tractable, proper approximations and assumptions need to be introduced for the joint geometry and material constitutive properties. Validity of the assumptions and simplifications can only be made through properly conducted experiments and observations, and subsequent micromechanics analyses.

In this section, proper geometric and material models are established for the subsequent study of a threaded composite tubular joint. The efforts include

1) establishing a detailed geometric model for threaded composite joints,

2) conducting microscopic observations and an X-ray diffraction (XRD) analysis to identify constituent material phases in the joints, and

3) determining constitutive properties of composite plies in the tube body, and of threads in the joint.

4.1 Geometric Features and Modeling of Threaded Composite Joints

Stress concentrations at thread roots of a joint are usually caused by the complicated geometry of the threads. The multiaxial loading, the stress transfer between the pin and the box, and material heterogeneity and discontinuity in the composite joint introduce additional difficulties to the problem. Detailed geometric features of the composite joint are critical in the present analytical and experimental investigations and need to be examined with great care.

4.1.1 Joint Geometry and Geometric Modeling

Two kinds of threaded composite tubular joints, i.e., threaded and coupled (T&C) joint and integral joint (IJ), are commonly used. In a T&C joint shown in Fig. 4-1(a), two pin members are connected by a coupler, which is a short tubular segment with a slightly larger inner diameter than that of pins but threaded internally from both ends. In an integral joint, as shown in Fig. 4-1(b), internal threads are made directly at one end of the tube (i.e., the box end), and external threads are made at the other end (i.e., the pin end). The composite tubulars are connected by making-up interference through the threads. A properly controlled amount of radial interference may be introduced in the integral joint because only one make-up process is needed in each connection.

To investigate the mechanics of composite joint leakage failure without loss of

generality, an integral composite tubular joint[1] made of filament-wound glass/epoxy is selected in this study. To obtain the detailed local geometry and material characteristics of an integral composite joint, the joint was cut, measured, and observed under an optical microscope. The overall geometry of a threaded integral joint specified by American Institute of Petroleum is shown in Appendix A.

4.1.2 Thread Geometry and Geometric Model

Threads in a joint are used mechanically to hold a pin and a box section together with a proper axial alignment. Threads are required to act as leakage resistant elements. For illustrative purposes, four types of threads [38,39]: line-pipe threads, round threads, buttress threads, and extreme-line threads, are shown in Appendix B. The line-pipe, round, and buttress threads are required to fit together during make-up such that with proper sealants, leakage resistance can be achieved through the threads[2] . The detailed thread geometry[3] in a selected threaded integral composite joint [38] is shown in Fig. 4-2. We note that a characteristic of the threads is that a taper in joint diameter (e.g., ~6.25%) exists; thus the pitch diameter of the threads varies along the axis of the joint. Because of the taper, an appreciable difference between diameters of the pin and the box is introduced during make-up. Obviously, both flanks of the thread may be subjected to complex contact loading, which is essential in sealing[4] the joint.

4.1.3 Geometric Imperfections

In reality, no joint is machined perfectly to nominal dimensions, and geometric imperfections always exist. In a threaded composite tubular joint, geometric imperfection in the form of thread taper may change the interference introduced into the joint during make-up, and consequently its leakage-resistant capacity. For a joint with different thread taper between pin-side threads and box-side threads, its leakage-resistant capacity can be significantly different. Typical thread taper of an integral composite tubular joint is shown in Appendix C.

4.2 Microstructure of Fiber Composite Joint Materials

(a) Microstructure of Thread Materials

Material constitutive equations and leakage failure modeling require clear understanding of various material systems used in the threaded composite joint. From detailed optical microscope observations, microstructures of the threads in the pin and box sections are presented in Figs. 4-3(a) and 4-3(b). A significant amount of fillers was found in the thread materials. Volume fractions of the fillers were approximately 25.5%

---

[1] The internal and external diameters of the tube body selected are 2.004 inches and 2.344 inches, respectively, for convenience and for the availability of tests.

[2] Threads in an extreme-line casing are not designed to be leak tight. The leakage resistance of an extreme-line connection is accomplished by a metal-to-metal seal.

[3] The dimensions of the thread in the figure are: $\theta=60^{o}$, $p = 0.1250$ inch, $H = 0.10825$ inch, $h_s = h_n = 0.07125$ inch, $s_{rs} = s_{rn} = 0.01700$ inch, and $s_{cs} = s_{cn} = 0.0200$ inch.

[4] There is a small clearance between crest and root of the thread. In order to provide reliable sealing, Teflon particles are sometimes recommended together with a thread lubricant to fill the clearance during making-up of the joint.

and 15.3%, respectively, in the threads of the pin and box sections. Only about 2% of the total volume was found to be voids in the pin-side threads, whereas a larger amount of voids, approximately 10%, was observed in the box side threads. The difference in the void volume fraction may be caused by difference in processing, and needs to be included in the micromechanics analysis of constitutive equations of the joint materials.

To determine interface characteristics between the threads and the tube body, both pin and box sections were sectioned, polished and observed under an optical microscope. A clear interface (Figs. 4-4(a) and 4-4(b)) was found between the pin-side threads and the composite pin tube body, Fig. 4-4(a), indicating that the pin-side threads were adhesively bonded to the pin. The interface was not clearly observable between the box-side threads and the composite box body in Fig. 4-4(b). Instead, glass fibers in the inner ply of the box were observed to meander along the profile of the box-side threads[1] .

(b) Filament-wound Composite Tube Bodies

The fiber volume fraction and ply configurations in the composite tubular joint (the pin and the box) were determined by an ASTM standard burn-out test conducted in an oven with a temperature at 530°C. The composite ply configurations were identified as $[\pm 55^{\circ}]_9$ in the pin and $[\pm 55^{\circ}]_{11}$ in the box section. Fiber volume fractions in the pin and in the box of the joint were also determined by the burn-out test. The volume fraction of glass fibers was found to be approximately 55%.

4.3 Material Systems and Their Constitutive Equations

(a) Thread Materials

An X-ray diffraction (XRD) method was used to identify the filler materials in the threads. Typical diffraction patterns of the pin and box thread materials are shown in Figs. 4-5(a) and 4-5(b), respectively. The fillers in the pin and in the box threads were identified as quartz (SiO_2) and graphite flakes, respectively.

The elastic moduli of the quartz and graphite flakes were 10.4 Msi and 1.5 Msi, respectively [40]. Assuming the fillers in the threads were 3-D randomly oriented, one may obtain elastic properties[2] of the particulate filled epoxy thread composites based on the following micromechanics equations [63]:

$$E = \frac{V_f}{6} E_f + [\, 1 + (1+\nu_m) V_f] \, E_m, \tag{4-1a}$$

$$\nu = V_f \nu_f + (1 - V_f) \nu_m, \tag{4-1b}$$

---

[1] In some cases, threads are machined into the composite tube. But the case of machined threads is not considered in this study.

[2] E = 0.48 Msi and υ = 0.3, for box-side threads.
E=0.67 Msi and υ = 0.3, for pin-side threads.

where quantities with subscripts f and m are related to the fiber and matrix, respectively, and V_f is the fiber volume fraction.

(b) Fiber Composite Tubular Bodies

In the tubular composite joints, an anhydride-cured epoxy resin was used. The reinforcements were E-glass fibers. Elastic properties of the unidirectional glass/epoxy composite, obtained from experiments [41] at room temperature, were

$$E_{11} = 6.53 \text{ Msi}, E_{22} = E_{33} = 1.74 \text{ Msi},$$
$$\upsilon_{12} = 0.28, G_{12} = 0.82 \text{ Msi},$$
$$V_f = 0.57, V_v = 0.012,$$

where subscripts 1, 2, and 3, refer to fiber, transverse and through-the-thickness directions in each glass/epoxy ply.

Glass transition temperatures, T_g, of the fiber composite and the thread materials were determined by a standard DSC (Differential Scanning Calorimetry) measurement. The T_g's of the glass/epoxy composite and the filled thread material were 115°C and 103°C, respectively, as shown in Figs. 4-6(a) and 4-6(b). Since the T_g value of the fiber composite was significantly higher than the ambient temperature, viscoelastic effects[1] of the composite were neglected in the present study of room-temperature failure behavior of the composite joint.

4.4 Failure Strengths of Fiber Composite Joint Materials

(a) Fiber Composite Tubular Body

The establishment of proper failure criteria is critical in the leakage failure study of the composite tubular joint. Rigorous physical-mechanism-based failure criteria, based on the results of a previous study [6], are introduced in the present progressive failure analysis of composite tube bodies[2].

(b) Composite Thread Materials

To predict leakage failure of a threaded composite tubular joint under combined internal pressure, axial and make-up loading, damage and failure of the threads must be taken into account. Since epoxy is relatively brittle, the well-known maximum principal stress failure criterion for brittle materials is used. Tensile and compressive strengths of the filled epoxy in the threads are found to be 9.5 ksi and 36 ksi, respectively [40].

(c) Thread-tube Body Interface

---

[1] A long-term moisture exposure of the composite joint may reduce Tg values of the composite and the thread material. Viscoelastic effects may become appreciable in this case and have to be considered.

[2] The failure strains of the unidirectional glass/epoxy composite obtained from experiments [41] are

$$\varepsilon_{22f}^{(T)} = 0.004, \quad \varepsilon_{22f}^{(C)} = 0.04, \quad \text{and} \quad \gamma_{12f} = 0.0504.$$

Here, superscripts T and C represent tension and compression, respectively.

The microstructural study reveals that the pin-side threads were molded on the tube body. The interface strength between the composite pin body and pin-side threads is important in determining the ultimate load bearing capability of the joint. Rigorous methodology to determine the interface strength between two composite systems remains still controversial, and various test methods have been introduced, but none is satisfactory. In this study, the interfacial strength between the thread and the tube body was obtained by an analytical procedure with back calculations from the experimental results of selected integral composite joints in an axial-loading dominated condition. The results show that the average interfacial (shear) strength between the filled threads and the composite tube body was approximately 1.6 ksi.

5. LEAKAGE FAILURE EXPERIMENTS

The experimental part of this research attempts to identify damage mechanisms associated with leakage failure and establish proper failure models. It is also used to validate the leakage failure analysis of a threaded composite tubular joint. The leakage failure experiments on threaded composite joints are much more involved than those on fiber-composite tube bodies, owing to the complex joint geometry, and loading and material parameters involved. Each leakage failure experiment on a threaded composite joint usually consists of following three steps which need to be considered carefully.

1) Make-up. Make-up (i.e., tightening) is a unique loading mode associated with threaded joint contact mechanics. During the make-up, a radial interference is introduced and its associated variables, such as make-up turn, torque, and associated deformations need to be included.

2) Multiaxial loading and leakage detection. Determination of leakage in the experiment, especially its onset in a threaded composite joint subjected to external loading, is controversial. Leakage failure modes are critical in understanding the functional failure and modeling the damage of the joint. The leakage failure envelope, i.e., the critical state of combined internal pressure, axial and make-up loading, is most important in understanding loading mode interactions in joint leakage failure.

3) Break-out. Break-out of a joint leads to determination of deformations involved and the amount of interference introduced in a tested joint. The information is needed to construct the leakage failure envelope.

The complicated threaded fiber-composite joint failure caused by applied multiaxial loading requires special considerations in:

1) Designing a proper test specimen with a simple geometry and a gripping system suitable for evaluation of failure modes and critical loads of the joint;

2) Developing a loading system for introducing various combinations of internal pressure, make-up and axial loads in a joint leakage test;

3) Devising proper measurement and data acquisition systems that all necessary information in the leakage test can be recorded correctly and conveniently;

4) Construction of a reliable leakage detection system to determine quantitatively the onset of the leakage failure;

5) Developing a control system which enables the micro-computer to govern different loading actuators, synchronize the measurements, and detect the leakage;

6) Conducting a critical bearing pressure study to establish the sealing capacity of a threaded tubular composite joint under various loading modes, and

7) Establishment of a leakage failure envelope for the threaded composite joint under different make-up interferences and other loading, and identify associated leakage failure modes for subsequent modeling and verification.

5.1 Experimental System Development

5.1.1 Threaded Composite Joint Specimen

The leakage test was conducted on threaded fiber-composite joints with finite-length pin and box sections subjected to combined make-up, internal pressure and axial loading. The applied loading was transmitted from loading grips to the specimen through surface contact. During the load transfer, local stress concentrations in the specimen were inevitably developed. If not properly designed, the specimen may fail prematurely and outside the gage section. The local stress concentrations were mostly related to the geometry of the grips, the bonded tab and the threads, and the material discontinuities between various contacts and fixtures.

Several types of tab designs for different tubular gripping systems have been reported in the literature [42,43]. Since in a threaded composite joint specimen, high stress concentrations generally occur in the thread contact region, thus, this will ensure the joint specimen fails first in the gage section rather than in the tube body. Therefore, a proper tab design for a composite tubular specimen should be also suitable for the composite joint specimen.

Extensive studies [41], experimentally and numerically, have been conducted on designing the tabs for a tube-body experiment in our laboratory. Based on the analytical and experimental results obtained in [41], specimen design for the leakage testing a threaded composite joint is presented in Figs. 5-1(a) and 5-1(b). The specimen tab was made of a hoop-wound glass/epoxy with a taper angle of 7.5º, as shown in Figs 5-1(a) and 5-1(b)[1].

5.1.2 Composite Tubular Joint Gripping System

In a leakage experiment, the threaded composite joint was subjected to multiaxial loading. The loading must be transferred to the specimen through a specifically designed gripping system. In an axial loading case, an in-house designed gripping system was used. The grip arrangement, shown in Fig. 5-2, consisted of a steel end plate with an internal plug, an aluminum spacer, and an outer steel flange. The axial load was transmitted from an actuator to the steel flange by bolts and was applied to the specimen through the surface contact between the tab and the spacer. Grips on both the pin side

[1] We note that using hoop-wound glass/epoxy as the tab material may not be the best in some cases, especially in the cases of high axial loading. However, the hoop-wound tab was easy to make and suitable for joints subjected to an intermediate level of axial loading. Since the internal diameter of the box near the box end varied along its axis, a relatively long specimen in the box side was employed.

and the box side of the joint were identical except the internal diameter of the spacer on the pin side, which was smaller than that on the box side.

An internal pressure was applied to the specimen by the water filled inside the specimen. Two alternatives could be used to conduct the pressurization. One was by sealing the gap between the steel plug on the end plate and the inner wall of the specimen; the other was by using a mandrel. The first method had some disadvantages[1] and was not used. The second approach, as illustrated in Fig. 5-3, could overcome these difficulties. With a mandrel being introduced, the amount of the pressure medium in the specimen could be kept to a minimum. Based on a self-equilibrated design of the mandrel, no internal pressure related axial load was needed when pressurizing the joint. Therefore, the axial-to-hoop loading ratio could be accurately controlled. Sealing between the mandrel and the specimen was achieved by using suitable O-rings, if dimensions of the mandrel, especially the OD and O-ring grooves, are designed and machined with close tolerances. The one-piece mandrel worked well for the test of a composite tubular body specimen. However, the experiment of threaded composite joints required additional attention, because diameters of the pin and the box would be changed after the make-up was applied, as illustrated in Fig. 5-4.

To achieve the best sealing[2] between the mandrel and the specimen without damaging the O-rings and the specimen, a two-piece screw connected aluminum alloy mandrel was used in the current gripping system, as shown in Figs. 5-5a and 5-5b. Each side of the mandrel was pushed into the joint from the end of the specimen, as shown in Fig. 5-5c, and then connected[3] .

5.1.3 Multiaxial Loading System

The development of a dependable multiaxial loading system was essential to the establishment of leakage failure envelopes and identification of failure modes in the composite joints. The multiaxial loading system developed for the joint leakage test is shown in Fig. 5-6. Two actuators were used in the experiments, one for applying the axial load up to 55 Kips and another for the internal pressure. The internal pressure was applied to the joint specimen by a pressure intensifier which could generate a pressure up to 10 ksi.

The pressure medium was salt water, which was supplied to the intensifier and

---

1 The disadvantages include (1) A large axial compressive loading must be applied to the specimen to offset the tensile loading caused by the internal pressure. This compressive load might buckle the specimen if the specimen was to experience a sudden drop in the internal pressure, and causing load control of the test to become difficult, and (2) A relatively large amount of the pressure medium (water) was needed, which might mess up the test system when the joint leaked or failed.

2 Owing to the radial interference introduced during make-up, dimensions of the box end increased and those of the pin end decreased. The reduction in the internal diameter at the pin-end caused difficulties in pushing the mandrel into the specimen and even damaged the O-rings and the specimen, especially for the joint with a high level of make-up. Reducing the outside diameter of the mandrel may avoid these difficulties, but it may also decrease the sealing pressure between the specimen and the mandrel.

3 The two-piece mandrel could also eliminate the inconveniences caused by the dimensional limitation in the tension-torsion test system when pushing the mandrel into the specimen.

the specimen through an inlet valve with an opened bleeding valve. After the intensifier and the specimen were filled with water, the bleeding valve and the inlet valve were closed. A prescribed level of internal pressure could be realized upon moving the piston in the intensifier by an analog controller. In an experiment without leakage, the piston in the intensifier would be controlled to a constant position to keep a desired level of pressure, as long as deformations in the specimen and in the test system were time independent. However, when leak occurred, the piston would be forced to move up to maintain the prescribed pressure.

5.1.4 Make-up Loading System

During make-up of a threaded composite joint, a radial interference was introduced, resulting in a bearing pressure on the thread surface. A simple and accurate joint make-up system was developed in this study, as illustrated schematically in Fig. 5-7. The design made full use of the existing equipment and the grips available in Multiaxial Materials and Structures Testing Laboratory. The grips were identical to those used in the leakage test and a 60:1 speed reducer, driven manually by a crank handle, was used as the torque application device. As shown in Fig 5-7, the box side of the joint would move up substantially during the make-up as the joint was tightened up. The movement could induce a significant amount of axial load to the threads of the joint and even damage the threads, if the actuator failed to follow the axial movement of the box section. To eliminate this induced axial load during the make-up, the axial actuator in the test system was set to a zero-load control mode, while the torsional actuator remained in a displacement-control mode. With the zero-load control, the axial actuator would follow the movement of the box during the make-up and protected the threads from being damaged.

5.1.5 Load Control Systems

During construction of the experimental facility in this study, control systems, involving a digital controller and an analog controller, were developed to govern the axial load and the internal pressure. With the digital controller, the applied axial load was controlled by a computer through a general purpose interface bus (GPIB) board, using the existing system configuration, whereas with the analog controller, the pressure applied was controlled by a computer with minor system modifications. Among various operational parameters, loading and unloading were the first concerns in the joint leakage test. Proper control of the loading path ensured that the applied axial loading and internal pressure could be introduced in-phase or along a prescribed path, while control of unloading provided safety if the specimen was damaged, leaked or in an emergency.

Two channels of digital I/O in a data acquisition board (MINI-16) were programmed as outputs and used for the load (pressure) control on the analog controller, as shown in Fig. 5-8. Two computer-driven solid state relays (SSR) were mounted behind the start button on a waveform generator unit and the actuator-off button on a hydraulic control unit of the analog controller. When the digital output of the data acquisition board was set to high (>2.4 volts), the voltage on the SSR (<2.6 volts) was not enough to close the relay and left the relay open. By setting the digital output to low (<0.4 volts), the voltage on the SSR (>4.6 volts) was sufficient to close the relay.

By closing or opening the relays, the computer was able to start the waveform generator to apply a prescribed internal pressure to the specimen or turn off the actuator for unloading. The SSRs also provided electrical isolation from the control devices. With these hardware modifications and a properly developed software, which controlled both data acquisition and GPIB boards, the multiaxial test system could simultaneously control the axial load and the pressure, measure joint deformations, detect leakage, and terminate the experiment when the onset of leakage was detected.

5.1.6 Multiaxial Deformation Measurement System

During joint make-up, a radial interference was introduced into the joint. Associated with the interference were deformations in both pin and box sections of the joint, and a make-up torque due to the friction generated between threads. Accurate measurements of make-up parameters, such as the deformation, torque, and turn, were essential [44] in quantitative evaluation of the make-up. A measurement system for the joint make-up, as shown in Fig. 5-9, was developed for this purpose. Deformations in a threaded joint during make-up were measured with strain gages mounted on the joint. A ten-turn potentiometer, mounted on the bottom of the speed reducer, was calibrated for the make-up turn measurement. The induced torque during the joint make-up was measured directly from the load cell of the tension-torsion test system.

In a leakage test, the detailed response of a threaded joint under a combined axial load, internal pressure, and make-up interference was determined, including deformations caused by the axial and pressure loading. Also, the critical load level at which leakage occurred, and the associated damage modes in the joint were identified and recorded in the test system.

Unlike the experiment on a tube body [41], which had a uniform field in the gage section, deformations in a threaded joint specimen were highly nonuniform with strains varying along the axis of the joint. Strain gages were also used at different locations along the joint axis to determine deformations. The internal pressure was measured by a transducer in the pressure intensifier, and the piston movement, by a linear variable displacement transducer (LVDT). Signals were sent to the analog-controller conditioning board. Signals from the strain gages, the pressure transducer, and the LVDT were processed through the data acquisition board and the microcomputer. The axial load measured by the load cell in the test system was recorded by the computer through the GPIB board. The complete measurement system developed for the leakage experiment of threaded composite joint is shown in Fig. 5-10.

5.1.7 Leakage Detection Systems

Determination of the load level at which the onset of threaded joint leak requires a sensitive and reliable leakage detection system. In this study, two leakage detection systems were constructed. Both methods were sensitive to detect the joint leak and a comparative evaluation was easily made to assess their validity.

(a) Conducting Metal Mesh Method.

By wrapping a fine conductive metal mesh on the outside surface of a specimen,

water leaked to the surface of the specimen was detected through a digital input measurement, as shown in Fig. 5-11. The method was based on the fact that a glass/epoxy composite was not a conductor. A conductive path was formed between the metal mesh and the mandrel when the salt-water filled specimen leaked, resulting in reduction in resistance between the mesh and the mandrel. The reduction was amplified by a PNP triode, leading to a forward active mode between its collector and an emitter. The mode would lower the digital input of the data acquisition board, which was set to be high initially, and thus would trigger an event detection system.

(b) Piston-Movement Method

The second method was developed on the basis that, at a constant pressure loading rate, the piston of a pressure intensifier would move faster in a leaked joint test than in the one without leakage in order to keep the same applied pressure. A schematic of a pressure-versus-piston movement in a joint test without leakage is given by the solid line in Fig. 5-12. After an initial adjustment, such as filling the fluid into the gap between the mandrel and the specimen, the slope approached to a constant value D_1, which depended on the stiffnesses of the specimen and the test system. If the specimen started to leak at a certain pressure level, the slope D would have to increase in order to maintain the same pressure, as shown by the dash line in Fig. 5-12. Given the loading rate and the diameter of the piston, one could determine quantitatively the amount of fluid leaked through the specimen at a given load by calculating the difference in the slope, $(D-D_1)$. If the leakage threshold was assumed as D_L, then the following expression may be used as leakage detection,

$$\text{Leakage occurs, when } D \geq D_1 + \frac{D_L}{(\text{Area of piston}) \times (\text{Loading rate})}. \qquad (5\text{-}1)$$

Based on the API recommendation [44], the threshold D_L for leakage detection was set as approximately 1 ml/minute in this study. An experiment was terminated, only when both leakage detection systems were triggered.

5.1.8 Data Acquisition System

Measurement devices for the aforementioned joint make-up and leakage test employed two data acquisition systems, namely, a data acquisition board and a GPIB board. Since no hardware synchronization existed between the two data acquisition systems and patterns of scanned data were different as described in Appendix D, a single reading mode was selected in the digital controller. Also, since the scanning frequency of the data acquisition board was relatively low in low noise and high resolution modes, certain sequences in the data acquisition must be determined first to obtain relatively well synchronized measurements. Here two single readings from the digital controller were placed one before and one after the data acquisition from the data acquisition board. The average of the two readings was used as a reference (or synchronized) for the data from the data acquisition board. At a low loading rate, this reading sequence gave good synchronization between the two data acquisition systems.

A schematic representation of the control and the data acquisition operations is

given in Fig. 5-13. After all test parameters were introduced, the computer took control from the digital controller and set the axial loading rate and magnitude. The prescribed axial load and internal pressure were applied by the computer almost instantaneously to ensure the correct loading ratio and path. During loading, the computer acquired the data in the aforementioned manner. The digital input from the leakage detection systems was also checked during loading. When a joint leak was detected, the computer would automatically terminate the test or beep to alarm the operator, depending on the options chosen.

In order to make the control program user friendly, the program was written in Visual-Basic 3.0. The menu-driven program, Fig. 5-14, would prompt the user with a corresponding sub-windows for the detailed input of loading parameters, strain gage arrangements, test profile display, and leak detection choices. Test parameters would also be saved in a file (or loaded into the system), based upon the selection of the file menu. The test results were displayed on two x-y-y plots through the computer screen, according to profile selection.

During a joint make-up, the torque was applied manually. In this case, the computer was used only for data acquisition and analysis purpose.

5.2 Experimental Procedure

(a) Composite Joint Makeup

Prior to a formal joint make-up, an initial tightening (IT)[1] was ascertained. At the mid-point of an anticipated, engaged thread section, two circumferentially oriented strain gages were mounted 180^{o} apart on the outside surface of the composite box section. Threads on both the pin and the box sides of the composite joint were brushed with a manufacturer-recommended thread compound [45]. The pin section was then screwed into the box in three turns below a finger tight position. The make-up of the connection was continued, using the aforementioned device shown in Fig. 5-7, until a prescribed number of turns was reached. During the make-up process, the make-up turn, the torque, and the hoop strains were all recorded and monitored with a micro-computer.

(b) Multiaxial Loading on Threaded Composite Joint

The leakage failure experiment of a threaded composite integral joint was conducted on the aforementioned multiaxial material testing system. Three circumferentially oriented and six axially oriented strain gages were mounted on the outer surface of a box section, as shown in Fig. 5-15. The three locations for mounting the strain gages corresponded to two end points and one mid point of the engaged threads. Unless otherwise noted, the experiments were conducted under proportional loading with a loading rate about 19 psi/sec for one-turn make-up and 21 psi/sec for two-turn

---

[1] The initial tightening is sometimes referred to as "finger tight position" (FTP). The FTP was determined by using two fingers to make-up the joint such that deformation in the joint at that position was minimal.

make-up. The pressure-to-axial-load ratio applied in the leakage experiments ranged from a pure internal pressure (1:0) case to a nearly uniaxial loading (~0:1) case.

(c) Leakage Detection

Salt water was used as the pressuring medium in all experiments. An aluminum mesh was wrapped on the outer surface of the threaded joint for accurate leak detection. The piston movement in the pressure intensifier was also monitored to determine the joint leakage. The test was terminated when results from both leakage detection methods were positive.

In this study a total of 37 tests have been conducted. The specimens were from two batches of samples sent by the manufacturer. The test matrix is shown in Table 5-1, which also gives loading and make-up conditions in each test.

6. BOUNDARY VALUE PROBLEM FOR LEAKAGE FAILURE OF THREADED COMPOSITE TUBULAR JOINTS

Consider a threaded composite joint subjected to combined internal pressure, axial load, make-up interference and, in some cases, bending. An accurate leakage failure analysis of the threaded composite joint under the complicated loading requires proper formulation of a nonlinear mechanics problem, involving thread surface contact, nonlinear material constitutive equations, and anisotropic coupling of extension, shearing, bending and torsion. In addition, a proper theoretical model for the joint leakage behavior should also include various failure modes, such as tube body damage, thread shear-off, thread/tube body interface failure and loss of bearing pressure between the threads in contact. In this section, formulation of a nonlinear boundary-value problem for a threaded composite joint, and an accompanying solution procedure are presented for studying the leakage failure of the joint. In the formulation of the boundary-value problem, the following subjects are specially addressed:

1) Assumptions and approximations for modeling a threaded composite joint, based on the experiments and observations, and information available in the literature;

2) Governing differential equations, and corresponding boundary and interface conditions for the joint subjected to multiaxial loading;

3) Uniqueness of a solution for the problem, and

4) Procedures for solving the boundary-value problem.

6.1 Approximations and Assumptions

6.1.1 Geometric Consideration

Except the helical threads, an important feature of a threaded tubular composite joint is its global structural axisymmetry. The nonaxisymmetric effect of the threads depends on the thread helical angle, which is a function of the nominal diameter of the joint and dimensions of the thread pitch, as shown in Fig. 6-1. The global geometric axisymmetry of a threaded joint is less disturbed in the case of threads with a small helical angle. In most commonly used threaded tubular joints [38,39], the helical angle is less than 2 degrees, as discussed in Appendix E. Therefore, in this study, it is assumed that the nonaxisymmetric effect of the threads with a small helical angle is negligible. The threaded joints considered are modeled as being geometrically axisymmetric in a cylindrical coordinate system.

6.1.2 Thread Contact

It is generally recognized that thread surfaces of a composite tubular joint are smooth due to high precision molding during manufacturing. Note that a lubricant is

commonly applied during make-up. Galling caused by an excessive make-up is not considered. Therefore, a small frictional force between thread contact surfaces is assumed.

6.1.3 Composite Joint Material System

Ply constitutive equations of the filament-wound composite tubular body are assumed to be transversely isotropic and uniform along the circumferential direction. The fiber composite considered in this study is a glass/epoxy composite, exhibiting highly nonlinear shear behavior, whereas tensile stress-strain relations in longitudinal and transverse directions remain approximately linear. The shear nonlinearity has been shown [6] to affect significantly deformation and leakage failure characteristics of the composite tubular. An analysis with linear material properties may grossly underestimate the composite leakage response. Experimental studies, as will be discussed later, show that matrix cracking, a damage mechanism in the composite tubular, is a major failure mode responsible the joint leakage. Therefore, in developing the current theoretical model, the composite tube body is assumed to have cylindrically anisotropic ply properties with substantial shear nonlinearity.

6.1.4 Interface

Macroscopically, two kinds of interface exist in a threaded composite tubular joint, (1) interfaces between composite plies with different winding angles in the tube body, and (2) the interface between the composite lamina in the tube body and molded threads in the joint region. Perfect bonding between the composite plies and also between the composite lamina and the threads is assumed in the joint section.

6.1.5 Loading

In the study, a threaded joint is assumed to be subjected to a combined internal pressure, axial load, torsional make-up, and bending. In typical fluid transport and downhole environments, the bending is small and assumed to be negligible. Also, the composite tubular joint is supported axisymmetrically.

6.2 Governing Differential Equations

Based upon the aforementioned assumptions and approximations, a threaded composite tubular joint can be referred to a cylindrical coordinate system (Fig. 6-2) with the z coordinate being coincident with the tube axis. In the cylindrical coordinates, the engineering strain, ε_i, in each composite ply are given by

$$\begin{aligned} \varepsilon_r &= \frac{\partial u}{\partial r}, & \varepsilon_{\theta z} &= \frac{\partial v}{\partial z} + \frac{1}{r}\frac{\partial w}{\partial \theta}, \\ \varepsilon_\theta &= \frac{1}{r}\frac{\partial v}{\partial \theta} + \frac{u}{r}, & \varepsilon_{rz} &= \frac{\partial u}{\partial z} + \frac{\partial w}{\partial r}, \\ \varepsilon_z &= \frac{\partial w}{\partial z}, & \varepsilon_{r\theta} &= \frac{1}{r}\frac{\partial u}{\partial \theta} + \frac{\partial v}{\partial r} - \frac{v}{r}, \end{aligned} \tag{6-1}$$

where u(r, θ, z), v(r, θ, z), and w(r, θ, z) are displacement components in each ply along r, θ, and z directions, respectively.

The ply composite material constitutive equations with in-plane shear nonlinearity are expressed as

$$\varepsilon_i = S_{ij}(\tilde{\sigma})\,\sigma_j \quad (i,j=1,2,3,4,5,6). \tag{6-2}$$

In Eq. (6-2), S_{ij} is nonlinear compliance of the individual composite plies, and is function of ply fiber orientations Θ_k and the state of stress $\tilde{\sigma}$. The σ_j and ε_j are stresses and strains in contracted notation with $[\sigma_1, \sigma_2, \sigma_3, \sigma_4, \sigma_5, \sigma_6]=[\sigma_{11}, \sigma_{22}, \sigma_{33}, \sigma_{23}, \sigma_{13}, \sigma_{12}]$ and $[\varepsilon_1, \varepsilon_2, \varepsilon_3, \varepsilon_4, \varepsilon_5, \varepsilon_6]=[\varepsilon_{11}, \varepsilon_{22}, \varepsilon_{33}, \varepsilon_{23}, \varepsilon_{13}, \varepsilon_{12}]$.

The constitutive equations for the threads follow Hooke's law $\varepsilon_i = S^*_{ij}\,\sigma_j$, where S^*_{ij} is a linear compliance of the thread material. Equilibrium equations in the cylindrical coordinates are

$$\begin{aligned}
&\frac{\partial \sigma_r}{\partial r} + \frac{(\sigma_r - \sigma_\theta)}{r} + \frac{1}{r}\frac{\partial \tau_{r\theta}}{\partial \theta} + \frac{\partial \tau_{rz}}{\partial z} = 0\,,\\
&\frac{\partial \tau_{r\theta}}{\partial r} + \frac{1}{r}\frac{\partial \sigma_\theta}{\partial \theta} + \frac{\partial \tau_{\theta z}}{\partial z} + \frac{2\tau_{r\theta}}{r} = 0\,,\\
&\frac{\partial \tau_{rz}}{\partial r} + \frac{1}{r}\frac{\partial \tau_{\theta z}}{\partial \theta} + \frac{\partial \sigma_z}{\partial z} + \frac{\tau_{rz}}{r} = 0\,.
\end{aligned} \tag{6-3}$$

Since all geometric parameters, external loads, and ply material properties are assumed to be independent of θ, the ply displacements, strains and stresses in the composite should also be independent of θ. Thus, the strain-displacement relations can be simplified as

$$\begin{aligned}
&\varepsilon_r = \frac{\partial U}{\partial r}\,, && \varepsilon_{\theta z} = \frac{\partial V}{\partial z}\,,\\
&\varepsilon_\theta = \frac{U}{r}\,, && \varepsilon_{rz} = \frac{\partial U}{\partial z} + \frac{\partial W}{\partial r}\,,\\
&\varepsilon_z = \frac{\partial W}{\partial z}\,, && \varepsilon_{r\theta} = \frac{\partial V}{\partial r} - \frac{V}{r}\,,
\end{aligned} \tag{6-4}$$

where U(r, z), V(r, z) and W(r, z) are ply displacements, and are functions of r and z only. Similarly, equilibrium equations in the cylindrical coordinates have the forms as

$$\frac{\partial \sigma_r}{\partial r} + \frac{(\sigma_r - \sigma_\theta)}{r} + \frac{\partial \tau_{rz}}{\partial z} = 0\,,$$

$$\frac{\partial \tau_{r\theta}}{\partial r} + \frac{\partial \tau_{\theta z}}{\partial z} + \frac{2\tau_{r\theta}}{r} = 0 \,, \qquad \frac{\partial \tau_{rz}}{\partial r} + \frac{\partial \sigma_z}{\partial z} + \frac{\tau_{rz}}{r} = 0 \,. \tag{6-5}$$

Note that in Eqs. (6-4) and (6-5), the strains (ε_i) and stresses (σ_i) are functions of r and z only. Therefore, the boundary-value problem of a threaded composite tubular joint can be formulated in terms of r and z in the cylindrical coordinate system. Note also that while the composite joint problem is formulated in the same manner as a traditional axisymmetric problem, the deformations and stresses in the threaded composite joint are inherently *three-dimensional*, since all components of field variables are present in the above equations.

As mentioned earlier, the constitutive equations for a fiber composite lamina (Eq. (6-2)) generally involve severe shear nonlinearity. The nonlinear shear behavior of a fiber composite requires a proper mathematical description. Based on the strain energy density consideration and symmetry of deformation in a rectilinear anisotropic solid, Hahn and Tsai have proposed [46,47] a power-law type constitutive equation to describe the nonlinear behavior of fiber composites. (A discussion of the strain energy density function for the nonlinear material is provided in Appendix F). Following the Tsai-Hahn representation [46,47], the power-law relationship given in Eq. (6-6) is used in the study:

$$\varepsilon_6 = \bar{S}_{66}\sigma_6 + \bar{S}^h_{66}\sigma_6^3 \,, \tag{6-6}$$

where $\bar{S}_{66}$ corresponds to the linear in-plane shear compliance and $\bar{S}^h_{66}$ is a high-order term, which can be determined by proper experiments.

Although the power-law expressions may be extended [48] to include the out of plane transverse nonlinear relationships between ε_{LZ} and σ_{LZ} and the coupling between the in-plane and out-of-plane deformations (in LZ and LT planes), only the decoupled in-plane shear nonlinearity is considered in this study.

Thus, constitutive equations of a transversely isotropic unidirectional fiber composite[1] can be expressed in the principal material coordinates as

[1] For the E-glass/epoxy composite used in the current study, the nonlinear shear compliance $\bar{S}^h_{66}$ has been found [41] to be 1.654×10^{-14} $(psi)^{-3}$.

$$\begin{Bmatrix}\varepsilon_1\\ \varepsilon_2\\ \varepsilon_3\\ \varepsilon_4\\ \varepsilon_5\\ \varepsilon_6\end{Bmatrix}=\begin{bmatrix}\bar{S}_{11} & \bar{S}_{12} & \bar{S}_{12} & & & \\ \bar{S}_{12} & \bar{S}_{22} & \bar{S}_{23} & & 0 & \\ \bar{S}_{12} & \bar{S}_{23} & \bar{S}_{22} & & & \\ & & & 2(\bar{S}_{22}-\bar{S}_{23}) & 0 & 0 \\ & 0 & & 0 & \bar{S}_{66} & 0 \\ & & & 0 & 0 & \bar{S}_{66}+\bar{S}^{h}_{66}\sigma_5^2\end{bmatrix}\begin{Bmatrix}\sigma_1\\ \sigma_2\\ \sigma_3\\ \sigma_4\\ \sigma_5\\ \sigma_6\end{Bmatrix}, \tag{6-7}$$

where

$$\bar{S}_{11}=\frac{1}{E_L}\ ,\ \bar{S}_{12}=\frac{-\nu_{LT}}{E_L}\ ,\ \bar{S}_{23}=\frac{-\nu_{TZ}}{E_T}\ ,\ \bar{S}_{22}=\frac{1}{E_T}\ \text{ and }\bar{S}_{66}=\frac{1}{G_{LT}}\ .$$

From Eq. (6-7), the constitutive equations, Eq. (6-2), in the structural (r-θ-z) coordinates can be easily obtained by a standard coordinate transformation.

6.3 Boundary and Interface Conditions

6.3.1 Applied Loading Conditions

For illustration, consider a threaded tubular joint made of a two-ply fiber composite (Fig. 6-3) subjected to a combined axial load p_a and internal pressure p_i, respectively. Along the boundary Γ_1, traction boundary conditions are

$$\sigma_z^{(1)}=\sigma_z^{(2)}=p_a,\quad \tau_{rz}^{(1)}=\tau_{rz}^{(2)}=0,\ \text{and}\ \ \tau_{\theta z}^{(1)}=\tau_{\theta z}^{(2)}=0, \tag{6-8}$$

where the superscripts 1 and 2 denote composite plies in the pin section of the joint.

An internal pressure p_i is applied on inner surfaces Γ_2, Γ_3, Γ_4 and Γ_5 of the joint. The corresponding traction boundary conditions along the boundaries Γ_2 to Γ_5 are as follows:

$$\sigma_r=-p_i,\quad \tau_{rz}=0,\ \text{and}\ \ \tau_{r\theta}=0,\qquad \text{on } \Gamma_2, \tag{6-9}$$

$$\sigma_z=-p_i,\quad \tau_{rz}=0,\ \text{and}\ \ \tau_{\theta z}=0,\qquad \text{on } \Gamma_3, \tag{6-10}$$

$$n_j^{(r)}\,\sigma_{1j}=-p_i,\quad n_j^{(r)}\,\sigma_{sj}=0\ ,\qquad \text{on } \Gamma_4 \text{ and } \Gamma_5, \tag{6-11}$$

$$(j=1,2,3;\ s=2,3;\ r=4,5),$$

where $n_j^{(r)}$ denote directional cosines of the normal to the boundary Γ_r.

Boundary conditions along all other surfaces of the joint, Γ_0, except those along the thread contact, are traction-free and can be expressed as

$$\sigma_{ij}\,n_j=0, \tag{6-12}$$

where n_j denote directional cosines of the normal to the boundary Γ_0.

Also, the following constraint conditions are applied along the boundary Γ_6 to prevent any rigid body motion of the joint:

$$V = 0, \quad W = 0. \tag{6-13}$$

Note that other constraint conditions may also be used, provided that they have the same statically equivalent effect on the thread region. Equation (6-13) is taken in this study because of its simplicity.

6.3.2 Thread Surface Contact Conditions

It is important to point out here that threads of a tubular joint not only transfer loads between the pin and the box but also serve the sealing function. The sealing integrity of a threaded joint is accomplished by the development of contact pressure on the thread surface. The contact pressure is caused by a radial interference[1], due to thread taper, between the external surface of the pin and the internal surface of the box after assemblage. A key element in the determination of thread-surface contact is a proper description of the contact condition. Unlike the commonly used displacement (or traction) boundary conditions in a boundary-value problem, the exact solution along the contact boundary is unknown in the present threaded joint problem, and it changes with the applied boundary loading. However, the surface contact conditions can still be determined through an iterative method, by employing a properly introduced solution procedure.

Generally, three situations may occur on a contact surface when two bodies are brought in contact, opening (on ∂R_{open}), sliding contact (on ∂R_{slide}), and sticking contact (on ∂R_{stick}). In each case, two types[2] of boundary conditions need to be satisfied, i.e., basic contact and constraint contact conditions.

(a) Opening Case

In an opening case, two bodies do not contact along ∂R_{open} and traction-free boundary conditions need to be met,

$$\sigma_n^{(i)} = \sigma_n^{(j)} = 0, \quad \tau_{nt}^{(i)} = \tau_{nt}^{(j)} = 0, \text{ and } \tau_{n\theta}^{(i)} = \tau_{n\theta}^{(j)} = 0, \qquad \text{on } \partial R_{open}. \tag{6-14a}$$

---

[1] The radial interference, δ, may be approximated from the taper of the threads as

$$\delta \approx \frac{\text{(Turns for assemblage) x (Tapering)}}{\text{2 x (Number of Threads/inch)}}.$$

[2] Basic contact conditions are commonly given in the form of an equality, whereas constraint conditions are expressed by an inequality. In a mechanics analysis, the constraint contact conditions are used to describe the situations of a contact boundary and the basic contact conditions are for defining the local loading (or continuity), which are enforced along the corresponding boundaries.

Also, the required constraint conditions are

$$U_n^{(j)} - U_n^{(i)} > \delta_n, \quad \text{on } \partial R_{open}. \tag{6-14b}$$

The subscripts n, t, and θ in Eqs. (6-14a) to (6-14b) denote local normal, tangential, and circumferential directions along the contact boundary, respectively, as shown in Fig. 6-4. The superscripts i and j represent the bodies in contact, and δ_n is the normal component of the radial interference (or initial interference) on the contact surface.

(b) Sticking Contact

In the case of a sticking surface contact, the bodies are in contact along a segment of the surface, ∂R_{stick}. However, driving force in this case may not be sufficient to cause relative sliding to happen. Consequently, basic conditions for the sticking contact are

$$U_n^{(j)} - U_n^{(i)} = \delta_n, \quad U_t^{(j)} - U_t^{(i)} = \delta_{t0}, \quad U_\theta^{(j)} - U_\theta^{(i)} = \delta_{\theta 0}, \quad \text{along } \partial R_{stick}, \tag{6-15a}$$

$$\sigma_n^{(i)} - \sigma_n^{(j)} = 0, \quad \tau_{nt}^{(i)} - \tau_{nt}^{(j)} = 0, \quad \tau_{n\theta}^{(i)} - \tau_{n\theta}^{(j)} = 0, \quad \text{along } \partial R_{stick}, \tag{6-15b}$$

where δ_{t0} and $\delta_{\theta 0}$ in Eq. (6-15a) are relative movements along the t and θ directions when sticking occurs. Constraint conditions for this case are

$$\sqrt{\tau_{n\theta}^2 + \tau_{nt}^2} < f\left|\sigma_n\right|, \tag{6-15c}$$

$$\sigma_n^{(i)} = \sigma_n^{(j)} < 0, \tag{6-15d}$$

where f is the coefficient of friction[1], and $\sqrt{\tau_{n\theta}^2 + \tau_{nt}^2}$ is called an "equivalent frictional stress".

(c) Sliding Contact

When the equivalent frictional stress reaches a critical value, $f\left|\sigma_n\right|$, along ∂R_{slide} sliding contact occurs. The basic conditions for the sliding contact are

$$U_n^{(j)} - U_n^{(i)} = \delta_n, \tag{6-16a}$$

$$\sigma_n^{(i)} - \sigma_n^{(j)} = 0, \quad \tau_{nt}^{(i)} = \tau_{nt}^{(j)} = \frac{-f\left|\sigma_n\right|\delta_t}{\sqrt{\delta_t^2 + \delta_\theta^2}}, \quad \tau_{n\theta}^{(i)} = \tau_{n\theta}^{(j)} = \frac{-f\left|\sigma_n\right|\delta_\theta}{\sqrt{\delta_t^2 + \delta_\theta^2}}, \tag{6-16b}$$

where δ_t and δ_θ are relative sliding displacements along the t and θ directions, respectively. Constraint conditions for the sliding contact are

$$\sigma_n^{(i)} = \sigma_n^{(j)} < 0, \quad \text{on } \partial R_{slide}. \tag{6-16c}$$

---

[1] In this study, the f is considered to be isotropic because the particle-filled thread composites in the pin and box regions are statistically homogeneous and isotropic.

In general, a combination of ∂R_{open}, ∂R_{stick}, and ∂R_{slide} constitutes the entire thread contact surface.

6.3.3 Interface Conditions

Basic equations given in Section 6.4.1 are for each composite ply and for the thread materials. Thus, solutions obtained for individual composite plies and for the threads have to satisfy continuity conditions along the interface. Since plies of the threaded composite joint are assumed to be perfectly bonded, the following displacement and traction continuity conditions along the interface need to be met:

$$\left.\begin{aligned} U^{(1)} = U^{(2)},\ V^{(1)} = V^{(2)},\ W^{(1)} = W^{(2)} \\ \sigma_n^{(1)} = \sigma_n^{(2)},\ \tau_{nt}^{(1)} = \tau_{nt}^{(2)},\ \tau_{n\theta}^{(1)} = \tau_{n\theta}^{(2)} \end{aligned}\right\} \text{ on } \Gamma_{int1}, \tag{6-17a}$$

$$\left.\begin{aligned} U^{(2)} = U^{(3)},\ V^{(2)} = V^{(3)},\ W^{(2)} = W^{(3)} \\ \sigma_n^{(2)} = \sigma_n^{(3)},\ \tau_{nt}^{(2)} = \tau_{nt}^{(3)},\ \tau_{n\theta}^{(2)} = \tau_{n\theta}^{(3)} \end{aligned}\right\} \text{ on } \Gamma_{int2}, \tag{6-17b}$$

$$\left.\begin{aligned} U^{(4)} = U^{(5)},\ V^{(4)} = V^{(5)},\ W^{(4)} = W^{(5)} \\ \sigma_n^{(4)} = \sigma_n^{(5)},\ \tau_{nt}^{(4)} = \tau_{nt}^{(5)},\ \tau_{n\theta}^{(4)} = \tau_{n\theta}^{(5)} \end{aligned}\right\} \text{ on } \Gamma_{int3}, \tag{6-17c}$$

$$\left.\begin{aligned} U^{(5)} = U^{(6)},\ V^{(5)} = V^{(5)},\ W^{(6)} = W^{(6)} \\ \sigma_n^{(5)} = \sigma_n^{(6)},\ \tau_{nt}^{(5)} = \tau_{nt}^{(6)},\ \tau_{n\theta}^{(5)} = \tau_{n\theta}^{(6)} \end{aligned}\right\} \text{ on } \Gamma_{int4}, \tag{6-17d}$$

where superscripts represent the corresponding plies in a threaded composite tubular joint (Fig. 6-3). The subscripts n, t, and θ denote normal, tangential, and circumferential directions of a ply interface.

6.4 Boundary-Value Problem for Threaded Composite Joint

In the context of nonlinear, anisotropic elasticity and contact mechanics, the boundary-value problem for a threaded composite joint under multiaxial loading may be written as follows:

$$\nabla \cdot \boldsymbol{\sigma} = \mathbf{0}, \quad \text{in } \Omega_{cb}, \Omega_{cp}, \Omega_{tb}, \text{ and } \Omega_{tp}, \tag{6-18a}$$

$$\boldsymbol{\varepsilon} = \tfrac{1}{2}\left(\nabla \mathbf{u} + (\nabla \mathbf{u})^T\right), \quad \text{in } \Omega_{cb}, \Omega_{cp}, \Omega_{tb}, \text{ and } \Omega_{tp}, \tag{6-18b}$$

$$\boldsymbol{\varepsilon} = \mathbf{S}(\tilde{\sigma})\,\boldsymbol{\sigma}, \quad \text{in } \Omega_{cb} \text{ and } \Omega_{cp}, \tag{6-18c}$$

$$\boldsymbol{\varepsilon} = \mathbf{S}^{*}\boldsymbol{\sigma}, \quad \text{in } \Omega_{tb}, \text{ and } \Omega_{tp}, \tag{6-18d}$$

$$\mathbf{N} \cdot \boldsymbol{\sigma} = \mathbf{t} \quad \text{on } \Gamma_0 \text{ to } \Gamma_5, \tag{6-18e}$$

$$\mathbf{u} = \bar{\mathbf{u}} \quad \text{on } \Gamma_6, \tag{6-18f}$$

$$\mathbf{N} \cdot \boldsymbol{\sigma}^j - \mathbf{N} \cdot \boldsymbol{\sigma}^i = \mathbf{0}, \quad \mathbf{u}^j - \mathbf{u}^i = \mathbf{0}, \quad \text{on } \Gamma_{interface}, \tag{6-18g}$$

$$\left.\begin{aligned} &(u_n^j - u_n^i - \delta_n) \geq 0, \quad \sigma_n \leq 0, \\ &(u_n^j - u_n^i - \delta_n)\,\sigma_n = 0, \\ &|\sigma_t| < -f\,\sigma_n, \quad \text{then } \delta_t = 0, \\ &|\sigma_t| = -f\,\sigma_n, \quad \text{then } \lambda \geq 0 \text{ s.t. } \delta_t = -\lambda\sigma_t, \end{aligned}\right\} \text{ on } \partial R_{open} \cup \partial R_{stick} \cup \partial R_{slide}, \quad (6\text{-}18h)$$

where Ω_{cb}, Ω_{cp}, Ω_{tb}, and Ω_{tp} in Eqs. (6-18a) to (6-18d) represent domains of the box, the pin, the box-side threads, and the pin-side threads, respectively.

The constitutive equations of a fiber-composite ply involving in-plane nonlinearity are given in Eq. (6-18c). Hooke's law for the threaded material is expressed by Eq. (6-18d). The interface $\Gamma_{interface}$ is between dissimilar materials. The expressions given in Eqs. (6-18h) are contact conditions along thread surfaces.

The external loading in the boundary value problem, as described in Section 6.5.1, is a combination of internal pressure, axial load, and make-up interference. The internal pressure and the axial load are applied to the joint as traction boundary conditions given in Eq. (6-18e). The make-up interference is introduced to the joint as a displacement mismatch δ_n along the contact surface $\partial R_{open} \cup \partial R_{stick} \cup \partial R_{slide}$ in Eq. (6-18h).

6.4.1 Uniqueness of Solutions

It is recognized that the boundary-value problem presented in the aforementioned Eqs. (6-18a) to (6-18h) involves two kinds of nonlinearity. The first is material nonlinearity of the fiber composite in the pin and box bodies. The second is traction nonlinearity along a thread contact surface. It is important at this point that the uniqueness of the solution for the nonlinear problem can be established first.

Consider an anisotropic, nonlinear elastic material R having shear nonlinearity in the 1-2 plane. Constitutive equations of the material are given as

$$\varepsilon_{ij} = \bar{S}_{ijmn}\,\sigma_{mn} + \frac{1}{2}\,(\delta_{i1}\delta_{j2} + \delta_{i2}\delta_{j1})\,\bar{S}^h_{66}\,\sigma^3_{12}, \quad (6\text{-}19)$$

where $\bar{S}_{ijmn}$ corresponds to linear material compliance and is positive-definite, and $\bar{S}^h_{66}$ is the high-order compliance.

Assume that the material is subjected to a prescribed traction $\mathbf{t}^a$ on ∂R_t, a displacement $\mathbf{u}^a$ on ∂R_u, and a body-force $\mathbf{f}$ in R. Then, the solutions should meet the equations given in Eq. (6-19) and the governing field equations,

$$\sigma_{ij,j} + f_i = 0 \qquad \text{in R}, \quad (6\text{-}20)$$

$$n_j\,\sigma_{ij} = t_i^a \qquad \text{on } \partial R_t, \quad (6\text{-}21)$$

$$u_i = u_i^a \qquad \text{on } \partial R_u. \quad (6\text{-}22)$$

If $(\sigma^{(1)}, \mathbf{u}^{(1)})$ and $(\sigma^{(2)}, \mathbf{u}^{(2)})$ are two different solutions and $\varphi^* = \varphi^{(1)} - \varphi^{(2)}$ is assumed for any φ, then one has

$$\sigma^*_{ij,j} = 0 \qquad \text{in R,} \tag{6-23}$$

$$n_j \sigma^*_{ij} u^*_i = 0 \qquad \text{on } \partial R^1, \text{ and} \tag{6-24}$$

$$\varepsilon^*_{ij} = \bar{S}_{ijmn} \sigma^*_{mn} + \frac{1}{2} (\delta_{i1}\delta_{j2} + \delta_{i2}\delta_{j1}) \bar{S}^h_{66} (\sigma^{(1)2}_{12} + \sigma^{(1)}_{12}\sigma^{(2)}_{12} + \sigma^{(2)2}_{12}) \sigma^*_{12}. \tag{6-25}$$

From Eq. (6-24), one has

$$0 = \int_{\partial R} n_j \sigma^*_{ij} u^*_i \, dS. \tag{6-26}$$

Using the divergence theorem, one obtains

$$\begin{aligned} &\int_{\partial R} n_j \sigma^*_{ij} u^*_i \, dS \\ &= \int_R (\sigma^*_{ij} u^*_i)_{,j} \, dV \\ &= \int_R (\sigma^*_{ij,j} u^*_i + \sigma^*_{ij} u^*_{i,j}) \, dV \\ &= \int_R \sigma^*_{ij} \varepsilon^*_{ij} \, dV \\ &= \int_R \{\sigma^*_{ij}\bar{S}_{ijmn}\sigma^*_{mn} + \bar{S}^h_{66} (\sigma^{(1)2}_{12} + \sigma^{(1)}_{12}\sigma^{(2)}_{12} + \sigma^{(2)2}_{12}) \sigma^{*2}_{12}\} \, dV = 0. \end{aligned} \tag{6-27}$$

Since $\left|\sigma^{(1)}_{12}\sigma^{(2)}_{12}\right| \le \frac{1}{2} (\sigma^{(1)2}_{12} + \sigma^{(2)2}_{12})$ and

$$\begin{aligned} \sigma^{(1)2}_{12} + \sigma^{(1)}_{12}\sigma^{(2)}_{12} + \sigma^{(2)2}_{12} &\ge \sigma^{(1)2}_{12} + \sigma^{(2)2}_{12} - \left|\sigma^{(1)}_{12}\sigma^{(2)}_{12}\right| \\ &\ge \sigma^{(1)2}_{12} + \sigma^{(2)2}_{12} - \frac{1}{2} (\sigma^{(1)2}_{12} + \sigma^{(2)2}_{12}) \\ &= \frac{1}{2} (\sigma^{(1)2}_{12} + \sigma^{(2)2}_{12}), \end{aligned} \tag{6-28}$$

one has $\sigma^{(1)2}_{12} + \sigma^{(1)}_{12}\sigma^{(2)}_{12} + \sigma^{(2)2}_{12} \ge 0$. Since $\bar{S}_{ijmn}$ is positive-definite and $\bar{S}^h_{66} \ge 0$, it follows that σ^*_{ij} vanishes throughout R. Consequently, ε^*_{ij} must vanish as well, whereas u^*_i may have, at most, the form of a rigid-body displacement.

Therefore, one concludes that solutions for stress and strain are unique in this

---

[1] From Eqs. (6-21) and (6-22), one has $n_j\sigma^*_{ij} = 0$ on ∂R_t and $u^*_i = 0$ on ∂R_u. Consequently, one has Eq. (6-24), provided that $\partial R = \partial R_t \cup \partial R_u$.

problem. The uniqueness of the displacement solution depends on having sufficient external constraints.

If there is a small difference in boundary conditions between Case 1 and Case 2, then Eq. (6-24) becomes

$$n_j \sigma_{ij}^* = t_i^{a*}, \qquad \text{on } \partial R_t, \tag{6-29a}$$

$$u_i^* = u_i^{a*} \qquad \text{on } \partial R_u. \tag{6-29b}$$

By assuming that

$$\left| n_j \sigma_{ij}^* \right| = \sqrt{n_j \sigma_{ij}^* n_k \sigma_{ik}^*} < M_1 \qquad \text{on } \partial R_u, \tag{6-30a}$$

$$\left| u_i^* \right| = \sqrt{u_i^* u_i^*} < M_2 \qquad \text{on } \partial R_t, \tag{6-30b}$$

where M_1 and M_2 are positive constants, one has

$$\int_R \{\sigma_{ij}^* \bar{S}_{ijmn} \sigma_{mn}^* + \bar{S}_{66}^h (\sigma_{12}^{(1)^2} + \sigma_{12}^{(1)}\sigma_{12}^{(2)} + \sigma_{12}^{(2)^2}) \sigma_{12}^{*2} \} \, dV$$
$$< M_1 \int_{\partial R_u} |\mathbf{u}^{a*}| \, dS + M_2 \int_{\partial R_t} \left| \mathbf{t}^{a*} \right| dS. \tag{6-31}$$

Consequently, one obtains

$$\lim_{|u^{a*}| + |t^{a*}| \to 0} \sigma_{ij}^* = 0 \ , \tag{6-32}$$

$$\lim_{|u^{a*}| + |t^{a*}| \to 0} \varepsilon_{ij}^* = 0. \tag{6-33}$$

Therefore, the solutions for stress and strain continuously depend upon the boundary conditions.

We remark here that the existence of a unique solution for a contact problem has been discussed by Oden, et al. [49] with a series of mathematical theorems. For the thread contact in a tubular joint discussed in this study, the existence and uniqueness of solutions, according to Oden, et al., are guaranteed.

6.4.2 Convergence of Solutions

In Eq. (6-6), shear deformation is expressed as a function of stress and experimental data can be used to determine the S_{66} and S_{66}^h well. Expressing the stresses as functions of strains and using the Taylor series expansion, one can rewrite Eq. (6-6) in term of ε_6 as

$$\sigma_6 = f(\varepsilon_6) = \frac{\varepsilon_6}{S_{66}} \sum_{n=0}^{\infty} A_n \left(\frac{S_{66}^h \varepsilon_6^2}{S_{66}^3}\right)^n, \tag{6-34}$$

where A_n are constants, with A_0=1, A_1=-1, A_2=3, A_3=-12, A_4=55 and A_5=189, etc. The convergence condition of Eq. (6-34) can be expressed as

$$\lim_{n \to \infty} \left| \frac{A_{n+1}}{A_n} \right| \left| \frac{S_{66}^h \varepsilon_6^2}{S_{66}^3} \right| < 1. \tag{6-35}$$

Limited numerical values of A_n show that

$$\left| \frac{A_{n+1}}{A_n} \right| \geq 1. \tag{6-36}$$

Therefore, one obtains

$$\varepsilon_6 < \sqrt{\frac{S_{66}^3}{S_{66}^h}}. \tag{6-37}$$

For the fiber composite system used in this study, the value of $\sqrt{S_{66}^3 / S_{66}^h}$ is 0.0105, which is below the shear failure strain of the glass/epoxy composite. Therefore, the radius of convergence of Eq. (6-34) may cause "collapse" in expressing the shear stress as a polynomial of shear strain.

6.4.3 Solution Procedure

Solving the boundary-value problem with the aforementioned material and traction nonlinearities in a closed analytical form is possible only in an extremely simple case, e.g., a long cylinder subjected to pure torsion. In most other cases, solutions for this class of boundary-value problems require an iterative numerical procedure in which such technique as the Newton-Raphson method needs to be employed.

Most theoretical studies [61,62] on finding deformation and contact force of elastic bodies under certain boundary (and loading) conditions are restricted to the special case in which no friction exists on the contact surface. In order to solve a contact mechanics problem with a finite frictional force on the contact surface, Oden, et al. [49] have proposed an iterative procedure. The procedure is based on a sequential-approximation approach. Two special cases have been investigated with success, (i) contact with a prescribed tangential stress, and (ii) contact with a prescribed normal stress along the boundary.

The numerical solution procedure for the present nonlinear contact problem is introduced with the following iterative steps:

1) Solve the special case (i) with an assumed tangential stress σ_t on the contact surface. As a result, the normal stress σ_n on the contact surface is also obtained.

2) Using the normal stress σ_n, one may solve the special case (ii). As a result, a new tangential stress σ_t is computed

3) Check the convergence of the solution. If the prescribed tolerance limit of convergence is not attained, repeat Steps (1) and (2).

Details of the numerical solution procedure are given in Section 8.

6.5 Remarks

6.5.1 Boundary-Value Problem

The boundary-value problem for a threaded composite joint subjected to multiaxial loading has been formulated in a cylindrical coordinate system involving only r and z. However, anisotropy of fiber composite properties leads to severe coupling between ply axial and shear deformations and, globally, coupling among extension, bending as well as twisting. Therefore the resulting deformations and stresses are inherently three dimensional.

Formulation of the threaded composite joint problem involves material nonlinearity and contact nonlinearity caused by thread surface closure and sliding. The uniqueness of the solution is shown to be guaranteed for the composite material system used in current study. Solving this class of boundary-value problems requires development of a new iterative solution procedure involving two kinds of iteration to account for both material nonlinearity and thread surface contact nonlinearity.

6.5.2 Material Nonlinearity of Fiber Composites

The nonlinear constitutive equations for fiber composites used in this study are first developed by Hahn and Tsai [30], based on the complementary energy density function expressed in a polynomial form proposed by Green, et al. [55]. Similar constitutive equations have also been obtained by Hashin, et al. [56], using the classical deformation plasticity approach. This kind of nonlinear shear response has been found for almost all composite systems [6, 43]. Accordingly, a general expression may be deduced from the complementary energy density function, yielding the commonly used power-law type constitutive relationship of the following form for fiber composites:

$$\varepsilon_6 = S_{66}\sigma_6 + S^h_{66}\sigma^3_6. \tag{6-38}$$

Note that Eq. (6-34) may be viewed as a truncated polynomial of the third order. The second-order terms are excluded because: (1) the complementary energy density function of a fiber composite is invariant [55], and (2) the material is indifferent to the change of direction of shear loading in the material symmetry plane of the composite.

It is also noted that the constitutive equation, Eq. (6-34), involves only physical (material) nonlinearity. Consideration of only the material nonlinearity (and neglecting the kinematic nonlinearity) has led to the development of a broad range of theory of physically nonlinear elasticity. This class of nonlinear mechanics theory has been used to address many important engineering problems in plasticity [57], fracture mechanics [58], and composites [5, 48].

Recent developments in finite elasticity [59,60] have shown that nonlinear elasticity, involving only physical nonlinearity, may have some shortcomings. For example, constitutive relations based on physically nonlinear elasticity do not consider the difference between Piola-Kirchkoff and Cauchy stresses [60], and the infinitesimal strain may not be invariant under superimposed finite rigid-body motions [59].

Following the common approach of finite elasticity, the second Piola-Kirchkoff stress of an elastic material may be expressed as an expansion of a function f(**E**), where **E** is a finite strain tensor, defined by

$$\mathbf{E} = \mathbf{e} + \frac{1}{2}\mathbf{H}^{\mathrm{T}}\mathbf{H}, \qquad \mathbf{e} = \frac{1}{2}(\mathbf{H}^{\mathrm{T}} + \mathbf{H}), \tag{6-39}$$

in which **H** is a displacement gradient, and **e** is the infinitesimal strain tensor. Assuming that f(**E**) is twice differentiable at **0**, one may express the second Piola-Kirchkoff stress $\mathbf{T}^{(s)}$ as

$$\mathbf{T}^{(s)} = \mathbf{L}(\mathbf{E}) + \mathbf{Q}(\mathbf{E}, \mathbf{E}) + o(|\mathbf{E}|^2), \tag{6-40}$$

where **L** and **Q** are fourth and sixth order tensors determined by f(**E**). Note that in physically nonlinear elasticity, deformations are assumed to be infinitesimal and no distinction is made among the Cauchy stress **T**, the first Piola-Kirchhoff stress $\mathbf{T}^{(p)}$ and the second Piola-Kirchhoff stress $\mathbf{T}^{(s)}$. Therefore, the stress $\mathbf{T}^{(pn)}$ in physically nonlinear elasticity is

$$\mathbf{T}^{(pn)} = \mathbf{L}(\mathbf{e}) + \mathbf{Q}(\mathbf{e}, \mathbf{e}) + o(|\mathbf{e}|^2). \tag{6-41}$$

The difference between the second Piola-Kirchkoff stress $\mathbf{T}^{(s)}$ obtained from finite elasticity and the stress $\mathbf{T}^{(pn)}$ from physically nonlinear elasticity is

$$\mathbf{T}^{(s)} - \mathbf{T}^{(pn)} = \frac{1}{2}\mathbf{L}(\mathbf{H}^{\mathrm{T}}\mathbf{H}) + o(|\mathbf{H}|^2). \tag{6-42}$$

Decomposing the displacement gradient **H** into symmetric and skew-symmetric parts, one has

$$\mathbf{H} = \mathbf{e} + \mathbf{w}, \tag{6-43}$$

where **w** is a rotational tensor expressed as

$$\mathbf{w} = \frac{1}{2}(\mathbf{H}-\mathbf{H}^T) = -\mathbf{w}^T. \tag{6-44}$$

Then, Eq. (6-42) may be expressed as

$$\mathbf{T}^{(s)} - \mathbf{T}^{(pn)} = \frac{1}{2}\mathbf{L}(\mathbf{e}^2 + \mathbf{ew} - \mathbf{we} - \mathbf{w}^2) + o(|\mathbf{H}|^2). \tag{6-45}$$

From Eq. (6-45), it is clear that the constitutive equations obtained from the physically nonlinear elasticity approach, Eq. (6-41), may not be comprehensive. Certain terms are not included when finite strains are considered, as shown in the results from finite elasticity, Eq. (6-40).

To illustrate this concern, consider the problem of an elastic solid under simple shear in which displacement components in a Cartesian coordinate system (X, Y, Z) in the reference configuration are

$$u_1 = 2\theta Y, \tag{6-46a}$$
$$u_2 = u_3 = 0, \tag{6-46b}$$

where the 2θ is the amount of the shear applied. From Eq. (6-45), the difference in stresses obtained from a finite elasticity approach and from the physically nonlinear elasticity approach may be determined as

$$T_{ij}^{(s)} - T_{ij}^{(pn)} = 2L_{ij22}\,\theta^2 + o(\theta^2). \tag{6-47}$$

From the above discussion, we remark that for a composite structure under large deformation, development of complete constitutive equations to account for both material and kinematic nonlinearities are needed (to include finite deformations and/or rotations in the formulation.)

At present, the property database of fiber composites under finite deformations does not exist. Including rotations **w** in the nonlinear constitutive relations also introduce practical difficulties in experiments, i. e., complexities in measuring the rotation **w**. While the physical nonlinear constitutive equation is recognized to have its short-comings for the composites under large deformations, the proposed physically nonlinear elasticity model is employed in the leakage failure study, since deformations in the composite joint remain small.

7. APPROXIMATE MODELS FOR OF THREADED COMPOSITE TUBULAR JOINTS

Except the few very simple cases discussed previously, solving the boundary-value problem formulated in Section 6 in a closed form could be difficult because of the complicated thread geometry and the material and contact nonlinearities involved. Since dimensions of the threads in a joint are much smaller than those of the tubular joint body, the boundary-value problem may be modeled on different scales (i.e., global and local) [14]. As will be shown later, modeling of a tubular composite joint can be greatly simplified on a global scale. Furthermore, coupling the global approach with a local model may provide an efficient and effective way to determine the complicated details of the nonlinear boundary-value problem.

Two distinct models are introduced in this section for analyzing a threaded composite joint, i.e., direct full-field model and coupled global-local model. Formulation of a direct full-field model is relatively straightforward, as compared to a coupled global-local model. However, details of local deformation and contact stress can only be obtained from the coupled global-local model, leading to a better understanding of the joint leakage failure problem. The objectives of the present efforts are to

1) develop a direct, full-field model and an accompanying analysis;

2) introduce a coupled global-local model for a threaded composite tubular joint;

3) formulate an "equivalent thread layer" to approximate the threads on the global scale for the coupled model;

4) establish governing equations for the coupled global-local model and develop an accompanying analysis.

7.1 Direct Full-Field Model

A straightforward approach to the threaded composite joint problem is to solve the boundary-value problem given in Eqs. (5-19a)-(5-19h) numerically. Various numerical methods could be used for this purpose. Direct discretization, i.e., full-field modeling, of the entire joint by a solid finite element method provides a direct solution for the problem. The full-field modeling and analysis should include the following features:

1) Anisotropic, nonlinear material properties of composite plies in both the pin and the box section.

2) Detailed geometric modeling of both pin-side and box-side threads.

3) Contact between thread surfaces and the effect of thread surface friction.

With the direct full-field model, deformations and stresses in the threads, along the thread contact surface, and in the tubular joint body may be obtained in one comprehensive analysis. However, costs of the analysis could be prohibitive and solution accuracy may not be easily established.

7.2 Coupled Global-local Model

In coupled global-local modeling, unique characteristics of a threaded composite tubular joint are recognized; i.e., the threads are dimensionally small and geometrically and mechanically complicated. The approach attempts to combine a detailed local formulation of the individual thread response with a global structural joint analysis. Thus, the boundary-value problem may be decomposed into two inter-related parts on two different (i.e., global and local) scales. The global-scale model concentrates on overall deformation of the threaded joint and provides proper input boundary conditions for a selected local domain with a substructure of a thread contact region. The local-scale analysis, however, focuses on detailed deformation and local stress concentrations in the threads and along the thread contact surface.

7.2.1 Assumptions and Approximations

In addition to the assumptions made in Section 6, the following approximations are introduced in the global-local modeling of the threaded joint.

1) In the global-scale model, the thread region in a tubular joint may be represented by an "equivalent thread layer", which will be discussed in the next section.

2) The "effective stiffness" of the equivalent thread layer is anisotropic and can be related to thread geometry and thread surface friction.

3) Effective stresses in threads may be evaluated in a selected domain with a substructure and boundary conditions determined from the global model.

A schematic of the coupled global-local model is given in Fig. 7-1. The detailed thread geometry needs not to be seen in the global-scale modeling, whereas on a local scale, detailed thread geometry is fully considered.

7.2.2 Formulation of Equivalent Thread Layer

In the global model, the overall deformation of a threaded tubular joint is of primary concern. Thus, all engaged threads in the joint may be represented by an "equivalent thread layer" with an "effective stiffness". The effective stiffness of this equivalent thread layer may be related to constitutive properties of the threads and individual thread geometry. Following the work of Bretl and Cook [12], the effective stiffness within the equivalent thread layer is formulated such that the layer

would not take the stress tangent to the "load-bearing plane". Therefore, the stiffness of the equivalent thread layer may be approximated by

$$\begin{Bmatrix} \sigma_{11} \\ \sigma_{22} \\ \sigma_{33} \\ \tau_{23} \\ \tau_{13} \\ \tau_{12} \end{Bmatrix} = \begin{bmatrix} 0 & 0 & 0 & 0 & 0 & 0 \\ 0 & C_{22} & C_{23} & 0 & 0 & 0 \\ 0 & C_{32} & C_{33} & 0 & 0 & 0 \\ 0 & 0 & 0 & 0 & 0 & 0 \\ 0 & 0 & 0 & 0 & C_{55} & 0 \\ 0 & 0 & 0 & 0 & 0 & 0 \end{bmatrix} \begin{Bmatrix} \varepsilon_{11} \\ \varepsilon_{22} \\ \varepsilon_{33} \\ \gamma_{23} \\ \gamma_{13} \\ \gamma_{12} \end{Bmatrix}, \tag{7-1}$$

where C_{ij} is elastic stiffness component of the equivalent thread layer. Here subscripts 1, 2, and 3 represent directions on the "load-bearing plane"; the 2 direction is normal to the plane, and 1 and 3 directions tangent to the plane with the 3 direction being coincident with the θ direction as shown in Fig. 7-2.

The load-bearing plane in an equivalent thread layer is defined and determined from thread geometry and thread contact conditions. If frictional force is neglected, the load-bearing plane is the physical surface of a thread. In the presence of frictional force, the load-bearing plane is defined to be perpendicular to the resultant of normal and frictional forces on a contact surface.

For a pair of threads illustrated in Fig. 7-2, the direction γ of the load-bearing plane for each contact case is defined as

$$\varepsilon_{AB} < 0 \qquad \begin{cases} \gamma_{ABDC} = \beta_1 + \alpha \\ \gamma_{ABFE} = \beta_2 - \alpha, \end{cases} \tag{7-2a}$$

$$\varepsilon_{AB} > 0 \qquad \begin{cases} \tau_{rz} > 0: \quad \gamma_{ABDC} = \gamma_{ABFE} = \beta_1 - \alpha \\ \tau_{rz} < 0: \quad \gamma_{ABDC} = \gamma_{ABFE} = \beta_2 + \alpha, \end{cases} \tag{7-2b}$$

where ε_{AB} is an average strain through the thickness direction of the equivalent thread layer; τ_{rz} is the shear stress at B; and γ_{ABDC} and γ_{ABFE} are directions of the load bearing planes in ABDC and ABFE, respectively. The angle of friction α is defined as

$$f = \tan \alpha, \tag{7-3}$$

where f is a frictional coefficient.

We note that the ε_{AB} in Eqs. (7-2a) and (7-2b) indicates the contact situation between threads. The conditions represented by Eq. (7-2a) are for the case that both

load and stab flanks of a thread are in contact, which is important in joint sealing. Equation (7-2b), however, represents the case of a single thread surface contact. Equations (7-2a) and (7-2b) are unique for the threaded tubular joint problem, which generally has a taper along the joint axis, and both thread flanks in contact are physically feasible.

7.2.3 Governing Equations for Global-Scale Model

In the global-scale model of a threaded composite joint with an effective thread layer, the governing equations for the problem may be stated as follows:

$$\nabla \cdot \boldsymbol{\sigma} = \mathbf{0}, \quad \text{in } \Omega_{cb}, \Omega_{cp}, \Omega_t, \tag{7-4a}$$

$$\boldsymbol{\varepsilon} = \frac{1}{2}(\nabla \mathbf{u} + (\nabla \mathbf{u})^T), \quad \text{in } \Omega_{cb}, \Omega_{cp}, \text{ and } \Omega_t, \tag{7-4b}$$

$$\boldsymbol{\varepsilon} = \mathbf{S}(\bar{\sigma})\,\boldsymbol{\sigma}, \quad \text{in } \Omega_{cb} \text{ and } \Omega_{cp}, \tag{7-4c}$$

$$\boldsymbol{\sigma} = \bar{\mathbf{C}}\,\boldsymbol{\varepsilon}, \quad \text{in } \Omega_t, \tag{7-4d}$$

$$\mathbf{N} \cdot \boldsymbol{\sigma} = \mathbf{t} \quad \text{on } \Gamma_0 \text{ to } \Gamma_5, \tag{7-4e}$$

$$\mathbf{u} = \bar{\mathbf{u}} \quad \text{on } \Gamma_6, \tag{7-4f}$$

$$\mathbf{N} \cdot \boldsymbol{\sigma}^j - \mathbf{N} \cdot \boldsymbol{\sigma}^i = \mathbf{0}, \quad \mathbf{u}^j - \mathbf{u}^i = \mathbf{0}, \quad \text{along } \Gamma_{interface}, \tag{7-4g}$$

where Ω_{cb}, Ω_{cp}, and Ω_t in Eqs. (7-4a)--(7-4d) represent domains of the box, the pin, and the thread layer, respectively. Constitutive equations for a fiber composite lamina, involving the in-plane nonlinearity, are given in Eq. (7-4c). Elastic stiffness of an equivalent thread layer in the joint is given in Eq. (7-4d) with detailed formulation expressed in Eq. (7-1). The $\Gamma_{interface}$ represents an interface between dissimilar materials. The loading boundary conditions, as described in Section 5, are combined internal pressure, axial load, and make-up interference.

7.2.4 Governing Equations for Local-scale Model

The local model requires a detailed description of each thread geometry and involves complex nonlinear contact mechanics formulation of thread engagement. The local modeling is conducted for selected domains, as shown in Fig. 7-3, much smaller than those in the full-field analysis. The boundary conditions in the local model are interpreted from the resulting displacement solution for a global model. The boundary-value problem for the local model is given as follows:

$$\nabla \cdot \boldsymbol{\sigma} = \mathbf{0}, \quad \text{in } \Omega^*_{cb}, \Omega^*_{cp}, \Omega_{tb}, \text{ and } \Omega_{tp}, \tag{7-5a}$$

$$\boldsymbol{\varepsilon} = \frac{1}{2}(\nabla \mathbf{u} + (\nabla \mathbf{u})^T), \quad \text{in } \Omega^*_{cb}, \Omega^*_{cp}, \Omega_{tb}, \text{ and } \Omega_{tp}, \tag{7-5b}$$

$$\boldsymbol{\varepsilon} = \mathbf{S}(\bar{\sigma})\,\boldsymbol{\sigma}, \quad \text{in } \Omega^*_{cb} \text{ and } \Omega^*_{cp}, \tag{7-5c}$$

$$\boldsymbol{\varepsilon} = \mathbf{S}^*\boldsymbol{\sigma}, \quad \text{in } \Omega_{tb}, \text{ and } \Omega_{tp}, \tag{7-5d}$$

$$\mathbf{u} = \bar{\mathbf{u}} \quad \text{on } \Gamma^*, \tag{7-5e}$$

$$\mathbf{N} \cdot \boldsymbol{\sigma}^j - \mathbf{N} \cdot \boldsymbol{\sigma}^i = \mathbf{0}, \quad \mathbf{u}^j - \mathbf{u}^i = \mathbf{0}, \quad \text{along } \Gamma_{interface}, \tag{7-5f}$$

$$\left.\begin{aligned} &(u_n^j - u_n^i - \delta_n) \geq 0, \quad \sigma_n \leq 0, \\ &(u_n^j - u_n^i - \delta_n)\,\sigma_n = 0, \\ &|\sigma_t| < -f\,\sigma_n, \quad \text{then } \delta_t = 0, \\ &|\sigma_t| = -f\,\sigma_n, \quad \text{then } \lambda \geq 0 \text{ s.t. } \delta_t = -\lambda\sigma_t, \end{aligned}\right\} \text{ on } \partial R_{open} \cup \partial R_{stick} \cup \partial R_{slide}, \quad (7\text{-}5g)$$

where Ω^*_{cb} and Ω^*_{cp} in Eqs. (7-5a) to (7-5d) represent the selected local domains with detailed substructures. The Ω_{tb} and Ω_{tp} are local domains of pin-side and box-side threads, respectively Constitutive equations for a composite ply involving the aforementioned material nonlinearity are given in Eq. (7-5c). Hooke's laws for threaded materials are expressed in Eq. (7-5d). The interface $\Gamma_{interface}$ is between two different materials. The expressions given by Eq. (7-5g) are contact conditions along a thread surface. Loading conditions for the local model are prescribed displacements along the boundary Γ^*, which are obtained from the global model.

7.2.5 Remarks on Coupled Global-local Model

The coupled global-local model for a threaded composite tubular joint contains two boundary-value problems formulated on different scales. The local-scale modeling is generally well-defined and its details are almost identical to the one described in Section 6. The solution for the local model may be obtained by the same procedure described in the last section.

The equivalent thread layer conditions, Eqs. (7-2a) and (7-2b), developed in this study extend the work of Bretl, et al. [12], to account for the unique feature of both thread surfaces in contact in a threaded tubular joint . These expressions are more comprehensive than Bretl's model. By replacing the engaging threads with an equivalent thread layer, the global-scale model does not involve the thread-contact details. Therefore, its numerical details are much simpler than those of the direct full-field modeling. The global-scale model is effective, especially when overall structural deformations of a threaded tubular joint are of interest. The two-scale model is computationally efficient and operationally simple to address the complex composite threaded joint problem.

8. LEAKAGE FAILURE CRITERIA FOR THREADED COMPOSITE TUBULAR JOINTS

To predict accurately the leakage failure in a threaded composite tubular joint, different failure modes must be identified first and associated leakage failure criteria need to be properly established. In this section, the commonly observed leakage failure modes and associated failure criteria are addressed for a threaded composite joint under combined internal pressure, axial load and make-up interference.

8.1 Leakage Failure of Fiber-composite Tube Body

Leakage of a fiber-composite tube body is commonly associated with formation of through-thickness, interconnected ply transverse cracks[1] [5, 6]. Formation and growth of the interconnected cracks are mainly caused by low matrix-dominated, transverse and shear strengths of a fiber composite. To predict the transverse cracks in a tubular composite, detailed transverse normal and shear deformations at the ply level need to be accurately evaluated. In this study, the physical-mechanism-based composite ply failure criteria are used to determine the ply cracking in a composite laminate tube body. For the glass/epoxy composite used in the study, the following failure criteria are employed:

$$\text{Transverse cracking (tensile):} \quad \varepsilon_{22} \geq \varepsilon_{22f}^{(T)}, \tag{8.1a}$$

$$\text{Transverse cracking (compressive):} \quad \pm\varepsilon_{22} \geq \varepsilon_{22f}^{(C)}, \tag{8.1b}$$

$$\text{Ply shear failure:} \quad \left|\gamma_{12}\right| \geq \gamma_{12f}, \tag{8.1c}$$

where $\varepsilon_{22f}^{(T)}$, $\varepsilon_{22f}^{(C)}$ and γ_{12f} are transverse tensile, compressive and shear failure strains of the hoop-wound glass/epoxy composite, respectively.

8.2 Leakage Failure of Composite Threads and Thread-tube Interface

Thread failure may also cause leakage in the threaded composite joint. A common form of the thread failure is fracture of the thread material when local stress concentrations reach a critical value (i.e., strength). The other possible form of thread failure is due to reduction of thread height, usually caused by repeated make-up and break-out, which are not considered in the present study.

Leakage has also been observed as a result of debonding of the thread-tube body

---

[1] This is true only for the case of a fiber composite laminate tube containing a brittle liner or without a liner. For a fiber composite laminate tube with a ductile liner, burst failure commonly occurs due to fiber-dominated ply fracture.

interface. Unlike a threaded metal tubular joint, threads in a fiber composite tubular joint are usually molded on the composite tube body. Bond failure at the interface between the molded threads and the tube body may occur due to high interfacial stresses and low interfacial strength. The experimental study, which will be discussed later, shows that interface failure in a threaded composite tubular joint can be a major failure mode in joint leakage.

Since the thread materials and the molded interface both consist of highly crosslinked thermoset polymers with particulate reinforcements, the following brittle strength criteria are used to assess their failure:

$$\text{Thread failure:} \quad \sigma_I \geq \sigma_f^t \quad \text{for} \quad \sigma_I > 0, \tag{8-2a}$$

$$\left|\sigma_{III}\right| > \sigma_f^c \quad \text{for} \quad \sigma_{III} < 0, \tag{8-2b}$$

$$\text{Interface failure:} \quad \left|\tau_{12}^{(i)}\right| \geq \tau_{12f}^{(i)}, \tag{8-2c}$$

where σ_I and σ_{III} are principal stresses in a thread; σ_f^t and σ_f^c are the tensile and compressive strengths of the thread material, and $\tau_{12f}^{(i)}$ is the interfacial shear strength.

8.3 Sealing Failure Along Thread Contact Surface

A threaded composite joint may lose its sealing integrity even without any matrix cracking, when the fluid leaks through the thread contact surface. Understanding of this leakage mechanism requires detailed information of the thread surface pressure distribution during thread contact in the joint.

8.3.1 Sealing Along Thread Contact Surface

In the threaded composite joint considered, thread-to-thread sealing may be achieved, provided certain conditions[1] can be met. A key step to achieve the sealing integrity is to ensure an appropriate level of bearing pressure along the thread contact surface by a proper make-up. Theoretically, the higher the bearing pressure, the better the joint is sealed. However, a high bearing pressure is usually accompanied by large mechanical deformations in the threads and, consequently, may cause local thread damage. An optimal thread bearing pressure may be achieved by introducing a proper make-up interference into a joint under a combined internal pressure and axial load without damaging the joint. Therefore, establishment of a quantitative relationship between thread bearing pressure and the applied external loading is essential in designing

---

[1] These conditions may include:
1) Proper thread cleaning eliminates dirt or other foreign materials which may interfere with mating of thread surfaces.
2) Solid-bearing thread compounds, applied to the threads, fill the small (< 0.002 inch) clearance between crests and roots of the threads.
3) A proper assembly interference is introduced to provide enough bearing pressure between thread surfaces.

a leakage-free threaded joint.

8.3.2 Relationship Between Leakage Pressure and Thread-surface Bearing Pressure

Establishing a proper relationship in an analytical form between the applied internal pressure and the thread-surface bearing pressure to achieve pressure sealing is difficult, because of complexities associated with surface sealing mechanisms, especially when the surface is not perfectly smooth. The basic sealing principle [15] developed earlier for a metallic joint requires that the bearing pressure P_B must exceed the internal pressure P_i. This is a straightforward, minimum requirement in static balance to achieve a reliable sealing[1] and is expressed as

$$P_B > P_i \tag{8-3}$$

To quantify the sealing capability of a threaded joint, a leakage tightening factor, $\tilde{X}$ may be introduced, where $\tilde{X}$ is the ratio of contact (bearing) pressure to internal pressure in a joint at onset of leakage. Based on the minimum bearing-pressure requirement for sealing, Eq. (8-3), the leakage tightening factor $\tilde{X}$ must be greater than one. Owing to many uncertainties, such as surface roughness, involved in manufacturing and joint surface preparation, sealing capabilities may be different for two joints subjected to the same make-up and external loading.

Thus, it is appropriate to define a joint tightening factor X, which basically is a safety factor, relating the contact pressure to the internal pressure in order to achieve a leak-free joint. The joint tightening (safety) factor accounts for the joint sealing variability and provides a proper criterion for a leakage-free joint design. The joint tightening (safety) factor X should be greater than the leakage tightening factor $\tilde{X}$ with a certain degree of confidence. Obviously, accurate determination of the joint tightening (safety) factor requires a systematic investigation[2].

The level of the tightening (safety) factor reflects an allowable leakage probability, as shown in Fig. 8-1. The lower the leakage probability is allowed, the higher the tightening safety factor is required. When a bearing pressure is less than the

---

[1] Systematic experiments have been conducted by Buchter [50] to study the sealing behavior of a bolted steel flange joint. Several important observations relevant to the current study are:
1) The relationship between leakage internal pressure and contact pressure is linear, when a contact surface is very smooth.
2) The roughness of a contact surface can influence the joint sealing. (A well-polished surface provides better sealing than a rough surface.)
3) The viscosity of the oil applied on a sealing surface has a significant influence on sealing. (An oil with a higher viscosity provides better sealing, especially on a rough surface.)
4) The viscosity of the pressure medium used also influences the joint sealing. (A higher contact pressure is required to seal a pressure medium with a lower viscosity.)

[2] Buchter [50] has suggested the following criteria for selecting the joint tightening (safety) factor X for determining contact pressure in a leak-free *steel bolted flange* joint:
1) X=1.5 for static pressure up to 14 ksi and a joint diameter not exceeding 2 inches.
2) X=2.0 for pressures up to 28 ksi and a joint diameter larger than 2 inches.
3) X>2.0 for pressure greater than 28 ksi.

product of internal pressure and tightening safety factor, the leakage probability increases. The leakage probability is equal to one, theoretically, when a bearing pressure is equal to the internal pressure. Based on the leakage probability consideration, three regions may be defined in Fig. 8-1 for different levels of bearing pressure P_B as

$$\text{Leak region:} \quad 0 < P_B < P_i ,$$
$$\text{Leak-prone region:} \quad P_i < P_B < XP_i ,$$
$$\text{Leak-free region:} \quad XP_i < P_B .$$

In the leak region, the leakage probability is high, say 99%, which means that, in most cases, a bearing pressure is not enough to provide sealing. In the leak-free region, the leakage probability is required to be very low, e.g., 0.0005%, as suggested by the API [44]. The leak-prone region is a transitional region, in which the bearing pressure may or may not be enough to hold the pressure medium inside the joint.

8.4 Leakage Failure Criteria for Threaded Composite Tubular Joints

Based on the aforementioned discussion, the following leakage failure criteria are introduced in the leakage analysis of a threaded composite tubular joint subjected to complex external loading:

1) Joint leakage, if $P_B < P_i$.

2) Joint leakage, if a through-thickness crack is developed in a composite tube body, i.e., Eq. (8-1).

3) Joint leakage, if thread fracture or debonding along the thread-tube interface occurs, i.e., Eqs. (8-2a) to (8-2c).

4) Joint leakage free, if $XP_i < P_B$.

Based on the aforementioned criteria, a schematic leakage-failure envelope (Fig. 8-2) may be constructed for a threaded composite joint under a combined axial loading, internal pressure and makeup. Different regions under the leakage envelope correspond to different governing leakage failure modes. Leak, leak-prone, and leak-free regions are determined, based on the ratio of bearing pressure to internal pressure for the cases caused by loss of bearing pressure. Allowable loads for a reliable threaded composite tubular joint should fall in the leak-free region.

8.5 Remarks

The mechanism-based failure criteria introduced in this study distinguish different modes of leakage failure in a threaded composite joint. In the case of leakage caused by loss of bearing pressure, uncertainties involved in sealing between thread contact surfaces are taken into account by introducing a tightening (safety) factor, and

the leakage probability can be determined accordingly. The leakage failure envelope introduced here contains regions governed by the stiffness of a composite joint and a region governed by the strength of the fiber-composite material. In the strength-dominated failure region, the leakage may be determined by proper use of damage and failure mechanics, whereas in the stiffness-dominated regions, the present contact mechanics and failure theories can only provide a range where leakage may occur because of the uncertainties involved.

Note also that the leakage failure criteria developed in the study are valid only for a threaded fiber-composite joint with a brittle matrix and brittle threads, in which transverse (matrix) cracking governs the leakage failure. For a threaded composite joint with a ductile matrix, other mechanisms of damage may occur and, consequently, different leakage failure criteria may be required.

9. NUMERICAL METHODS FOR LEAKAGE FAILURE ANALYSES OF THREADED COMPOSITE JOINTS

As indicated in Section 6, deformations and stresses in a threaded composite tubular joint are inherently three-dimensional with all six components of stresses (and strains) in existence simultaneously. For the threaded composite tubular joint under complex combined loading, the aforementioned thread and joint geometry, lamination variables, and nonlinear material constitutive properties make the boundary-value problem extremely complicated. The progressive damage in the fiber composite in a joint and the unknown surface contact in the threads introduce such mathematical complications that generally prevent one from obtaining a closed-form solution. Thus, proper advanced numerical methods must be used.

Among various commonly used numerical methods, the well-known finite element method is considered here because of its flexibility in handling complicated geometry for solid modeling, loading and boundary conditions, and the unique nonlinear material constitutive equations. Obviously, conventional axisymmetric finite element formulation for an isotropic material is not adequate for the present problem. A quasi-three dimensional formulation, based on generalized plane deformation theory of anisotropic solids, needs to be developed for the present threaded composite tubular joint leakage problem.

We note here again that the numerical method for analyzing the leakage failure of a threaded composite joint must be able to include the important issues of material nonlinearity, thread surface contact, different modes of failure, and progressive damage of tube bodies, threads and the thread/tube body interface. All of these complications warrant the present development of accurate and efficient numerical methods in this study.

9.1 Nonlinear Finite Element Method for Analysis of Threaded Composite Joint

9.1.1 Formulation of Generalized Plane Elements

As discussed in Section 6, all field variables in the basic equations for a threaded composite joint are functions of r and z only. Following the standard displacement-based element formulation, one may express element displacements, U(r,z), V(r,z) and W(r,z), as

$$\begin{aligned} U &= \sum_{i=1}^{p} N_i(r,z)\, U_i \,, \\ V &= \sum_{i=1}^{p} N_i(r,z)\, V_i \,, \\ W &= \sum_{i=1}^{p} N_i(r,z)\, W_i \,, \end{aligned} \tag{9-1}$$

where N_i are shape functions; n is the number of nodes in an element, and U_i, V_i, and W_i are displacement components at the i-th node.

In this study, eight-node isoparametric ring elements are formulated. The N_i are standard quadratic interpolation functions [52]. Equation (9-1) may be expressed in a matrix form as

$$\{\mathbf{u}\} = [\mathbf{N}]\,\{\mathbf{q}^e\}\,, \tag{9-2}$$

where $\{\mathbf{u}\}$ are element displacements; $[\mathbf{N}]$, shape functions; and $\{\mathbf{q}^e\}$, element nodal displacements.

Applying the strain-displacement relationship Eq. (5-4), one may express the element strains $\{\varepsilon\}$ in term of $\{\mathbf{q}^e\}$, i.e.,

$$\{\boldsymbol{\varepsilon}\} = [\mathbf{B}]\{\mathbf{q}^e\}, \tag{9-3a}$$

where

$$[\mathbf{B}] = [\partial][\mathbf{N}]\,, \tag{9-3b}$$

$$[\partial] = \begin{bmatrix} \frac{\partial}{\partial r} & 0 & 0 \\ \frac{1}{r} & 0 & 0 \\ 0 & 0 & \frac{\partial}{\partial z} \\ 0 & \frac{\partial}{\partial z} & 0 \\ \frac{\partial}{\partial z} & 0 & \frac{\partial}{\partial r} \\ 0 & \frac{\partial}{\partial r} - \frac{1}{r} & 0 \end{bmatrix}. \tag{9-3c}$$

The compliance of a unidirectional composite is given by

$$[\bar{S}] = \begin{bmatrix} \bar{S}_{11} & \bar{S}_{12} & \bar{S}_{12} & & & \\ \bar{S}_{12} & \bar{S}_{22} & \bar{S}_{23} & & & \\ \bar{S}_{12} & \bar{S}_{23} & \bar{S}_{22} & & & \\ & & & 2(\bar{S}_{22}-\bar{S}_{23}) & 0 & 0 \\ & & & 0 & \bar{S}_{66} & 0 \\ & & & 0 & 0 & \bar{S}_{66}+\bar{S}^h_{66}\sigma_6^2 \end{bmatrix}. \tag{9-4}$$

Note that in Eq. (9-4), the nonlinear shear compliance $(\bar{S}_{66} + \bar{S}^h_{66}\sigma_6^2)$ is a function of σ_6.

Using the minimum potential energy theorem, one may establish the following global equilibrium equations for the problem:

$$[\mathbf{K}]\{\mathbf{q}\} = \{\mathbf{Q}\}, \tag{9-5}$$

where $[\mathbf{K}]$ is the global stiffness matrix; $\{\mathbf{q}\}$, global nodal displacements; and $\{\mathbf{Q}\}$, equivalent nodal forces. The stiffness matrix and the equivalent load are

$$[\mathbf{K}] = \sum \int_V [\mathbf{B}]^T [\mathbf{C}(\tilde{\varepsilon})][\mathbf{B}]\, r dr dz, \tag{9-6a}$$

$$\{\mathbf{Q}\} = \sum \int_s [\mathbf{N}]^T \{\mathbf{p}^{(e)}\}\, r dl. \tag{9-6b}$$

In Eqs. (9-6a)-(9-6b), $\{\mathbf{p}^{(e)}\}$ is an element loading vector, and $[\mathbf{C}(\tilde{\varepsilon})]$ is a nonlinear material stiffness matrix in the physical coordinates of the joint.

9.1.2 Lagrangian Multiplier for Thread Surface Contact

Accurate determination of bearing pressure on a thread surface is critical in the leakage analysis of a threaded joint. Proper formulation of a thread contact problem requires the constraint conditions in Eqs. (6-15a)-(6-17b) be imposed along the thread surface when different contact situations occur.

Along a surface with no thread contact, applying the traction-free boundary conditions is trivial. However, on a contact surface, the constraints imposed by Eqs. (6-16a) and (6-17a) may not be straightforward in the element formulation. A numerical procedure, which is generally very involved, requires a continuous change in degrees of freedom of active nodes during the incremental/iteration steps. This is especially true when the contact surface configuration and associated tractions change continuously during loading and unloading. In this study, an efficient procedure, based on the well-known Lagrangian-multiplier technique is introduced. For illustration, consider the sticking contact of a thread surface with the constraint condition Eq. (6-17a). The term, $\lambda(U_n^{(j)} - U_n^{(i)} - \delta_n)^2$, is added to the potential energy functional of the system, where λ is the Lagrangian multiplier. Minimizing the functional, one may obtain the following constraint conditions, containing $U_n^{(i)}$ and $U_n^{(j)}$, in addition to the equilibrium equations Eq. (9-5):

$$\begin{bmatrix} \lambda & -\lambda \\ -\lambda & \lambda \end{bmatrix} \begin{Bmatrix} U_n^{(j)} \\ U_n^{(i)} \end{Bmatrix} = \lambda \begin{Bmatrix} \delta_n \\ -\delta_n \end{Bmatrix}, \tag{9-7}$$

where $U_n^{(i)}$ and $U_n^{(j)}$ are nodal displacements, and δ_n, the make-up interference. Examining the left side of Eq. (9-7), one finds that it has a form similar to the equilibrium of a bar element. Therefore, the Lagrangian multiplier method used for the thread contact problem is equivalent to imposing a zero-length "bar" element with a stiffness λ connecting the i-th and j-th nodes along the normal on the contact surface. An obvious advantage of using the Lagrangian multiplier is that no change in degrees of freedom of

active nodes in the contact region is required during numerical iteration. Thus, computationally, modifications of the global stiffness matrix can be minimal in the contact analysis.

9.1.3 Incremental-iterative Procedure for Material Nonlinearity

The global equilibrium equations Eq. (9-5) are nonlinear since the element stiffness matrix Eq. (9-6c) involves composite stresses. Solving the equations requires a numerical incremental iterative procedure, as shown schematically in Fig. 9-1. During computation, nodal displacements $\underset{\sim}{u}_m^{(k)}$ in the m-th iteration are calculated at the k-th step loading $\underset{\sim}{Q}^{(k)}$ as follows:

$$\underset{\sim m+1}{\mathbf{u}}^{(k)} = \underset{\sim}{\mathbf{K}}_m^{-1} \underset{\sim}{\mathbf{Q}}^{(k)}, \tag{9-8}$$

where $\underset{\sim}{K}_m$ is a nonlinear stiffness matrix at the load level $\underset{\sim}{Q}^{(k)}$.

Convergence of the solution requires that $\left|(\underset{\sim}{u}_m^{(k)} - \underset{\sim}{u}_{m+1}^{(k)}) / \underset{\sim}{u}_m^{(k)}\right| \le \gamma$, where γ is a prescribed tolerance limit and is taken as 3% in this study.

9.1.4 Iterative Procedure for Thread Surface Contact

An iterative procedure is also necessary to address the thread contact problem because of the load-dependent contact surface conditions. In the finite element formulation, surface traction and deformation of contact along a thread surface is related to nodal variables. The iterative procedure involves the following steps:

1) Assume an initial contact area along the thread surface.

2) Apply proper contact conditions, and solve approximate equilibrium equations.

3) Check constraint conditions along the contact surface. If the conditions are inconsistent with the assumed contact configuration, then update the contact surface conditions, and return to Step 2.

4) Check the solution convergence. If the updated solution meets the prescribed convergence criterion, the load level is increased and return to Step 1. Otherwise, return to Step 2.

9.1.5 Numerical Scheme for Progressive Damage in a Threaded Joint

Three kinds of damage modes leading to leakage failure in a threaded composite joint are considered in the present study: thread fracture, thread-tube interface debonding, and ply cracking in the composite tube body. The composite damage degrades material properties, affects deformations and redistributes the stress in a joint. The magnitudes and states of the stresses in individual plies and threads at a given load

level are critical in assessing the damage evolution. To study the leakage failure modes and the corresponding damage progression in the joint[1] , the local failure criteria discussed in Section 8 are introduced and proper numerical algorithms are developed here.

1) Thread fracture

The materials used in the (pin-side) threads are identified as epoxy filled with quartz particulates, and epoxy with graphite flakes (box-side). Elastic properties of the thread composite materials are determined by micromechanics theories. Principal stresses at Gaussian stations in each element in the threads are checked against the brittle failure criteria given in Section 8. If a thread fracture is identified, the stiffness of the thread element is degraded to zero at the Gaussian point and the incremental procedure continues.

2) Thread-tube body interface debonding

To develop the numerical algorithm for the thread-tube body debonding the interface failure criterion given in Section 8 is used. Along the debonded interface, tractions varnish and the stiffness matrix (in local coordinates) at the Gaussian point near the interface of the tube-body element (Fig. 9-2) is modified as

$$[\tilde{C}] = \begin{bmatrix} 0 & 0 & 0 & 0 & 0 & 0 \\ 0 & \tilde{C}_{22} & \tilde{C}_{23} & \tilde{C}_{24} & 0 & 0 \\ 0 & \tilde{C}_{32} & \tilde{C}_{33} & \tilde{C}_{34} & 0 & 0 \\ 0 & \tilde{C}_{42} & \tilde{C}_{43} & \tilde{C}_{44} & 0 & 0 \\ 0 & 0 & 0 & 0 & 0 & 0 \\ 0 & 0 & 0 & 0 & 0 & 0 \end{bmatrix}, \tag{9-9}$$

where $\tilde{C}_{ij}$ represent composite stiffness components in the interfacial coordinates 1-2-3.

3) Composite tube body damage

In the case of leakage caused by ply cracking in a fiber composite tube body, the mechanism-based failure criteria, Eqs. (8-1a) to (8-1c), are employed. Material degradation associated with the ply damage requires instantaneous unloading and the composite with ply cracking is assumed to partially lose its partial load-bearing capacity. The stiffness matrix at a Gaussian point in the material coordinate system in a degraded element is changed to

---

[1] Wear of the pin threads is a potential problem, but it is not included in the study.

$$[\bar{C}] = \begin{bmatrix} \bar{C}_{11} & 0 & \bar{C}_{13} & & & \\ 0 & 0 & 0 & & & \\ \bar{C}_{13} & 0 & \bar{C}_{33} & & & \\ & & & 0 & 0 & 0 \\ & & & 0 & \bar{C}_{55} & 0 \\ & & & 0 & 0 & 0 \end{bmatrix}. \quad (9\text{-}10)$$

The following incremental-iterative solution procedure is introduced to determine the tube-body damage:

1) At a given load, global equilibrium equations for the entire joint are calculated with degraded material stiffness matrices in damaged elements.

2) The global nonlinear equilibrium equations are solved with an iteration procedure given in Sections 9.1.3. and 9.1.4 to include the material nonlinearity and thread contact.

3) Local stresses and strains are then determined in each element and along the thread-tube interface in the thread joint.

4) Stresses and strains are examined at each Gaussian point in all elements and along the thread-tube interface, and checked against the failure criteria.

5) If new damage is initiated, the loading is kept unchanged. An updated damage zone and failure modes are introduced, and the computation returns to Step. 1. Otherwise, a load increment is introduced and the procedure will continue from Step 1.

9.1.6 Numerical Procedure for Leakage Analysis

To predict the leakage onset, detailed stresses and deformations in the entire joint need to be obtained, and failure modes and damage evolution have to be determined at each load level. The efficiency and accuracy of the solutions have a direct consequence on the leakage failure prediction. The proposed iterative-incremental procedure can be accomplished within a computational loop with its exit being controlled by the following conditions:

1) The difference in deformation solutions between two iteration steps is within a prescribed tolerance limit (e.g., 3%).

2) Along all possible contact surfaces, contact surface configurations must be compatible with the corresponding constraint conditions.

3) The difference in bearing pressure along a contact surface between two iteration steps is small.

The solution procedure is terminated when a prescribed load is reached or when the leakage failure criteria are met. A flow chart of the incremental-iterative algorithm for analyzing and predicting the joint leakage problem is given in Fig. 9-3.

We note here that the present solution procedure combines numerical iterations for material nonlinearity and thread contact into one with multiple convergence conditions. This procedure greatly reduces the number of iterations during computation and expedites the incremental solution scheme.

9.1.7 Solution Accuracy and Convergence

To make efficient use of the computer memory, a one-dimensional storage technique with a variable semi-bandwidth is used. Equilibrium equations are solved by the well known Cholesky method. All real variables in the program are operated with double precision.

To check accuracy of the formulation and numerical algorithm, comparisons of the results with existing reference solutions are made. The first is on stresses in a linear glass-fiber composite tubing under a given internal pressure. The following geometry of the composite tubing and its material properties are used:

I.D. = 2.0 inches;	O.D. = 2.4 inches;	Tube length = 5.0 inches.
Ply fiber orientations:	$[+55^{o} / -55^{o}]_{s}$;	Internal pressure = 100 psi;
Composite ply properties:	E_{11}=6.53 Msi;	$E_{22}=E_{33}$=1.74 Msi.
	υ_{12}=0.28;	G_{23}=0.8 Msi.

In the analysis, the axial displacement W and the circumferential displacement V at one tube end are fixed, and free at the other end. One element per ply along the tube thickness direction is used. The stress solution at a distance 2.5 inches from the end of the composite tube is given in Table 9.1, and compared with the known solution [52] for an infinitely long composite tube. Excellent agreement between the reference solution and the current results is observed.

To establish the validity of the finite element formulation with material nonlinearity, a two-ply, long composite cylinder with shear nonlinearity under torsion is solved first in closed form. The closed-form, anisotropic elasticity solution for the problem is given in Appendix G. The geometry and ply material properties of the composite tube in the numerical solution are assumed as follows:

I.D. = 2.0 inches; O.D. = 2.4 inches; Ply thickness = 0.1 inch;
Length of Tube = 10 inches.

Outer ply properties:	E_{11}=6.53 Msi;	$E_{22}=E_{33}$=1.74 Msi;
	υ_{12}=0.28;	G_{12}=0.82 Msi.
	$\bar{S}^{h}_{66}=1.654 \times 10^{-14}$ (psi.)$^{-3}$.	
Inner ply properties:	E_{22}=6.53 Msi;	$E_{11}=E_{33}$=1.74 Msi;
	υ_{21}=0.28;	G_{12}=0.82 Msi.

$$\bar{S}^{h}_{66}=3.308 \times 10^{-14}\ (\text{psi})^{-3}.$$

In the computational analysis, at one end of the tube, the axial displacement W and the circumferential displacement V are fixed, and at the other end an end rotation is applied. Two elements per ply along the thickness direction and 12 elements along the axial direction of the cylinder are used. The shear stress τ_{12} obtained in the cross section at 5 inches from the end of the tube is shown in Fig. 9-4. Comparison is made between the numerical results and those determined from the elasticity solution given in Appendix G. In Fig. 9-4, excellent agreement is observed between the numerical results and the elasticity solution.

A convergence study on thread contact is conducted for a composite joint with different finite-element discretizations. The discretization, shown in Fig. 9-5b, is obtained by modifying and refining the mesh in Fig. 9-5a at both ends of the engaged threads. The convergence study is focused on the stresses in the end threads because loading on the threads are generally the highest and more complicated than that on the rest. The limited computer capacity is the other reason for the convergence study. (The node numbers of a nominal mesh and the locally enriched meshes are 6,598 and 8,027, respectively.) The external loading on the threaded joint is a two-turn make-up interference. The average normal contact pressure[1] on thread surfaces 1 to 6 and the maximum principal stresses at thread roots A to D shown in Figs. 9-5a and 9-5b are calculated. Comparisons of the results are made in Tables 9-2 and 9-3.

It is clear that the results obtained by different finite element discretizations are in excellent agreement. However, the maximum difference in the principal stress at a thread root is about 20%. The computational expense for the locally enriched mesh is almost two times as that for the case with a nominal mesh. Since stress concentrations obtained at a thread root are close from the two discretizations, the nominal mesh configuration is used in the subsequent calculations.

9.2 Numerical Method for Direct Full-Field Modeling

The generalized plane element formulation given in Sec. 9.1 is used to construct eight-node isoparametric elements for direct full-field modeling threaded composite tubular joints. The discretization shown in Fig. 9-6 contains 1,744 elements with 5,792 nodes. The axial displacement W and the circumferential displacement V at the left end of the joint are fixed . The numerical procedure for the direct full-field modeling is described in the previous section.

9.3 Numerical Method for Coupled Global-Local Modeling

Eight-node isoparametric elements are also used in the coupled global-local modeling of a threaded composite tubular joint. A mesh (1,016 elements with 3,255

[1] The tangent component of the contact pressure equals to the product of the normal pressure and the frictional coefficient, which is 0.08 in this case.

nodes) for the global-scale model is shown in Fig. 9-7. An associated local-scale model is shown in Fig. 9-8, which consists of 420 elements and 1,866 nodes. Nodal displacements along B_1 to B_5 in Fig. 9-8 are interpreted from the results of the global-scale analysis.

9.3.1 Iteration Procedure for Equivalent Thread Layer

In the global-scale model, the effective stiffness of the thread region is modeled by an equivalent thread-layer, involving determination of the aforementioned equivalent load-bearing plane, which is usually unknown in prior and is obtained through an iterative procedure. Before an element stiffness in the equivalent thread-layer is evaluated, an initial load-transfer direction and a thread surface contact are assumed. After solving the equilibrium equations, the shear stress and the average strain in Eqs. (7-2a) and (7-2b) are determined. If the results are consistent with the initial assumptions, the solution obtained is correct. If any inconsistency is found, the assumed load-transfer direction or the thread surface contact condition needs to be modified, and the equations are solved again. This iterative procedure continues until the consistency condition is reached in all thread-layer elements. Although the global-scale model involves the iterative procedure to determine the direction of the load-bearing plane, it is much conceptually simpler than that used in analyzing thread contact in the aforementioned direct full-field modeling.

9.3.2 Numerical Scheme for Local Modeling

The aforementioned local model of thread contact requires local boundary conditions obtained from the global model analysis be applied to the selected local domains with sufficient geometric details. Thread modeling at different scales is shown in Figs. 9-9a and 9-9b. Boundaries $\overline{CD}$ and $\overline{EF}$ of an equivalent thread layer correspond to boundaries $\overline{C'D'}$ and $\overline{E'F'}$ in a local model. However, applying displacements along $\overline{CD}$ and $\overline{EF}$ obtained directly from the global model to $\overline{C'D'}$ and $\overline{E'F'}$ in the local model may not lead to best results, because an equivalent thread layer only gives average deformations in the thread region. Deformations obtained at positions along $\overline{CD}$ and $\overline{EF}$ corresponding to the actual thread roots can be significantly different from their true solutions in the local model. A better solution of the local behavior may be obtained by conducting a local analysis on a selected domain including areas around the thread region, for example, regions A'B'D'C' and E'F'H'G', and ABDC and EFHG. (The applied displacement boundary conditions on $\overline{C'A'B'D'}$ and $\overline{E'G'H'F'}$ in the local model are obtained from the global analysis.)

9.4 Comparison of Results from Different Models and Solution Efficiency

9.4.1 Comparison Among different Models

With the two aforementioned approaches, threaded integral composite joints under one-turn and two-turn make-ups can be properly modeled. The composite material nonlinearity is included to ensure a full consideration of physical behavior of the system. Hoop deformations are obtained along the external surface of a box section ($\overline{AB}$ in Figs. 9-6 and 9-7) and along the internal surface of a pin section ($\overline{CD}$ in Figs. 9-6 and

9-7) in the engaged thread region. The results are shown in Figs. 9-10 to 9-13. As expected, the applied make-up radial interference results in tensile hoop strains along the external surface of the box section and compressive hoop strains along the internal surface of the pin section. The difference is found to be very small between the hoop strains at the external surface of the box obtained by the global and the direct full-field (linear material) models. Similarly, the computed hoop strains at the inner surface of the pin section along $z/p > 2.5$ (p is thread pitch), using the two different (linear material) models, are in close agreement. Discrepancies in the computed strains for $z/p < 2.5$ may result from the end effect of the tubular pin section.

Axial strains caused by the make-up load are shown in Figs. 9-14 to 9-17. On the external surface of the box section, axial strains are much smaller than those on the internal surface of the pin section. Better agreement is observed between the results from the two linear analyses along the external surface of the box than those obtained along the internal surface of the pin. However, in all cases studied, introduction of material nonlinearity in the direct full field model significantly affects the results.

Contact bearing pressures along the thread surfaces (i.e., stab and load surfaces Fig. 4-3b) are given in Figs. 9-18a and 9-18b, using both the direct full-field (linear material) model and the local (linear material) analysis, for both one-turn and two-turn make-up cases. The local model is conducted on the joint with the boundary conditions along boundaries B_1 to B_5 obtained from the global model. The local analysis addresses the details of individual thread contact, as shown in Fig. 9-8. Since the thread surface pressure is mainly caused by a radial make-up interference, good agreement is expected, and is indeed observed between the results from the two approaches in the region at $z/p > 2.5$. The end effect from the pin section is expected to affect the thread pressure in the region $z/p < 2.5$.

9.4.2 Solution Efficiency

All computations have been carried out on SunSparc-2 workstations. The CPU time used for a direct full-field model is approximately 225 minutes. The CPU time for a coupled global-local model requires 4.8 minutes for a global analysis and 28.3 minutes for a local analysis. The global-local modeling is much more efficient than the direct full-field modeling, and the requirement of computer capacity is much less. A global-local model needs only approximately 28% computer memory required for the corresponding direct full-field model.

9.5 Additional Remarks

The results obtained in this study indicate that overall deformations of a threaded composite tubular joint determined by a global-scale model compare well with those obtained from a direct full-field model. The detailed thread contact pressure obtained from an associated local analysis is also consistent with the results from a direct full-field model. From the view point of computational efficiency, the coupled global-local model appears more suited for the complex threaded composite joint problem without compromising the solution accuracy. However, the global-local model has severe

limitations, since an equivalent thread layer can not be constructed when the threads contain damage of different forms. Also accuracy of the global-local model is difficult to assess when the damage of the threads is included. Consequently, in construction of a leakage failure envelope for a threaded composite joint, the aforementioned direct full-field model with material nonlinearity is used to avoid the complications.

10. ANALYTICAL AND NUMERICAL SOLUTIONS FOR COMPOSITE JOINT LEAKAGE FAILURE, AND COMPARISON WITH EXPERIMENTS

The experimental, analytical and numerical methods developed in previous sections are used to investigate quantitatively the leakage failure of threaded tubular fiber composite joints. Leakage failure envelopes and associated failure modes of the threaded composite joints are determined for the cases under different combinations of axial load, internal pressure and make-up turns. Also included in the study are the influence of thread surface contact with varying bearing pressure, the effect of geometric imperfection, the probabilistic characteristics of composite joint leakage, and the determination of the tightening safety factor. Based on the results obtained, quantitative relationships are established among the joint sealing integrity, joint/thread materials and geometry, and external mechanical loading.

10.1 Deformations and Stresses of Threaded Composite Joints under Combined Loading

In a 2-3/8-inch diameter threaded composite joint with a thread compound, hoop strains ε_θ developed are shown in Figs. 10-1 and 10-2 for the cases of one-turn and two-turn make-ups. The hoop strains were measured at the midpoint of engaged threads on the external surface of the box section (i.e., hoop strain gage No. 2 as described in Section 5.4). Substantial deformation at the initial tightening (IT) position[1] was observed, especially in the joint with a low number of make-up turns, T. The start of the loading portion of a make-up-strain-versus-turn curve is difficult to delineate and define. Consequently, the exact amount of the make-up interference from a make-up curve may not be always accurately determined[2]. Experiments on disengagement of the composite joints (i.e., the break-out test) were conducted after the make-up tests. During a joint break-out, hoop strains and break-out turns were measured, as shown in Figs. 10-3 and 10-4, and the unloading could be easily identified[3, 4] in the figures.

---

[1] In a joint without a thread compound, the initial tightening is defined as

$$\varepsilon_\theta (Z^*) = 0, \text{ at } T=T_{IT},$$

$$\text{and } \varepsilon_\theta (Z^*) \neq 0, \text{ at } T=T_{IT} + \delta \text{ for } \forall\ \delta > 0,$$

where T is make-up turn, δ is a small constant and Z^* is the location of strain measurement, defined as the ratio of Z in Fig. 9-7 to thread pitch which is 0.125 inch for the joint studied.

[2] This was caused by the thread compound used in a make-up, which had a high viscosity and contained Teflon particles. During a make-up process, most of the applied thread compound was gradually squeezed out of the joint. Therefore deformations in the joint during the make-up depended significantly on the viscosity and process of thread compound squeezing. In order to eliminate the effect of thread compound viscosity, a break-out (untightening) study was conducted after the joint was tested.

[3] Ideally, the unloading portion is to decrease monotonically with the break-out turn, as illustrated schematically in Fig. 10-5. However, because of geometric imperfections, experimental results usually

In Fig. 10-6, measured hoop strains at the mid-point of engaged threads along the external surface of the box section during a make-up are shown. The results reveal that the actual make-up (corresponding to the unloading portion in a break-out curve) was usually, on an average, approximately 10% less than the number of turns passed the initial tightening position, due to the slight mismatch in the taper of the pin and the box. Therefore, in practice, to achieve a desired make-up interference, a ten percent over make-up may be needed if the initial tightening (IT) position is used as a reference.

Detailed deformations at the mid-point of engaged threads (Z^*=7.5) on the external surface of the box section in a threaded composite joint under one-turn and two-turn make-ups are also analytically determined by the aforementioned direct full-field model and are given in Fig. 10-6. Good agreement is observed between the measured hoop strains and the analytical solutions. The results for the joint with a linear ply properties are compared with the solutions obtained from the material constitutive model with ply nonlinearity. The relatively small interferences induced during the joint make-up do not seem to lead to significant nonlinear deformation in the joint.

In Figs. 10-7 to 10-8, typical load-deformation relationships are shown for a threaded composite joint subjected to increasing internal pressure (with T=2 and P_a=0). Hoop strains on the external surface of the box section changed nonlinearly with internal pressure. (A small amount of noise was recorded in the third hoop-strain gage when the applied internal pressure exceeded 3 ksi. The noise may be caused by local thread contact in the joint. The local contact may be also responsible for a slight jump of the hoop-strain measurement in the second gage.) Similar phenomena were observed in axial strain measurements. The onset of leakage was determined from the piston movement in the pressure intensifier during loading (Fig. 10-9). The initial movement of the piston was relatively fast in order to supply the fluid to fill the small gap between the specimen and the mandrel. The piston subsequently moved at an approximately constant velocity. When leakage occurred in the joint, the rate of the piston displacement increased, signaling the control system to terminate the experiment.

Principal stresses at the thread roots of the composite joint under two-turn makeup and 2:1 loading with internal pressure of 2000 psi. are shown in Figs. 10-10a and 10-10b. It is observed that the end threads usually carry higher loading. Interface shear stress between the threads and tube body, Fig. 10-11, also exhibits the similar features. The principal stress fields in the end threads are illustrated in Fig. 10-12a to 10-12d.

---

deviated from the expected linear relationship. In order to determine the separation point A in Fig. 10-5, a scheme was suggested to rationalize the experimental data. By a judicious choice of point A, the number of break-out turns could be determined such that the difference between the experimental results and the idealized curve could be minimized.

4 This is due to the fact that no compound was squeezed out of the threads and elastic unloading occurred

10.2 Leakage Failure Envelopes

Leakage failure envelopes were constructed for the threaded composite joints with one-turn and two-turn make-ups subjected to combined axial load and internal pressure[1] in a proportional loading mode and shown in Figs. 10-13 and 10-14. Failure predictions from the aforementioned full-field leakage analysis are also shown for comparison. Different leakage failure modes were identified and related to different combinations of internal pressure and axial loading. In the case of leakage failure caused by the loss of bearing pressure between thread surfaces, the experimental data obtained are in good agreement with the analytical predictions. Most experimental results were in leak and leak-prone regions of the failure envelopes. Leakage failure modes were found in consistency with the predictions. Scattering of experimental data was observed in the joints with a low level of make-up, and the data scatter is larger than that in joints with a higher level of make-up. Note that the numerical predictions are based on two different values of the tightening safety factor (X=1 and 2) as introduced in Section 8. The effect of the tightening factor on the leakage failure of a threaded composite joint will be addressed in Section 10.8.

In a joint subjected to a high axial load, leakage failure[2] caused by composite tube-body damage was not commonly observed in the experiments. Only in one test was composite tube body damage clearly found. Experimental results in this case were compared well with the numerical predictions, as shown in Fig. 10-14. Leakage failure by thread shear-off coupled with through-thickness cracking in the tube (pin) body was found in most experiments under a combined high axial loading and low internal pressure. However, analytically, only matrix-cracking-dominated leakage[3] and local thread-tube interface failure were predicted with no thread shear-off being analytically obtained in the numerical solutions. This will be discussed in detail in the next section.

10.3 Damage Mechanisms, Evolution and Associated Leakage Failure Modes

As indicated previously, several leakage failure modes were observed in the threaded composite joints under combined axial loading, internal pressure and thread make-up interference. In a hoop-stress dominated experiment, leakage failure was

---

1 As mentioned in Section 10.1, the amount of radial interference introduced into a composite joint during make-up could vary from joint to joint, even though the joint was tightened by the same number of make-up turns passing the initial tightening position. Therefore, each joint was prepared with different make-up levels. In order to construct accurately an experimental leakage failure envelope for a composite threaded joint, a rigorous scheme of normalization is introduced in Appendix F.

2 In a composite joint under high axial loading, the internal diameter of the joint decreased with an increasing load, due to Poisson's effect. In such a case, the piston displacement would not provide an accurate measure for the leakage detection since the piston of the pressure intensifier moved backward with an increasing load. Thus, the sensitivity of the leakage detection system could be reduced in the test conducted under high axial loading. The low sensitivity of the leakage detection system might cause the test system continue to apply loading to the joint after leakage was initiated, and eventually resulted in failure along the interface between the threads and the pin body.

3 We note that in some cases, the locations, where leakage is predicted, had a gap region of less than one-tenth of an inch between the pin and the box. Experimentally, using the aforementioned conducting-mesh technique to detect the leakage must be conducted with great care.

mainly caused by the loss of bearing pressure along the thread surface, as shown by the solid circles in the figures (Figs. 10-13 and 10-14). In these cases, the pressurized fluid leaked between the joint thread surfaces without causing material damage in the composite tube body or in the threads. The leakage failure was attributed to insufficient contact pressure developed among the threads.

In a composite joint dominated by combined high axial loading and internal pressure, leakage failure is predicted by pin-section composite tube-body damage. However, in the experiments, no leakage was actually detected in the tube body before the thread shear-off, except for the one case shown in Fig.10-14. (The conducting-mesh detection method usually gave a failure signal first, immediately followed by the thread shear-off. The piston movement detection method, however, did not give any advanced warning before failure in all the cases studied.) Failure by the pin-side thread shear-off (Figs. 10-15 and 10-16) was typical in the experiments under combined high axial loading and internal pressure, where interface fracture occurred between threads and the pin body. The pin-side composite tube was pulled out of the joint, leaving the pin-side threads in the box section.

Microscopic observations on the damaged pin sections indicated a significant amount of matrix cracking (Fig. 10-17) occurring in the failed region of the pressurized composite joint under high axial loading. Some through-thickness cracks were also found. To identify the damage failure mechanisms observed, the pin section with sheared off threads was subsequently pressurized internally. A significant amount of leakage was seen in the region where the threads were sheared off, as shown in Fig. 10-18, even though the pressure was as low as 80 psi. Leakage was also found at the end of the thread section. Clearly, leakage failure modes in these cases were thread shear-off combined with through-thickness cracking in the (pin section) tube body.

In the case of a composite joint failed by the aforementioned tube-body damage, the current numerical study predicts a failure mode in the form of pin-side tube-body damage (matrix cracking), as shown in Figs. 10-19a to 10-19c. The damage is predicted to initiate at the roots of the last two engaged pin-side threads near the mill end of the tube body and grow along the axial direction. Interfacial failure between the threads and the tube body occurs locally under the threads in the integral composite joint before a through-thickness crack is developed. The interfacial failure, which causes the threads to shear off, would occur if the applied loading continuously increases after the leak occurs.

10.4 Effects of Make-up Interference, Internal Pressure and Axial Loading

If the predicted leakage failure envelopes for a threaded composite joint are combined for the cases of one-turn and two-turn make-ups in Fig. 10-20, one finds that, in the region of failure by the loss of bearing pressure, the critical internal pressure in the joint depends significantly on the level of the make-up loading. In the case of combined high hoop stress and low axial loading, increasing the make-up interference could greatly increase the critical internal pressure, thus, the sealing capacity of the joint. However, in the tube-body-damage-dominated region, the critical axial load and internal pressure seem

not affected by the change of in make-up interference.

Thus, in the region that failure is dominated by the loss of bearing pressure, the tightening safety factor dictates the leakage-free region. High axial loading results in a low critical bearing pressure and consequently, reduces the sealing capability of the joint. The reduction in the bearing pressure appears to be approximately linear with an increase in external loading for the one-turn make-up case, whereas nonproportional changes are observed in a two-turn make-up case, due to complex interactions among material nonlinearity, thread contact and damage evolution. Obviously, these effects become more appreciable when the joint is subjected to higher loading.

For an illustrative purpose, relationships between the joint make-up level and the sealing capacity are shown in Figs. 10-21(a) to 10-21(c) for a 2-3/8-inch composite integral tubular joint under different hoop-to-axial loading ratios. The leakage-prone region is bounded by the tightening safety factors X=1 and X=2. Under a given (hoop-to-axial) loading ratio, the sealing capacity of the joint is approximately proportional to the make-up interference. An increase in the axial load requires an additional make-up to keep the same sealing integrity of the joint.

10.5 Effect of Geometric Imperfections

It is clear that in a joint leakage failure caused by the loss of bearing pressure, the critical internal pressure depends on the make-up interference and axial loading. For a joint with threads of a given pitch dimension, the magnitude of the make-up interference is a function of the make-up turn, thread taper and other geometric parameters, as expressed in Eq. (6-14). While the make-up turn is a global loading parameter independent of the joint geometry, the thread taper is an important local geometric parameter which requires carefully examination. The results of the threaded joint leakage failure presented in the previous sections are obtained under the assumptions that: (1) the radial interference is constant along the thread engagement region, and (2) the thread taper in both pin and box sections are nominal [38,39].

From Tables A-1 and A-2, taper of threads in a joint is clearly not constant but varies along the joint axis. The Tables also show that the pin-side and box-side thread taper are generally not the same[1]. To illustrate the effect of the geometric imperfection, two cases are investigated in the present study. The first is a so-called "fast-pin-and-slow-box" joint, in which pin-side threads have a taper of 6.5%, and box-side threads have a taper of 6.1%. The second is a "fast-box-and-slow-pin" joint, which has a geometry opposite to the first case. Obviously, in a joint with the thread taper being not nominal, the radial interference introduced during the make-up varies from point to point in the engaged thread region.

---

[1] API Standards [38,39] specifies that the tapering of round threads for an external-upset tubing can vary from 6.1% to 6.5% in diameter with a nominal value of 6.25%. Therefore, the maximum variation in tapering in a threaded composite joint may reach 0.4% in diameter, causing a substantial amount of interference between the two ends of the engaged threads and, consequently, affects the leakage pressure of the joint.

An illustration of the make-up interference in a fast-pin-and-slow-box joint is given in Fig. 10-22. The radial make-up interference along the left-hand side of the engaged thread region is smaller than that in a nominal joint if the interference at the mid-point of the engaged thread region is kept the same as that of a nominal joint. The reduction in the radial interference will result in a decrease in bearing pressure and, consequently, the sealing capability of the joint. In the case of a fast-box-slow-pin joint, it is plausible that the bearing pressure may increase in that region. Since in this research only reduction in sealing capability of a joint caused by the geometric imperfection is of concern, only the case of a fast-pin-slow-box composite joint is studied.

In the composite joint with a fast pin and a slow box, several parameters need to be introduced first to represent properly the make-up interference. Commonly, three physical make-up parameters need to be considered: (1) make-up torque, (2) make-up hoop strain at the mid-point in an engaged thread region, and (3) make-up interference at the mid-point in the engaged thread region. For comparison, the study on the effect of geometric imperfection conducted here assumes that all joints investigated, with or without a nominal thread taper, have the same amount of make-up.

The make-up torque and the make-up hoop strain at the mid-point of the engaged thread region on the outer surface of the box section in a joint with a fast pin and a slow box are determined numerically under a two-turn make-up interference at the mid-point in the engaged thread region. The solutions are compared with in a nominal joint with the same level of make-up. The results show that the ratio of the make-up torque on a nominal joint to that on a joint with a fast pin and a slow box is 1.004. The ratio of the make-up hoop strain on a nominal joint to that on a fast-pin-and-slow-box joint is 1.015. Since these two values are very close to one, it may be appropriate to approximate that the aforementioned three make-up parameters are generally equivalent. In the current analysis of a joint with a fast pin and a slow box, the make-up interference at the mid-point of an engaged thread region is used as the make-up parameter.

In Fig. 10-23, leakage failure envelopes are obtained for threaded, integral tubular composite joints with a nominal and with a non-nominal thread taper. It is important to note that in a joint with a fast pin and a slow box, the thread taper may cause a significant reduction in the leakage pressure of the joint. In order to quantify this geometric effect, a sealing reduction parameter ξ is introduced as the ratio of the critical leakage pressure for a non-nominal joint to that for a nominal joint subjected to the same proportional external loading. For the joints considered with a unit tightening factor, the ξ has values ranging from 0.795 to 0.886, and for joints with a tightening factor of two the ξ varies 0.786 to 0.852. Therefore, the critical leakage pressure of a joint with the non-nominal taper is lower than that of a nominal joint by about 22%. However, no appreciable effect of the taper imperfection is found in joints with the leakage failure being resulted from tube-body damage.

Note that the geometric-imperfection-induced ξ is only one of several geometric

imperfections contributing to the leakage resistance of a threaded composite joint. Other geometric and composite lamination parameters, such as wall and ply thicknesses, variations in material properties, thread height, truncating radii and flank angles, may lead to further reduction in the critical pressure.

10.6 Influence of Thread Surface Friction

In a leak-free threaded composite joint, the bearing pressure on a thread contact surface must be greater than the critical internal pressure[1]. The ratio of the bearing pressure to the critical internal pressure defines the joint sealing reliability. The higher the ratio, the more reliable the joint. Using a high make-up interference one may increase the ratio to improve the joint leakage resistance. However, a high level of make-up may also cause undesirable material damage in the joint even without external loading. Another approach is to change the tightening safety factor of the contact surface without losing the sealing reliability. The experimental study reported in [50] has shown that increasing the viscosity of the sealing compound applied on the thread surface may reduce the bearing pressure needed for sealing. Increasing the viscosity will raise frictional force between thread contact surfaces. The frictional effect is an important parameter and should be carefully examined.

In this section, leakage failure of a threaded integral composite joint with different thread surface friction is studied. For illustration, several coefficients of friction between the thread contact surfaces (e.g., 0.04, 0.08 and 0.16) are considered for determining the effect of the thread surface friction on the leakage-failure resistance of the composite joint. In Fig. 10-24, increasing the coefficient of friction between thread contact surfaces is found to raise the critical bearing pressure. In the region of leakage caused by the tube-body damage mode, the effect of thread surface friction is not significant. Thus, increasing the coefficient of friction between thread contact surfaces in a composite joint is expected to improve the sealing reliability of the joint, provided that the increase is not caused by raising the roughness of the contact surface.

10.7 Probabilistic Characteristics of Leakage Failure

In the joint leakage caused by the loss of thread bearing pressure, the magnitude of the tightening safety factor introduced earlier is critical. As mentioned in Section 8, proper determination of the tightening safety factor requires a combined experimental and analytical approach and clear understanding of leakage failure modes. With the analytical methods developed in this study, it is possible to determine quantitatively the tightening safety factor for a threaded integral composite tubular joint subjected to any combinations of internal pressure, axial load and make-up interference.

In this section, a systematic investigation of leakage failure has been conducted on two sets of threaded integral composite tubular joints. One is shown in Fig. 4-2 and the other, in Appendix G. The joints were tested under internal-pressure-dominated loading

---

[1] The critical internal pressure is XP_j.

with a hoop-to-axial load ratio ranging between 1:0 to 1:0.67 so that the leakage failure mode was governed by the loss of bearing pressure. Subsequent modeling and analyses are then conducted to determine the leakage tightening factors for individual cases. A cumulative leakage frequency diagram is then constructed, as shown in Fig. 10-25, based on the combined analytical and experimental results. The probabilistic leakage failure distribution function is determined, and it follows a normal distribution function F(X),

$$F(X) = \frac{1}{\sigma\sqrt{2\pi}} \int_{-\infty}^{X} e^{-(\frac{v-\mu}{\sigma})^2/2}\, dv, \tag{10-4a}$$

with

$$\mu = \frac{1}{n} \sum_{i=1}^{n} X_i\,, \tag{10-4b}$$

$$\sigma^2 = \frac{1}{n-1} \sum_{i=1}^{n} (X_i - \mu)^2, \tag{10-4c}$$

where μ is the mean value of X_i; σ is the standard deviation and n is number of samples. The values of μ and σ are found to be 1.61 and 0.48, respectively.

From the results, the tightening safety factors are given in Table 10-1 for the threaded composite joints with different sealing confidence levels. The length of the threaded composite tubing per leakage in the Table is calculated, based on the assumption that the composite tubing usually is 30 ft long with one threaded integral joint per segment. It is clear seen that the tightening safety factor X=2 corresponds to an 80% sealing confidence level, whereas the minimal sealing requirement, X=1, gives only 10% sealing confidence, which is consistent with the results shown in Section 8.

10.8 Approximate Relationship between Joint Sealing Integrity and Mechanical Loading

As a first-order approximation, a linear relationship is assumed to relate the leakage failure caused by the loss of thread bearing pressure to joint sealing capacity and make-up interference,

$$P_B \approx KT - \alpha P_i - \beta P_a, \tag{10-1}$$

where P_B is the bearing pressure on a thread contact surface; T is the make-up turn, and K, α, and β are constants. The terms P_i and P_a in Eq. (10-1) represent applied hoop and axial stresses, respectively. For a given hoop-to-axial load ratio $R = P_a / P_i$, Eq. (10-1) may be written as

$$P_B = KT - (\alpha + \beta R)\, P_i. \tag{10-2}$$

Taking the tightening safety factor X into consideration, one may determine the proper make-up for a threaded composite tubular joint under a prescribed axial and pressure loading by

$$T = \frac{P_B + (\alpha + \beta R)\, P_i}{K} = \frac{X + (\alpha + \beta R)}{K} P_i. \qquad (10\text{-}3)$$

Notes here that for a composite integral joint with a 2-3/8-inch diameter, the analytical solutions in the current study gives the values of K = 48,635 psi/turn, α = 1.355, and β = 0.9414. With Table 10-1 and Eq. (10-3), one may determine the suitable make-up for a threaded composite joint to achieve the desired level of sealing confidence under combined internal pressure and axial loading for a line pipe application.

10.9 Additional Remarks

The geometric variation in thread taper and viscosities of most thread compounds complicate quantitative determination of the joint make-up interference. A turn or torque criterion may not provide an accurate and adequate measure of the make-up interference. Consequently, the currently used representation of leakage failure loading for metal joints could be confusing. The scheme developed in this study elucidates the viscosity effect of a thread compound and provides a rational and quantitative measure of the make-up interference. A proper combination of the leakage loading representation and the make-up interference may provide an effective approach to this class of complicated problems. The leakage failure envelope obtained with these methods in this study reveals quantitatively some of the most important, fundamental nature of leakage failure of a threaded composite joint.

The analytical models developed in the current study have been shown to be effective in predicting leakage failure of a threaded composite joint under combined internal pressure, axial loading and make-up interference. Based on these models, an approximately linear relationship is introduced to relate the leakage failure to internal pressure, axial loading, make-up interference and sealing confidence of a threaded composite joint. The proposed approach provides an efficient and effective quantitative method for proper make-up determination. With the aid of the method developed in the study, the effect of thread taper imperfection is found to yield a geometry-related, joint sealing reduction parameter which is important in design of threaded composite joints.

However, the models and associated analytical methods developed in this study have the following limitations:

1) Geometry: The axisymmetric assumption of the joint thread geometry restricts the current model for the joints with small helix thread angles. The error introduced by the geometric model may increase with an increasing helix thread angle. In a metal joint with a helix thread angle of 5 degrees, neglecting the nonaxisymmetric effect of the helix angle may cause an error in the critical stress as much as 20% [13].

2) Loading: Nonaxisymmetric loading, such as bending, is not considered here. The circumferential θ–dependency of deformation and stress needs to be considered when the leakage failure of a joint under bending is studied. Using the well-known Coulomb's law to describe friction between thread contact surfaces may also introduce additional approximations in leakage prediction of a threaded composite joint under cyclic loading. Current hydrodynamic lubrication theory shows that Coulomb's law is only valid in describing the case of low-velocity sliding along a contact surface, as shown in Fig. 10-26. When the sliding velocity increases, the velocity-dependent frictional force has to be introduced.

3) Long-term leakage prediction: The glass-transition temperatures, T_g, of polymeric matrices in FRP joints are generally higher than room temperature. For short-term room temperature leakage prediction, it may be permissible to neglect the viscoelastic effect of the materials. However, long-term environmental parameters, such as moisture, may reduce the T_g of the material system. The viscoelastic effect during long-term loading on creep deformations and stress redistribution will become appreciable. Also the degradation of the polymeric materials and fibers in the composite during long-term mechanical and environment loading needs to be considered.

11. CONCLUSIONS

1) To understand the composite joint leakage failure phenomena and subsequently validate the analytical modeling, world-unique experimental facilities have been designed, constructed and fully used for this project. The facilities include a servo-hydraulic multiaxial (axial, pressure and torsional) loading system, digital and analog control systems, make-up interference application and measurement system, multiaxial deformation measurement systems (multiaxial extensometers), two leakage detection systems, and a fully computer-controlled data acquisition system.

2) Nonlinear, inelastic three-dimensional anisotropic composite mechanics models have been formulated for studying the complex deformation and damage developments in threaded composite tube bodies during leakage failure. The nonlinear moving boundary problem of local thread surface contact in a composite joint under combined internal pressure, axial and make-up loading is modeled by quasi three-dimensional contact mechanics formulation based on the Lagrangian multiplier method.

3) To account for the detailed thread geometry, local joint configuration, ply material nonlinearity, through-thickness material discontinuity, thread surface contact and damage (crack) growth in the composite joint, efficient and accurate incremental-iterative algorithms have been developed for both direct global modeling and coupled local-global modeling of the problem.

4) The complex failure modes, which govern the leakage failure of a threaded composite tubular joint, have been identified in the experiments on filament-wound E-glass/epoxy composite joints with molded threads and have also been confirmed in the analytical results. The failure modes include fiber- and matrix-dominated cracking through tube bodies, thread material fracture, tread/tube-body interface debonding, and the loss of bearing pressure in the thread surface contact region.

5) Quantitative failure criteria have been developed and established for each individual failure mode from failure theories of fiber and particulate composite mechanics and contact mechanics. These failure criteria have been successfully implemented into the computational algorithms of the leakage failure analysis and prediction methodologies developed in this research for threaded composite tubular joints.

6) Based on the experimental results and the analytical solutions, complete leakage failure maps (or envelopes) can be and have been constructed for filament-wound glass/epoxy composite joints with tube-body laminate lay-ups $[(\pm 55^{o})]_{n}$ (n= 9 for the pin and 11 for the box sections). The complete leakage failure map generally contains three distinct regions: leakage, leak-prone and leak-free regions under different combinations of internal pressure, axial and make-up loading.

7) Each region in the composite joint failure map is shown to be governed by the failure criteria associated with the distinct, individual failure modes identified, i.e., composite tube-body ply cracking, tube-thread interface debonding, thread material fracture, and loss of bearing pressure along the thread contact surface.

8) The inherent geometric and material variabilites of threads and thread surfaces in a composite tubular joint warrant the introduction of an important parameter, i.e., the tightening safety factor, in design, analysis and evaluation of the joint leakage failure problem. The value of the joint tightening safety factor is also affected by the roughness of the thread surface, the viscosity of the thread compound, the pressure medium used in the joint, and the allowable joint leakage failure probability.

9) Excellent agreement has been observed between the analytical predictions and the experimental results for the filament-wound glass/epoxy composite joints failed by the loss of bearing pressure. In the case of the composite joint leakage caused by a through-the-wall tube-body cracking mode, the discrepancy between the experimental data and predictions is small, since a high axial load is generally involved and the test system sensitivity is low in this condition.

10) In the case that a threaded composite joint failed by the loss of bearing pressure in the thread contact region, the leak-free, leak-prone and leakage-failure regions can be distinguished individually by different functional relationships among the applied axial and make-up loading, internal pressure, and the bearing pressure on a thread surface.

11) In the leakage failure of a composite joint caused by through-thickness tube-body cracking or thread material fracture, the influence of the make-up interference on the critical failure loads is found to be not appreciable. Consequently, in these cases increasing the make-up interference during the joint formation may not improve the sealing reliability of the threaded joint.

12) In the case of joint leakage failure by the loss of bearing pressure, the sealing capability of the joint, under a given biaxial loading and a safety tightening factor, increases almost proportionally with the amount of the make-up interference introduced in the joint. Therefore an additional make-up interference is required, as the applied axial load increases, to ensure the same joint sealing confidence.

13) The amount of thread tapering in a composite tubular joint significant affects the bearing pressure development in the thread contact region, and therefore influences the leakage failure of the joint. For a filament-wound glass/epoxy composite joint with a fast pin and a slow box, the sealing capability of the joint may be reduced by 22% when compared with the case with a nominal thread tapering configuration.

14) An increase in the frictional coefficient between the thread contact surfaces raises the bearing pressure, and consequently, improves the sealing capability of the

composite joint, provided that the change in the frictional coefficient is not caused by altering the roughness of the thread surface.

15) Based on the experiments and the failure analysis conducted in this study, the leakage failure probability of the filament-wound E-glass/epoxy composite joints is found to follow a normal distribution function. The standard deviation and mean values of the normal distribution function are 0.48 and 1.61, respectively, for the 2-3/8-inch integral FRP composite joints.

16) The present investigation on the joint tightening factor indicates that the minimum bearing pressure requirement for threaded joint sealing in a previous study [15] is not adequate to prevent leakage failure of a threaded composite joint. A higher bearing pressure is obviously needed to achieve a reliable, leakage-free performance of the composite joint.

17) In the API proposed procedure for ranking/qualifying threaded FRP composite joints/connectors, construction of both short-term and long-term failure envelopes should include the important make-up interference loading, in additional to the pressure and axial loading. The presently proposed representation of failure envelopes does not contain all the important applied external loading and can not adequately describe the joint leakage failure.

18) The currently recommended interpolation procedure in the API proposed ranking/qualification method may not be suitable for construction of proper leakage failure envelopes, especially for the case of long-term failure. From the present joint experiments and the related study on tube bodies, failure envelopes for both short-term and long-term leakage in a threaded joint are known to be highly distorted; the weighting method to interpolate the biaxial (hoop to axial) failure loading, even without considering the makeup interference, simply based on one intermediate, i.e., 1:1, biaxial loading ratio is obviously inadequate.

19) From the analytical and experimental studies conducted in this research, it becomes clear that additional parameters should be included in the API proposed procedure for establishing long-term joint leakage failure envelopes. These should include long-term creep deformation and stress relaxation in the threads, degradation of the thread compounds used in the joint, and time-dependent strength changes of both tube bodies and threads.

20) The reduction factor in the API proposed joint ranking procedure for obtaining the joint/connector service envelope from the long-term failure envelope needs to be lower than the current value, i.e., 0.67, based on the considerations of material and geometric variations in the composite joints and the statistical nature of the joint leakage failure characteristics, as reported by the experimental results and analytical solutions in this study

12. REFERENCES

[1] H. J. Taggart, "Acid Waste Recovery," *Composite Institute on Composites*, February/March 1995, pp. 5-6.

[2] R. M Jones, *Mechanics of Composite Materials*, Scripta Book Co., Washington, 1975.

[3] J. Mistry, "Theoretical Investigation into the Effect of the Winding Angle of the Fibers on the Strength of Filament Wound GRP Pipes Subjected to Combined External Pressure and Axial Compression," *Composite Structures*, Vol. 20, pp. 83-90 (1992).

[4] J. M. Whitney and J. C. Halpin, "Analysis of Laminated Anisotropic Tubes under Combined Loading," *Journal of Composite Materials*, Vol. 2, pp. 360-367 (1968).

[5] G. C. Eckold, D. Leadbetter, P. D. Soden and P. R. Griggs, "Lamination Theory in the Prediction of Failure Envelopes for Filament Wound Materials Subjected to Bi-axial Loading," *Composites*, Vol. 9, pp. 243-246 (1978).

[6] S. S. Wang, M. Karayaka, and S. Srinivasan, "Effect of Nonlinear Shear Constitutive Equations on Leakage Failure of Glass-Fiber Reinforced Epoxy Composite Laminate Tubes Subjected to Combined Axial Load and Internal Pressure," In preparation (1996).

[7] J. P. Den Hartog, "The Mechanics of Plate Rotors for Turbo Generators," *Transactions of ASME*, Vol. 51, pp. APM 51-1 (1929).

[8] J. N. Goodier, "The Distribution of Load on the Threads of Screws," *Journal of Applied Mechanics*, Vol. 7, pp. 10-16 (1940).

[9] D. G. Sopwith, "The Distribution of Load in Screw Threads," *Proc. Inst. Mech. Engrs.*, Vol. 159, pp. 373-383 and pp. 391-398 (1948).

[10] E. A. Patterson and B. Kenny, "A Modification to the Theory for the Load distribution in Conventional Nuts and Bolts," *Journal of Strain Analysis*, Vol. 21, pp. 17-23 (1986).

[11] E. Dragoni, "Effect of Thread Pitch and Frictional Coefficient on the Stress Concentration in Metric Nut-Bolt Connections," *Proceedings of the 11th International Conference on Offshore Mechanics and Arctic Engineering*, edited by M. M. Salama, et al., ASME, New York, pp. 355-362 (1992).

[12] J. L. Bretl and R. D. Cook, "Modeling the Load Transfer in Threaded Connections by the Finite Element Method," *International Journal for Numerical Methods in Engineering*, Vol. 14, pp. 1359-1377 (1979).

[13] H. C. Rhee, "Three Dimensional Finite Element Analysis of Threaded Joints," *Proceedings of the 9th International Conference on Offshore Mechanics and Arctic Engineering*, pp. 293-298 (1990).

[14] S. Andrieux and A. Leger, "Multiple Scaling Method for the Calculation of Threaded Assemblies," *Computer Methods in Applied Mechanics and Engineering*, Vol. 102, pp. 293-213 (1993).

[15] P. D. Weiner and F. D. Swell, "New Technology for Improved Tubular Connection Performance," *Journal of Petroleum Technology*, Vol. 19, pp. 227-343 (1967).

[16] J. B. Day, M. C. Moyer and A. J. Hirshberg, "New Makeup Method for API Connections", *Proceedings of 1989 Drill Conference*, pp. 635-642 (1989).

[17] L. B. Hilbert J. and I. A. Kalil, "Evaluation of Premium Threaded Connections Using Finite Element Analysis and Full-Scale Testing," *Proceedings of Drilling Conference*, pp. 562-580 (1992).

[18] A. P. Assanelli and E. N. Dvorkin, "Finite Element Models of OCTG Threaded Connections," *Computers and Structures*, Vol. 47, pp. 725-734, (1993).

[19] Y. Morita, H. Kawashima and K. Ishihara, "Finite Element Simulation of Jump-Out Behavior of Threaded Pipe Joints Used in Oil-Producing Wells," *Journal of Energy Resources Technology*, Vol. 119, pp. 27-33 (1988).

[20] H. Bahai, I. I. Esat and J. Lawrence, "A Hybrid Modeling Approach to 3 D Stress Analysis of Threaded Connections," *Engineering System Design and Analysis*, PD-Vol. 47-1, pp. 235-241 (1992).

[21] Y. W. Kwon, E. F. Klementlch and K. I. Ko, "An Efficient and Accurate Model for the Structural Analysis of Threaded Tubular Connections," *SPE Production Engineering*, pp. 261-264 (1990).

[22] M. Beghini, L. Bertini and E. Vitale, "Shrink Stress Density Functions in Conical Threaded Connections as a Function of Dimensional Tolerances," *Proceedings of the 11th International Conference on Offshore Mechanics and Arctic Engineering*, Vol. 3-B, pp. 383-389 (1992).

[23] G. Dilintas, "Investigation of a Composite Tubing Connection Performance," *Journal of Energy Resources Technology*, Vol. 113, pp. 40-48 (1991).

[24] G. Dilintas, "Influence of the Filament on the Performance of a Composite Tubing Connection," *Journal of Composite Materials*, Vol. 26, pp. 1443-1454 (1992).

[25] M. N. Nahas, "Survey of Failure and Post-failure Theories of Laminated Fiber-reinforced Composites," *Journal of Composite Technology and Research*, Vol. 8, pp. 138-153 (1986).

[26] S. W. Tsai and E. M. Wu, "A General Theory of Strength for Anisotropic Materials," *Journal of Composite Materials*, Vol. 5, pp. 58-80 (1971).

[27] Z. Hashin, "Failure Criteria for Unidirectional Fiber Composites," *Journal of Applied Mechanics*, Vol. 47, pp. 329-334 (1980).

[28] R. M. Christensen, "Tensor Transformations and Failure Criteria for the Analysis of Fiber Composite Materials," *Journal of Composite Materials*, Vol. 22, pp. 874-897 (1987).

[29] K. D. Chiu, "Ultimate Strengths of Laminated Composites," *Journal of Composite Materials*, Vol. 3, pp. 578-582 (1969).

[30] H. T. Hahn and S. W. Tsai, "On the Behavior of Composite Laminates After Initial Failures," *Journal of Composite Materials*, Vol. 8, pp. 280-308 (1974).

[31] P. H. Petit and M. E. Waddoups, "A Method of Predicting the Nonlinear Behavior of Laminated Composites," *Journal of Composite Materials*, Vol. 3, pp. 2-19 (1969).

[32] M. Hetenyi, "A Photo-elastic Study of Bolt and Nut Fastenings," *Journal of Applied Mechanics*, Vol. 10, pp. 93-100 (1943).

[33] B. Kenny and E. A. Patterson, "Load and Stress Distribution in Screw Threads," *Experimental Mechanics*, Vol. 25, pp. 208-213 (1985).

[34] K. Ishikama, M. Morikawa, Y. Ono, N. Kawasaki and A. Shimanuki, " Strength of Threaded Connections for Lifting Pipes," *Proceedings of the Third International Offshore and Polar Engineering Conference*, pp. 315-320 (1993).

[35] J. B. Traweek, C. J. Nini, D. Gardenier and B. Hasha, " Makeup Determination and External Testing of Internally Plastic-Coated Tuning Connections," *SPE 20125*, pp. 327-333 (1990).

[36] T. P. Broadbent and H. Fessler, "Stress Distributions in Screwed Tubular Joints for the Petroleum Industry," *Proceedings of the First International Offshore and Polar Engineering Conference*, pp. 484-491 (1991).

[37] T. Yamagata and X. Namba, "Study on Joining Method for Graphite Epoxy Tubes," *Proceedings of 24th International SAMPE Technical Conference*, pp. T1044-T1054 (1992).

[38] API Std 5B, "Specification for Threading Gauging and Thread Inspection of Casing, Tubing and Line Pipe Threads", American Petroleum Institute, Washington, D. C., 1982.

[39] API RP 5B1, "Recommended Practice for Gauging and Inspection of Casing, Tubing and Line Pipe Threads," American Petroleum Institute, Washington, D. C., 1988.

[40] M. M. Schwartz, *Composite Materials Handbook*, McGraw-Hill, New York, 1971.

[41] S. S. Wang, M. Karayaka and S. Srinivasan, "Nonlinear Shear Deformation and Failure and the Effect of Transverse Stress in Hoop-wound Glass-fiber Reinforced Epoxy Composite Tube under Combined Loading," In preparation.

[42] I. M. Daniel, "Experimental Mechanics of Composite Materials," *Mechanics of Composite Materials, Recent Advances*, Proceedings of IUTAM Symposium. on Mechanics of Composite Material, pp. 473-496 (1983).

[43] S. P. Swanson and A. P. Christoforou, "Response of Quasi-isotropic Carbon/Epoxy Laminates to Bi-axial Stress," *Journal of Composite Materials*, Vol. 20, pp. 457-471 (1986).

[44] A. S. Chiu, "Test Method for Defining Makeup-up Procedure of Fiberglass Connections," *Appendix H of API Specification 15HR*, Second Draft, 1994.

[45] *General Installation Instructions for Threaded Fiberglass Piping Systems*, Smith Fiberglass Products Inc. Little Rock, AR, 1992.

[46] H. T. Hahn and S. W. Tsai, "Nonlinear Elastic Behavior of Unidirectional Composite Laminae," *Journal of Composite Materials*, Vol. 7, pp. 102-118 (1973).

[47] H. T. Hahn, "Nonlinear Behavior of Laminated Composites," *Journal of Composite Materials*, Vol. 7, pp. 257-271 (1973).

[48] T. P. Yu and S. S. Wang, "Analysis of Cracks in Nonlinear Fiber Composite Materials," *ONR-URI Composites Program Technical Report No. 90-1*, National Center for Composite Materials Research (NCCMR), University of Illinois, Urbana, IL, 1990.

[49] J. T. Oden and G. F. Carey, *Finite Elements, Special Problem in Solid Mechanics*, Prentice-Hall, Englewood Cliffs, 1984.

[50] H. H. Buchter, *Industrial Sealing Technology*, John Wiley & Sons, New York, 1979.

[51] S. G. Lekhnitskii, *Theory of Elasticity of an Anisotropic Body*, Holden-Day, San Francisco, CA, 1963.

[52] O. C. Zienkiewicz, *The Finite Element Method in Engineering Science*, McGraw-Hill, London, 1971.

[53] S. Srinivasan, *"Leakage Failure of FRP Composite Tubing,"* PhD Dissertation (in preparation), University of Houston.

[54] R. P. Reed and A. F. Clark, *Materials at Low Temperatures*, American Society for Metals, Metals Park, OH, 1983.

[55] A. E. Green and J. E. Adkins, *Large Elastic Deformation and Nonlinear Continuum Mechanics*, Oxford, London, U. K. (1960).

[56] Z. Hashin, D. Bagchi and B. W. Rosen, "Nonlinear Behavior of Fiber Composite Laminates," *NASA CR-2313*, National Aeronautics and Space Administration, Washington, D. D. (1974).

[57] W. Ramberg and W. R. Osgood, "Description of Stress-strain Curve by Three Parameters," *NASA TN 902*, National Aeronautics and Space Administration, Washington, D. D. (1943).

[58] J. R. Rice and G. F. Rosengren, "Plane Strain Deformation Near a Crack Tip in a Power-law Hardening Material," *Journal of Mechanics and Physics of Solids*, Vol. 16, pp. 1-12 (1968).

[59] J. Casey and P. M. Naghi, "Physically Nonlinear and Related Approximate Theories of Elasticity, and Their Invariance Properties," *Archive for Rational Mechanics and Analysis*, Vol. 88, pp. 59-82 (1985).

[60] S. Bharatha and M. Levinson, "On Physically Nonlinear Elasticity," *Journal of Elasticity*, Vol. 7, pp. 307-324 (1977).

[61] S. P. Timoshenko and J. N. Goodier, *Theory of Elasticity*, McGraw-Hill, New York, 1970.

[62] W. Flügge, *Handbook of Engineering Mechanics*,. McGraw-Hill, New York, 1962.

[63] R. M. Christensen and F. M. Waals, "Effective Stiffness of Randomly Oriented Fiber Composites," Journal of Composite Materials, Vol. 6, pp. 518-532 (1972).

13. FIGURES

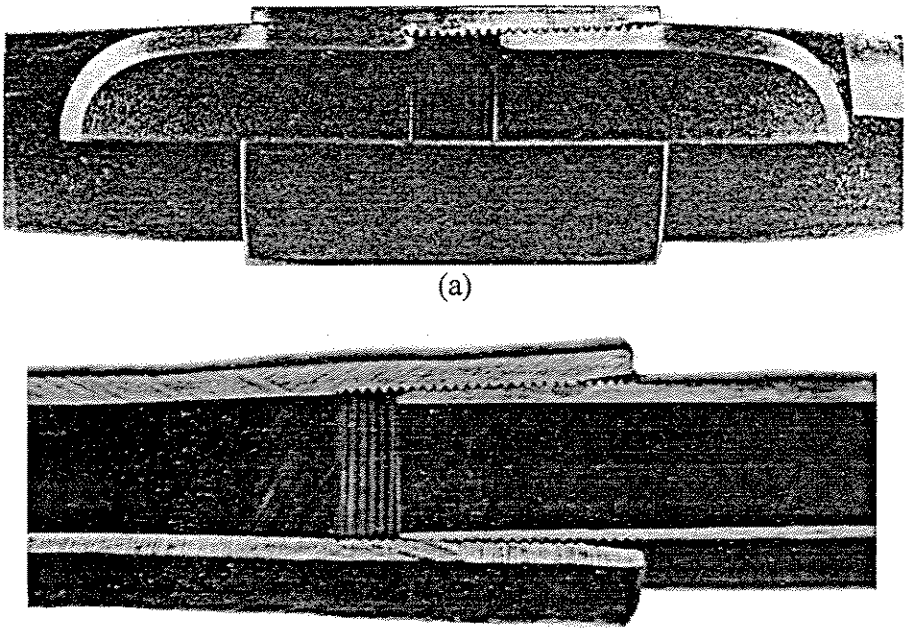

(a)

(b)

Fig. 4-1 Tubular Joints, (a) Threaded and Coupled (T&C) Joint, and (b) Integral Joint (IJ)

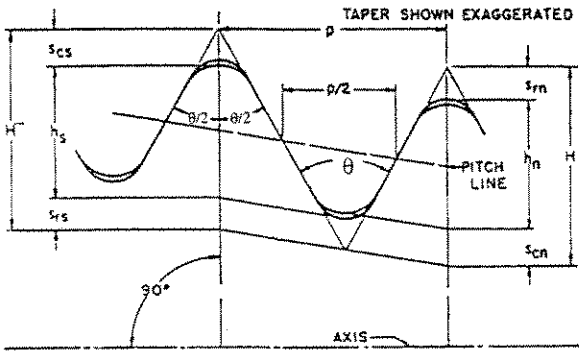

Fig. 4-2 Detailed Thread Geometry for Casing and Tubing Round Threads [38]

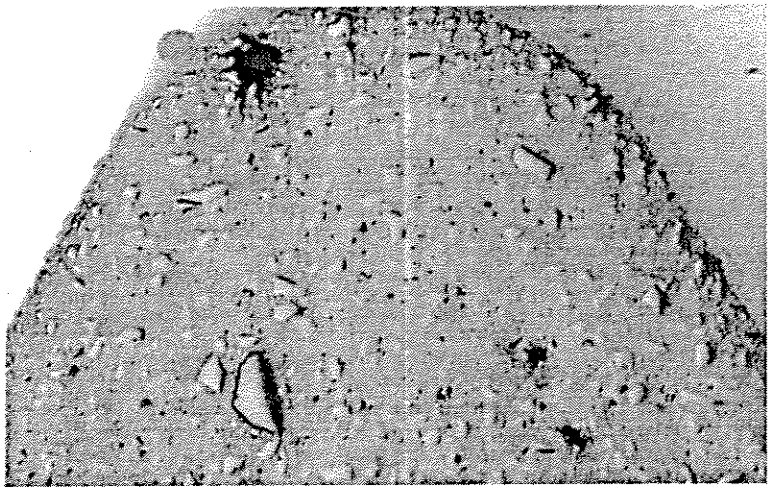

(a)

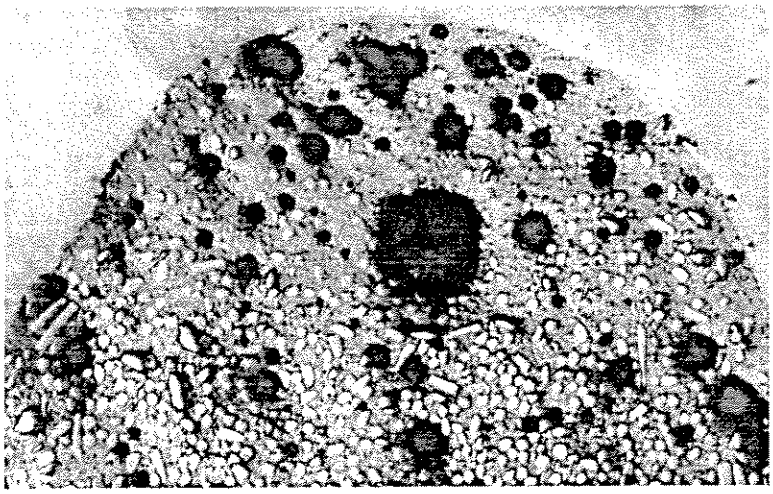

(b)

Fig. 4-3 Microstructure of Threads, (a) Pin-side Thread and (b) Box-side Thread

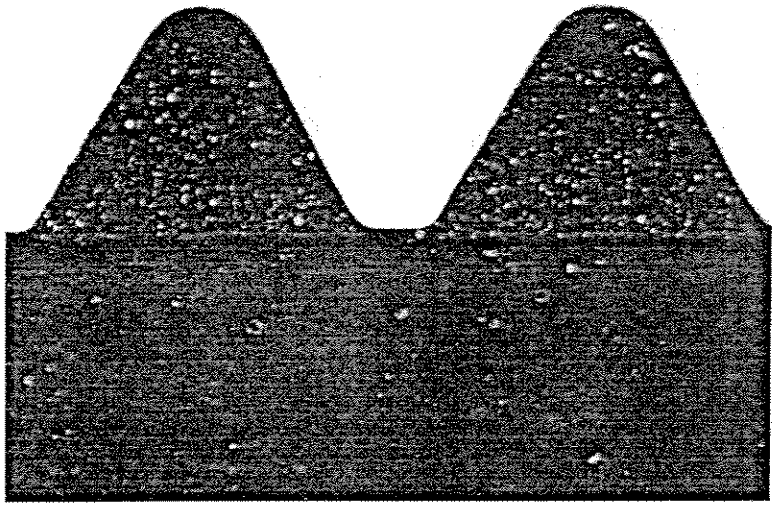

(a)

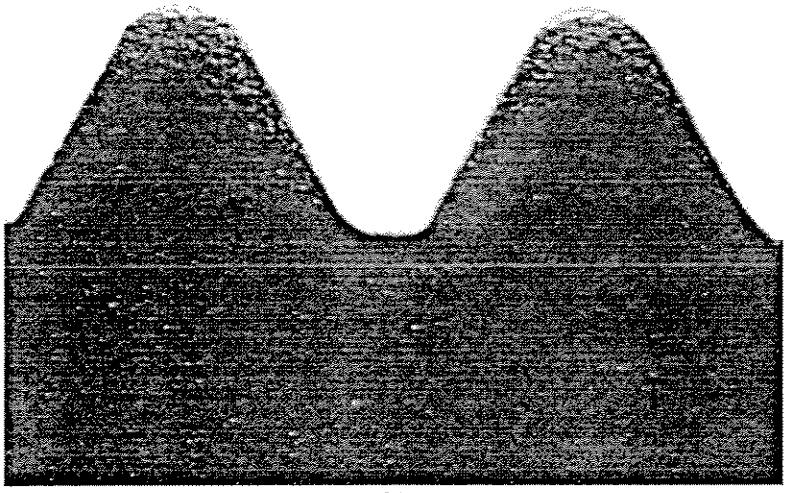

(b)

Fig. 4-4 Threads and Thread/Tube-body Interface at, (a) Pin Side and (b) Box Side, in Integral Composite Joint

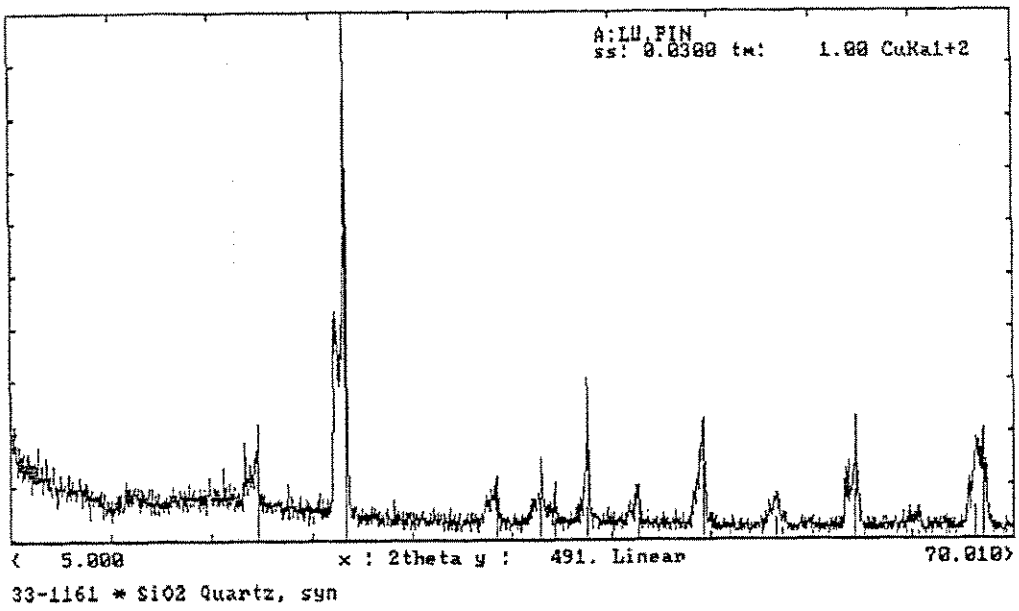

(a)

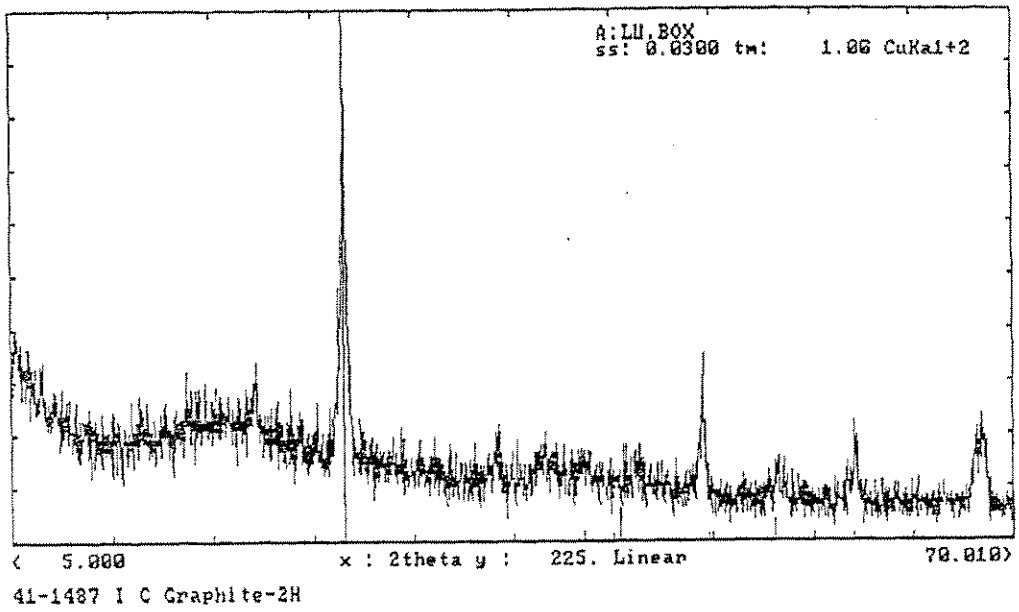

(b)

Fig. 4-5 XRD Patterns of Thread Materials in Integral Composite Joint: (a) Pin-Side Threads, and (b) Box-Side Threads

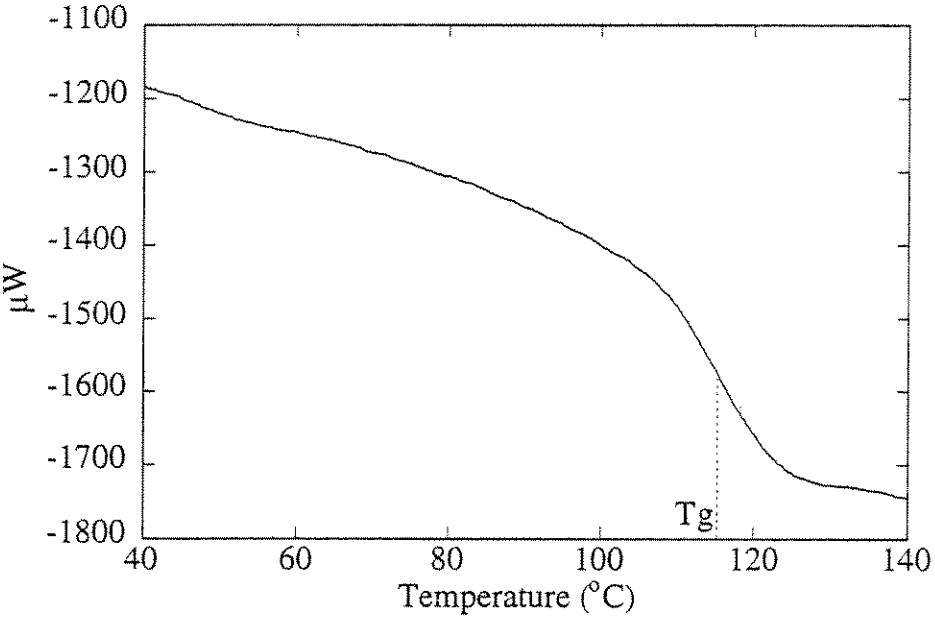

Fig. 4-6a Typical DSC Results of Glass/Epoxy Composite in Threaded Composite Joint

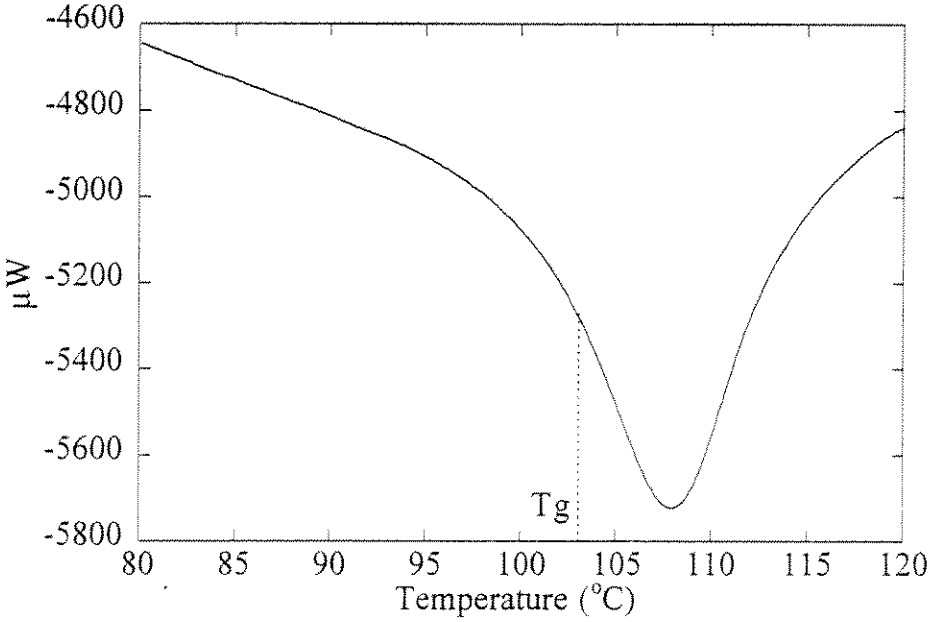

Fig. 4-6b Typical DSC Results of Epoxy Resin in a Filled Thread of an Integral Composite Joint

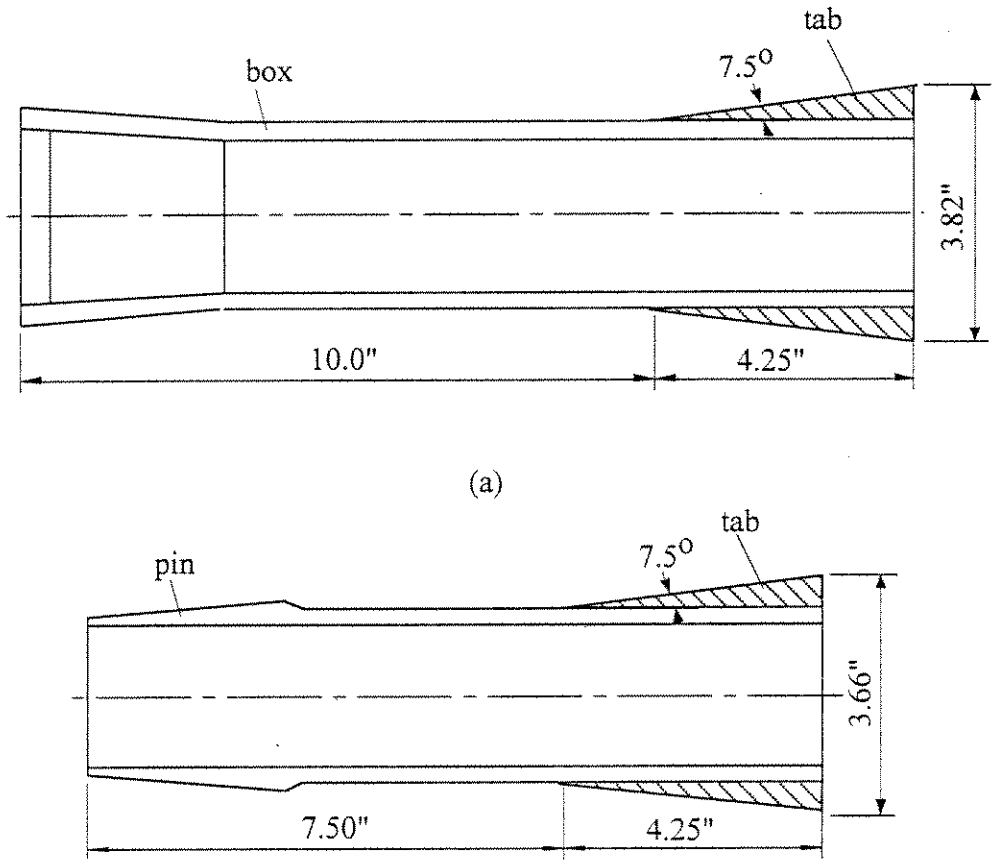

Fig. 5-1 Threaded Composite Joint Specimen, (a) Box Side, and (b) Pin Side

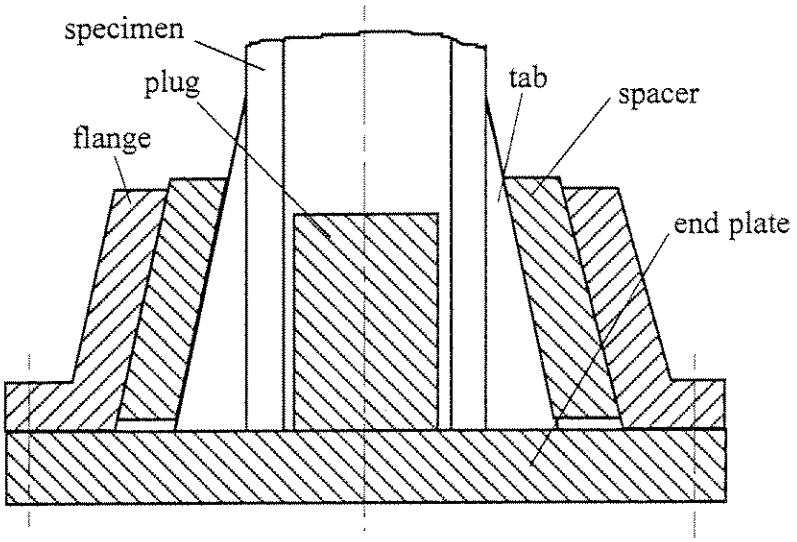

Fig. 5-2 End Gripping Arrangement

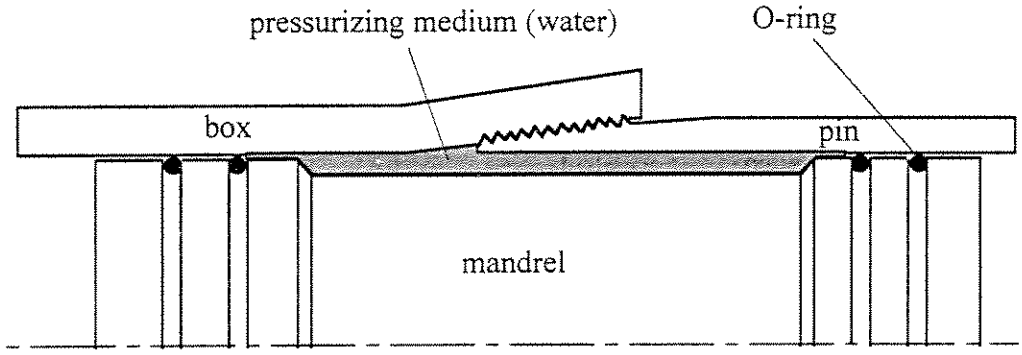

Fig. 5-3 Internal Pressurization (Using a Mandrel in Test System)

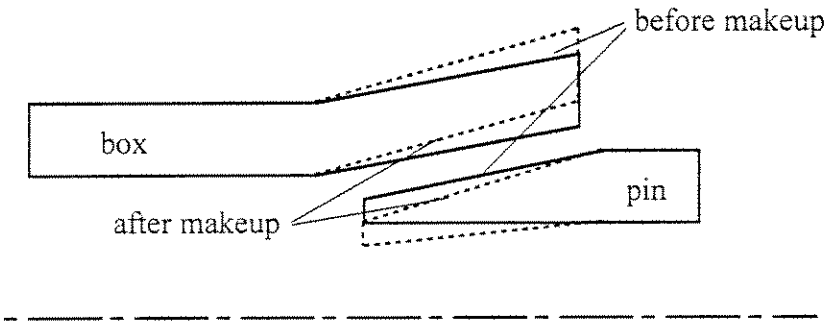

Fig. 5-4 Threaded Joint Deformation Caused by Make-up

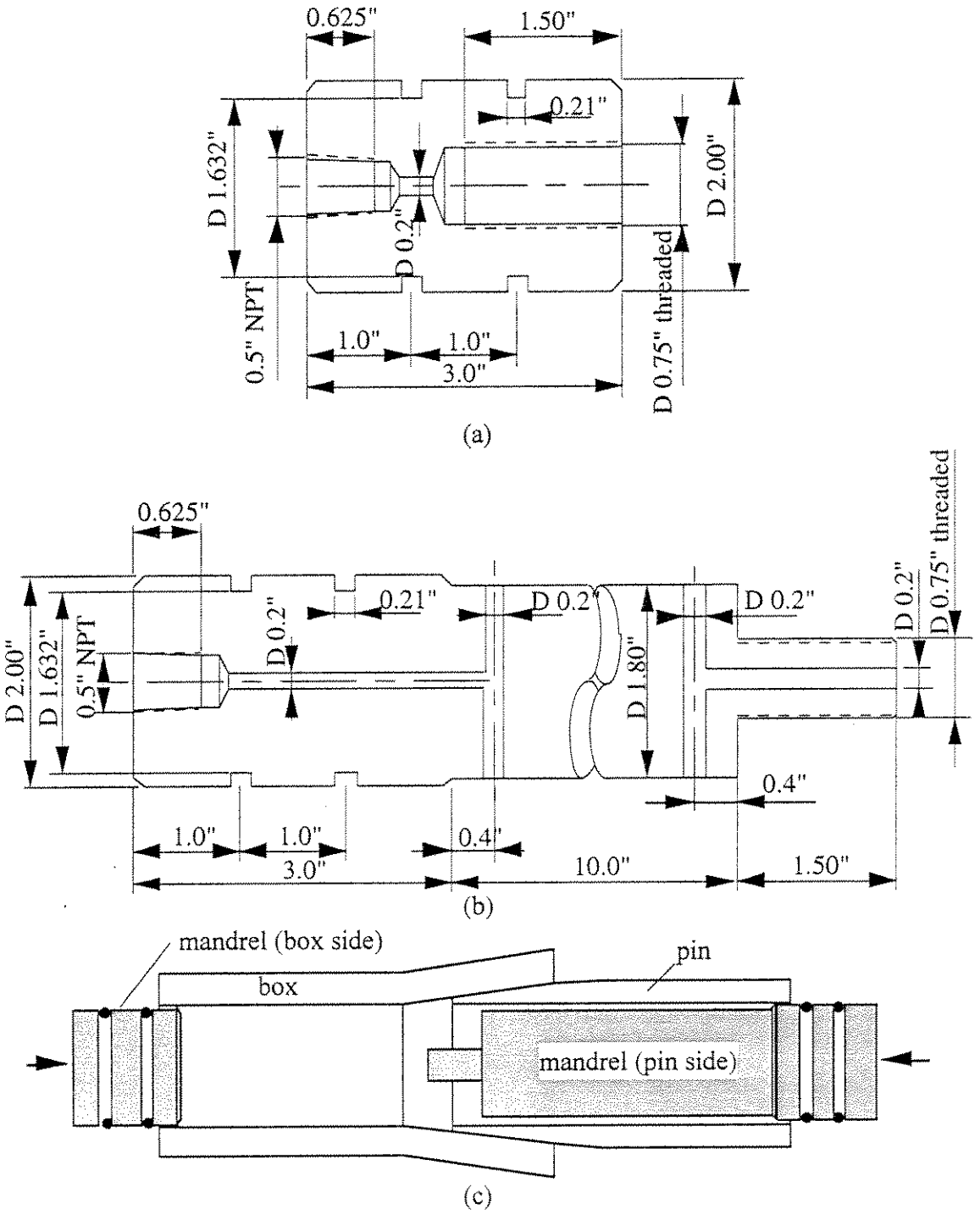

Fig. 5-5 Threaded Tubular Composite Joint Tests; (a) Pin-side Mandrel, (b) Box-side Mandrel, and (c) Installation of Two-piece Mandrel

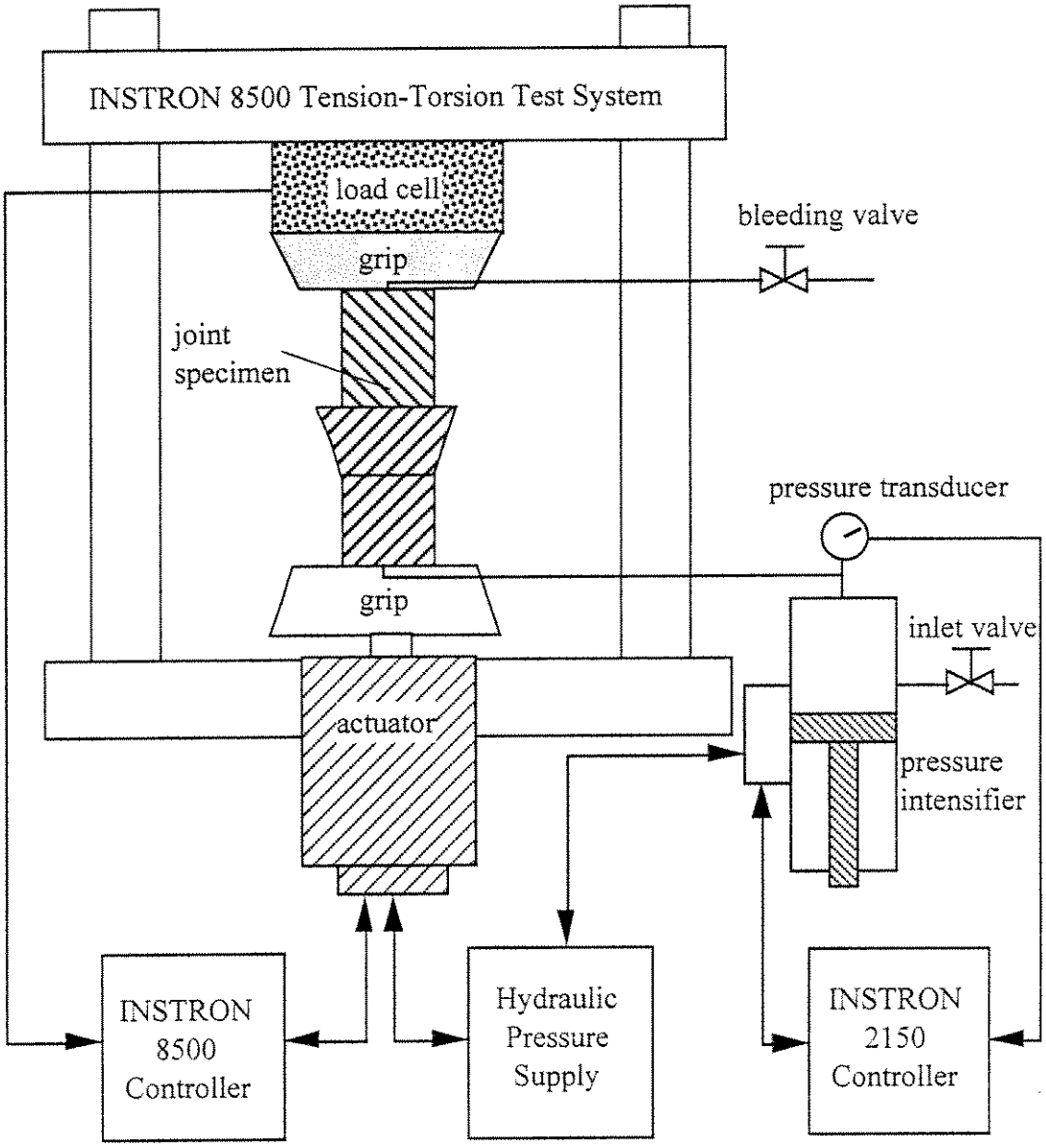

Fig. 5-6 Multiaxial Loading System for Leakage Test of Threaded Composite Joint

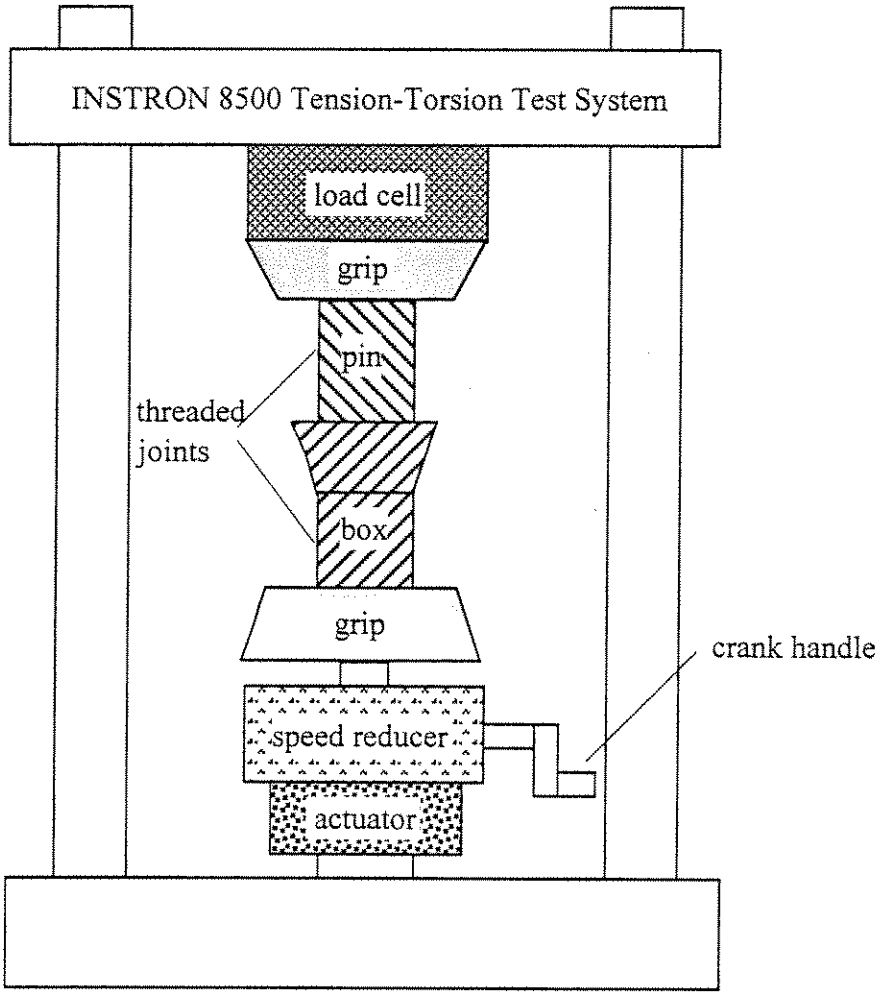

Fig. 5-7 Experimental Setup for Threaded Joint Make-up

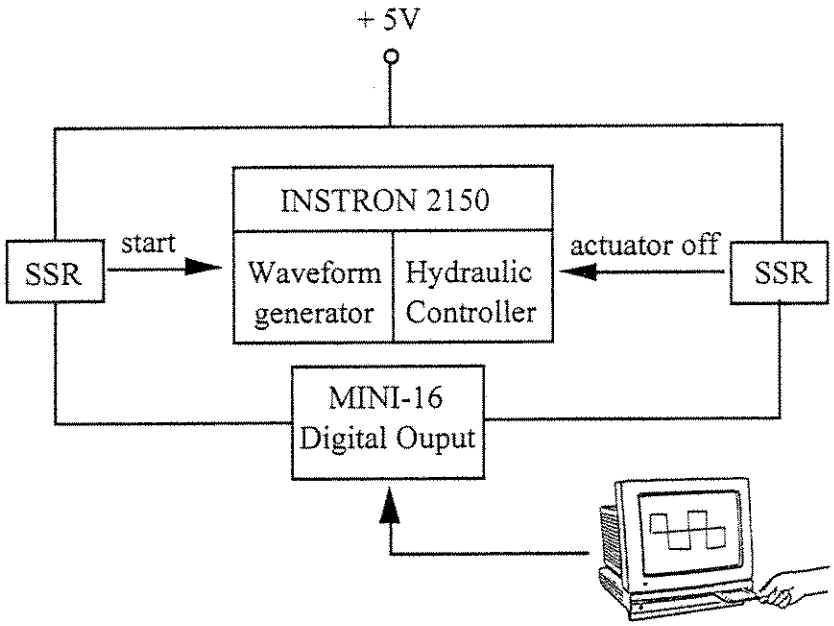

Fig. 5-8 Loading and Unloading Control of Internal Pressure

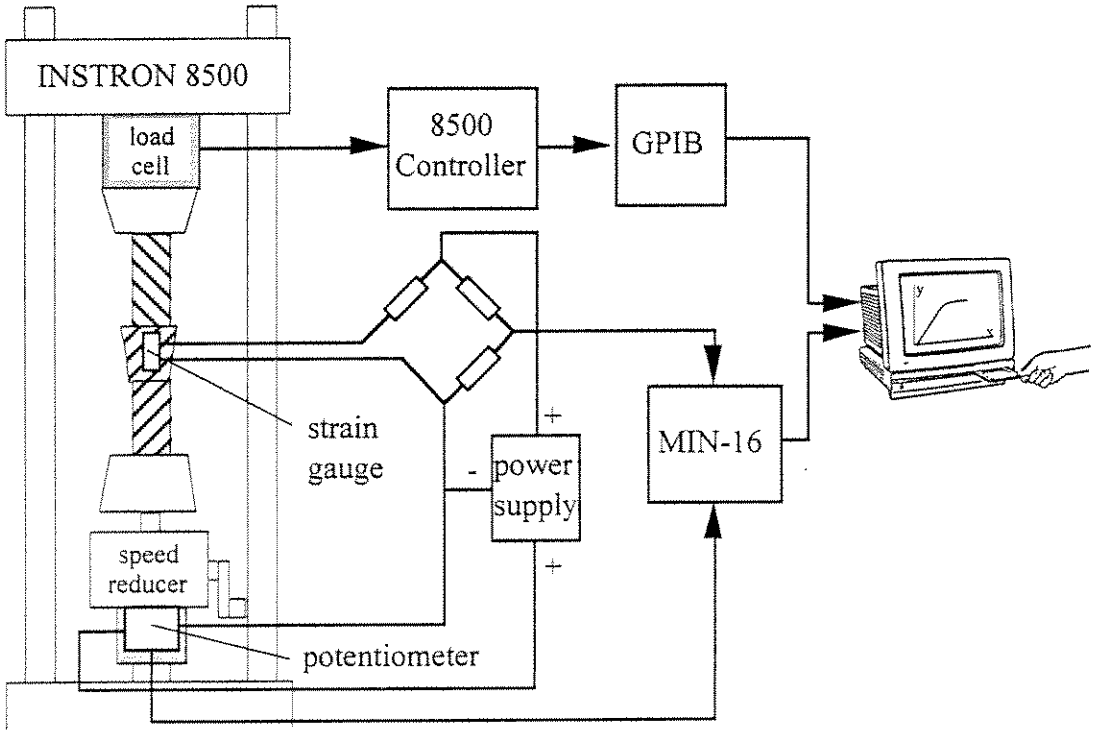

Fig. 5-9 Measurement System for Joint Make-up

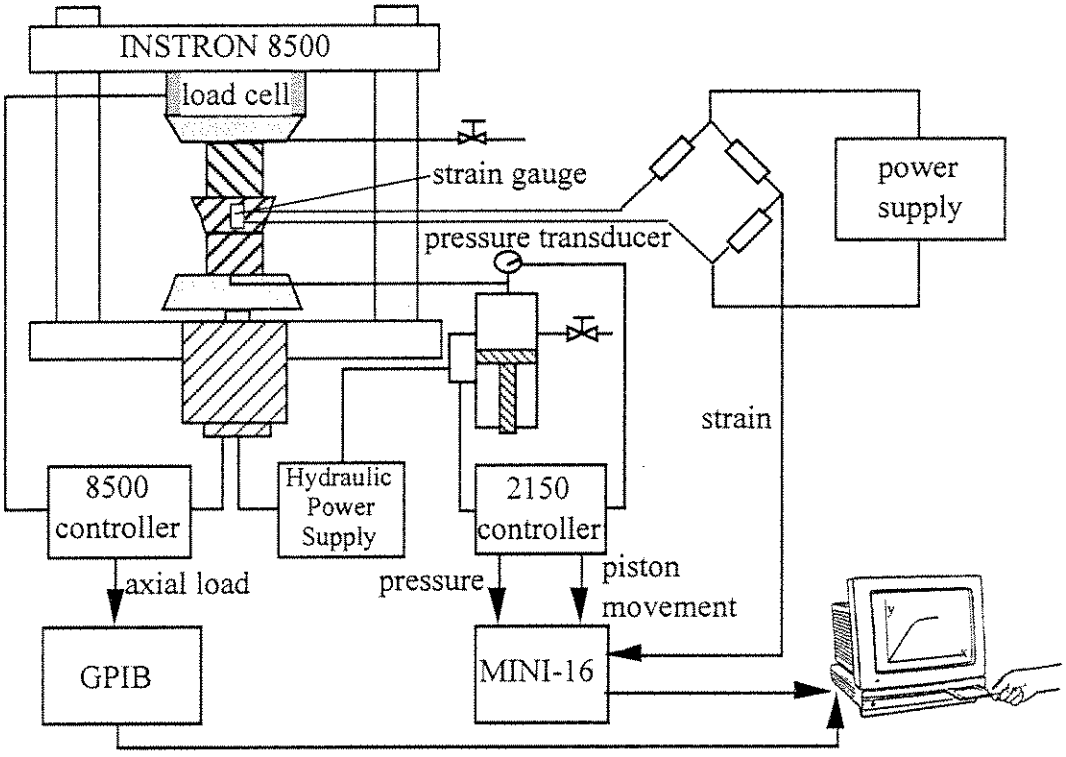

Fig. 5-10 Measurement System for Leakage Experiment of Threaded Composite Joint

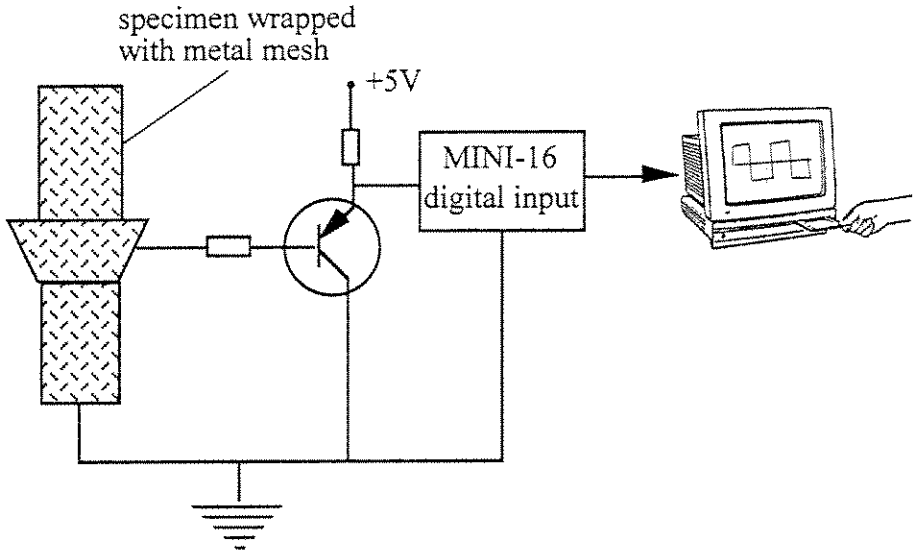

Fig. 5-11 Leakage Detection with Conducting Metal Mesh

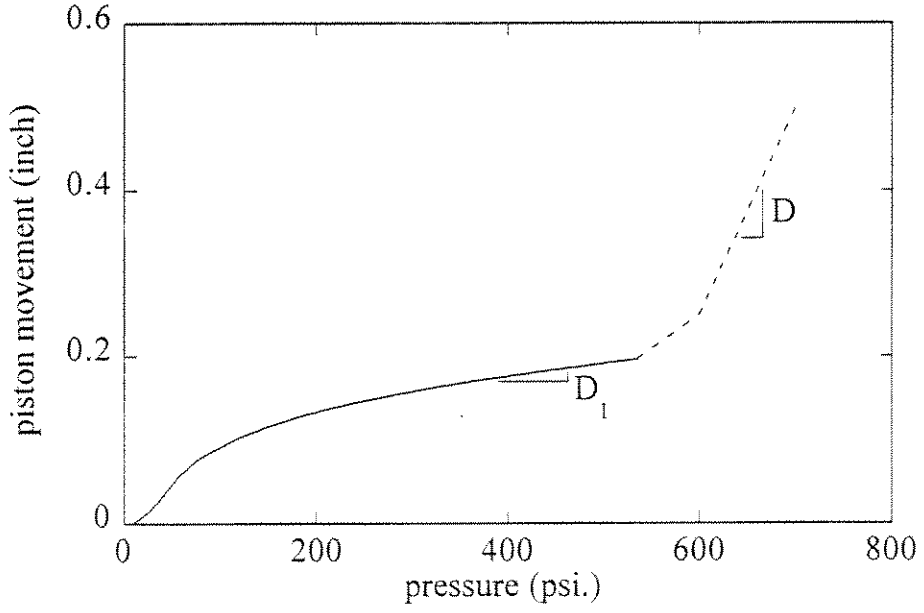

Fig. 5-12 Pressure versus Piston Movement During a Leakage Experiment

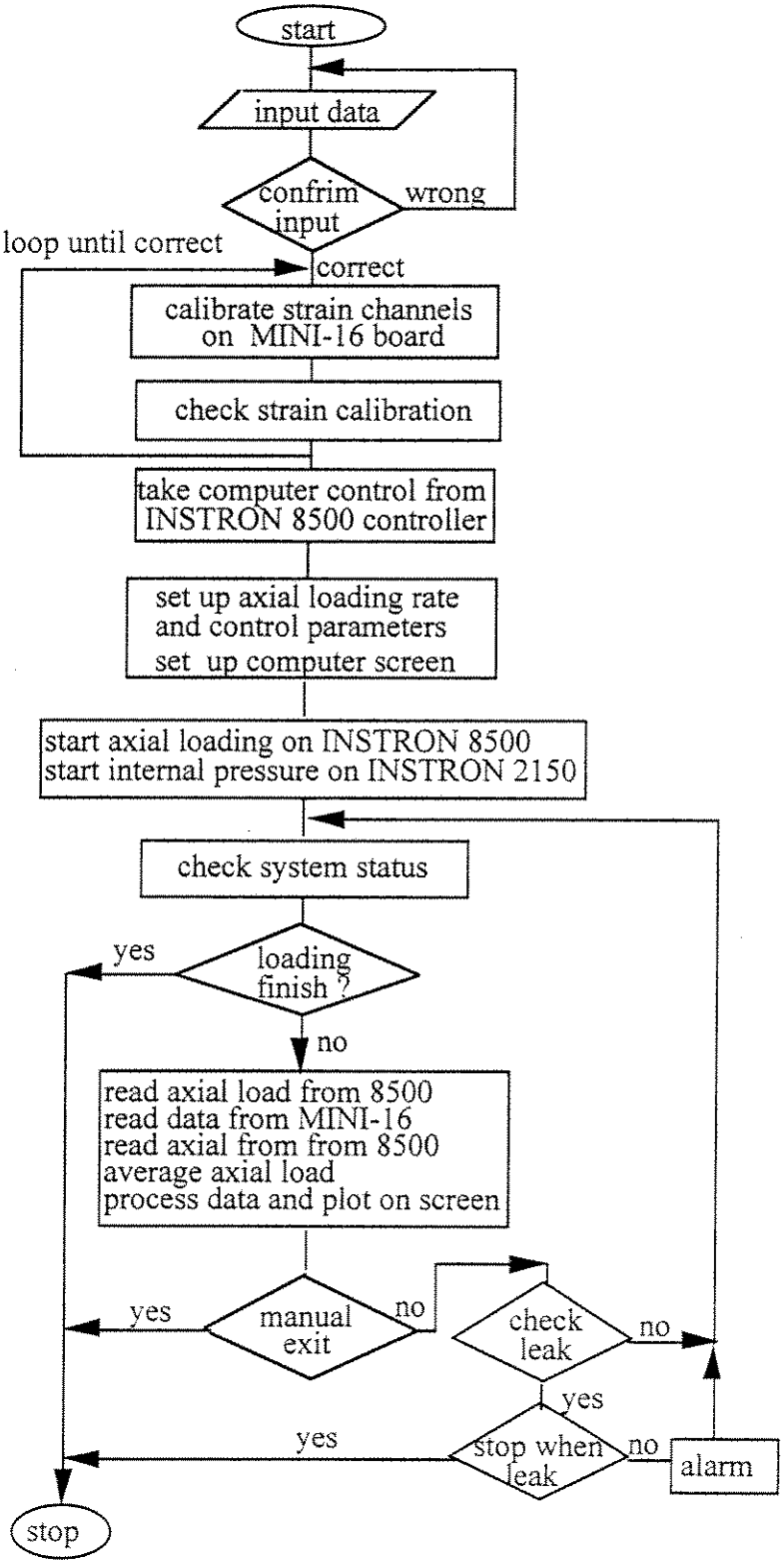

Fig. 5-13 Schematic Representation of Computer Control Program

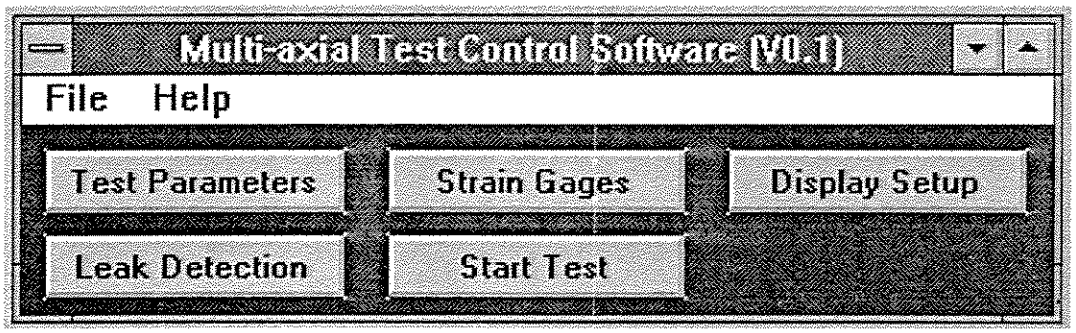

Fig. 5-14 Visual-Basic Computer Control Program

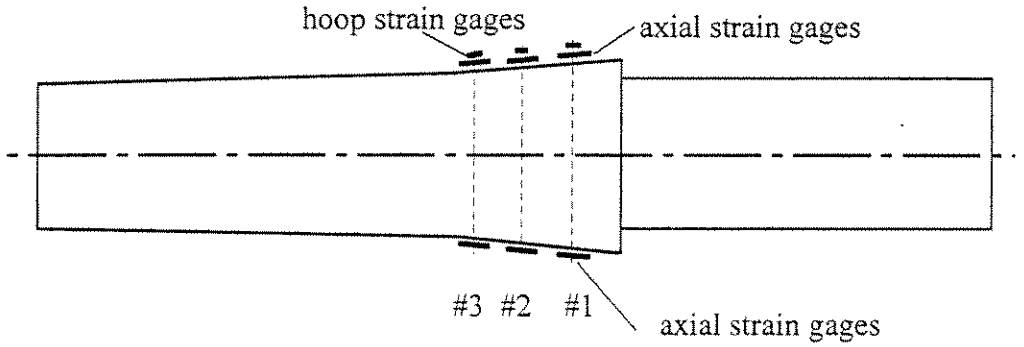

Fig. 5-15 Strain Gage Arrangement in Leakage Failure Experiment

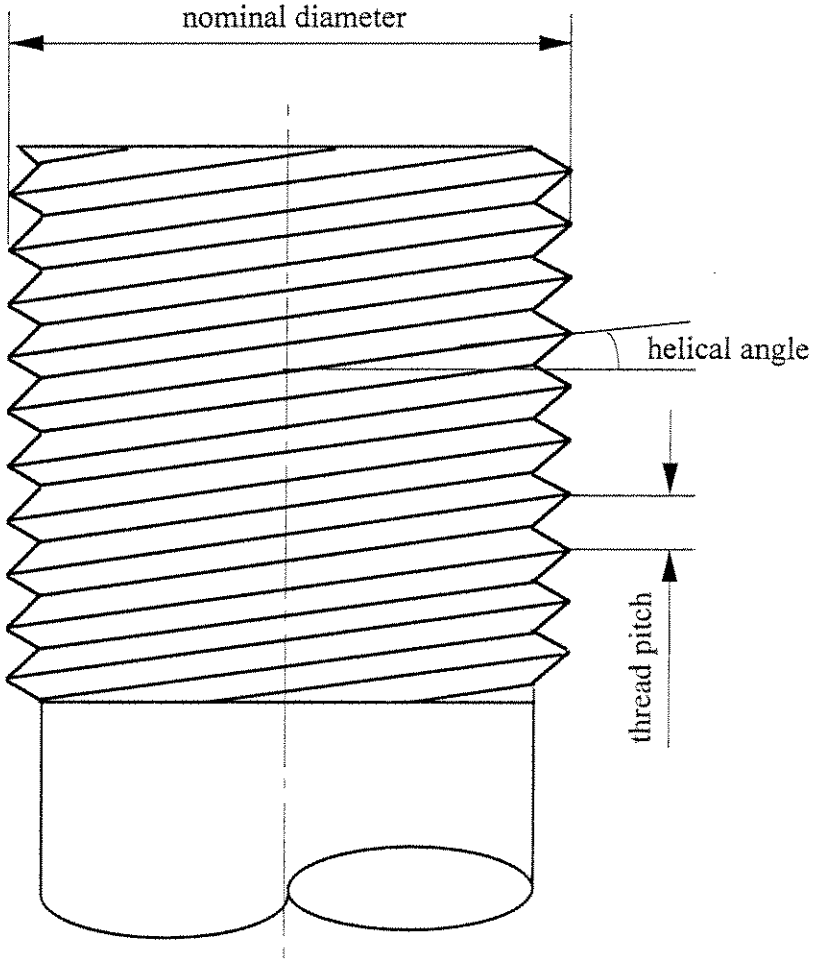

Fig. 6-1 Geometric Parameters of Threads in a Threaded Composite Joint

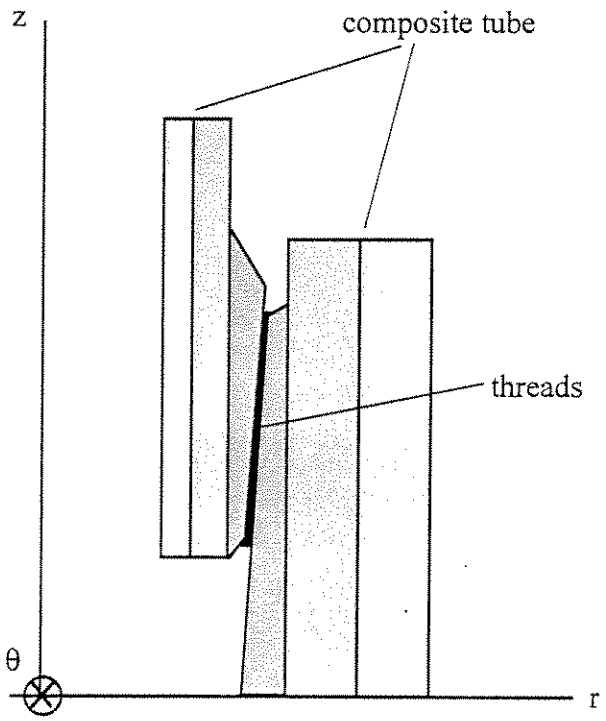

Fig. 6-2 Cylindrical Coordinate System Used in Formulation of Governing Differential Equations

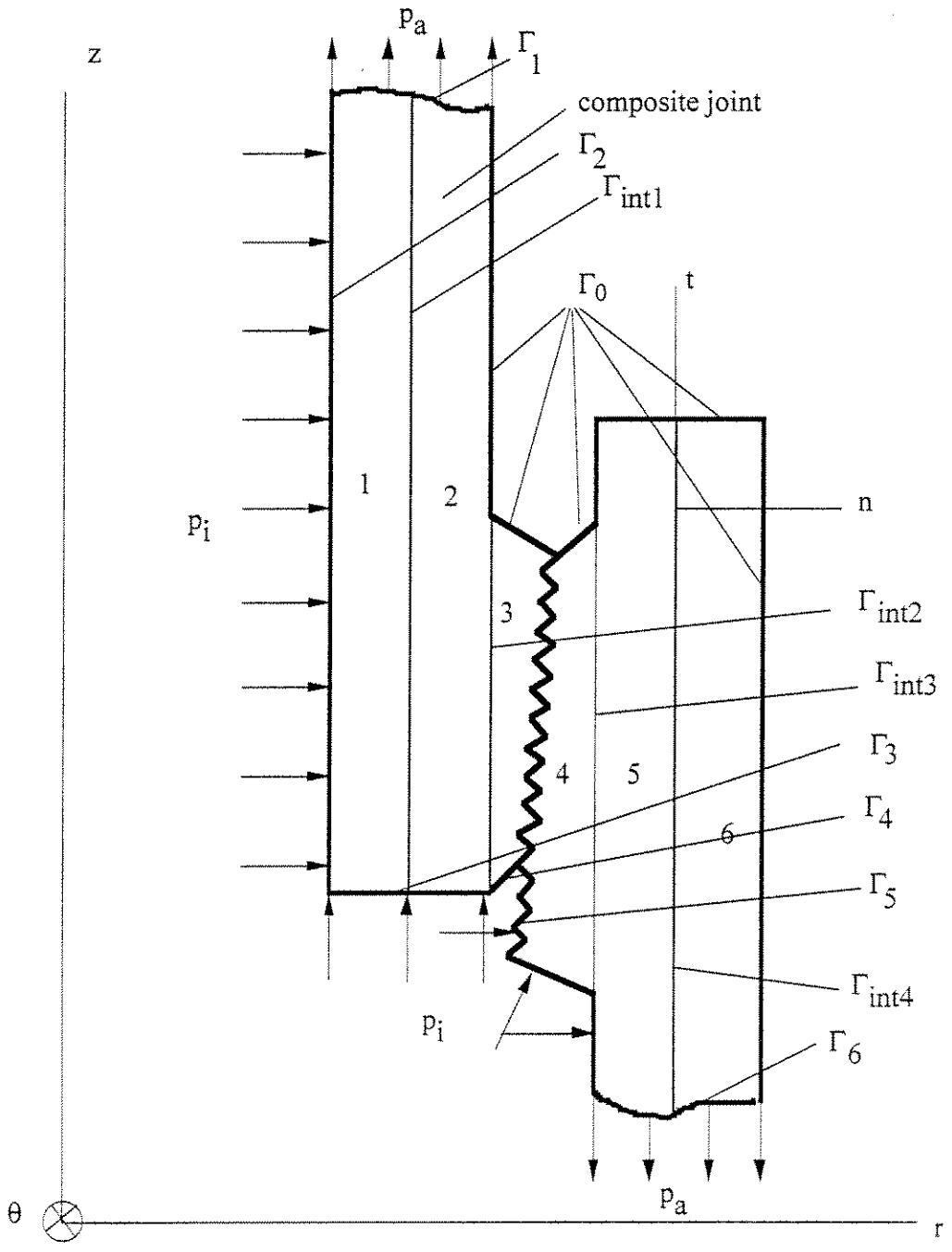

Fig. 6-3 Boundary and Interface Conditions for a Threaded Composite Tubular Joint

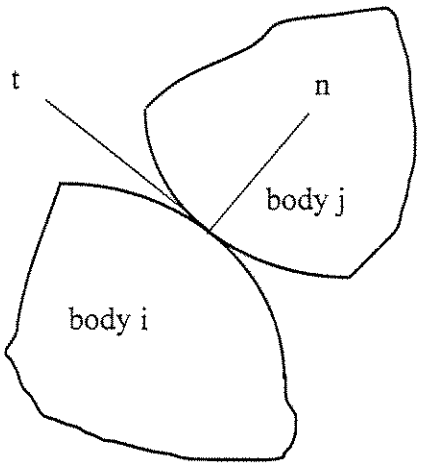

Fig. 6-4 Local Coordinates for Contact

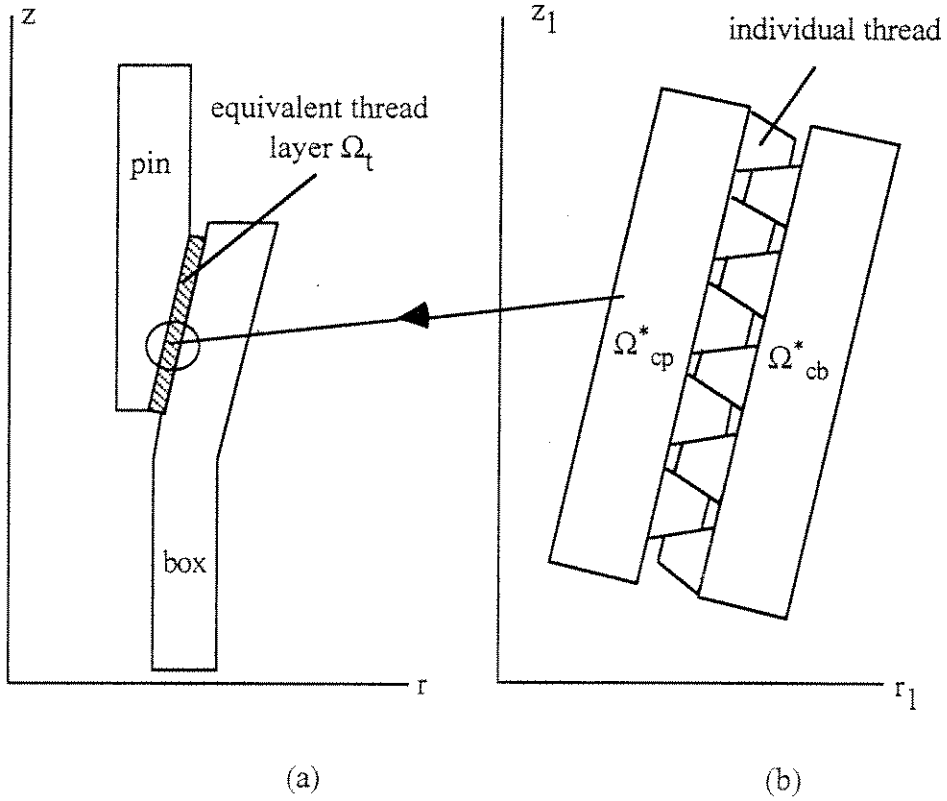

Fig. 7-1 Coupled Global-local Modeling of Threaded Tubular Composite Joint; (a) Global Modeling with an Equivalent Thread Layer, (b) Local Modeling of a Selected Domain with Detailed Substructure

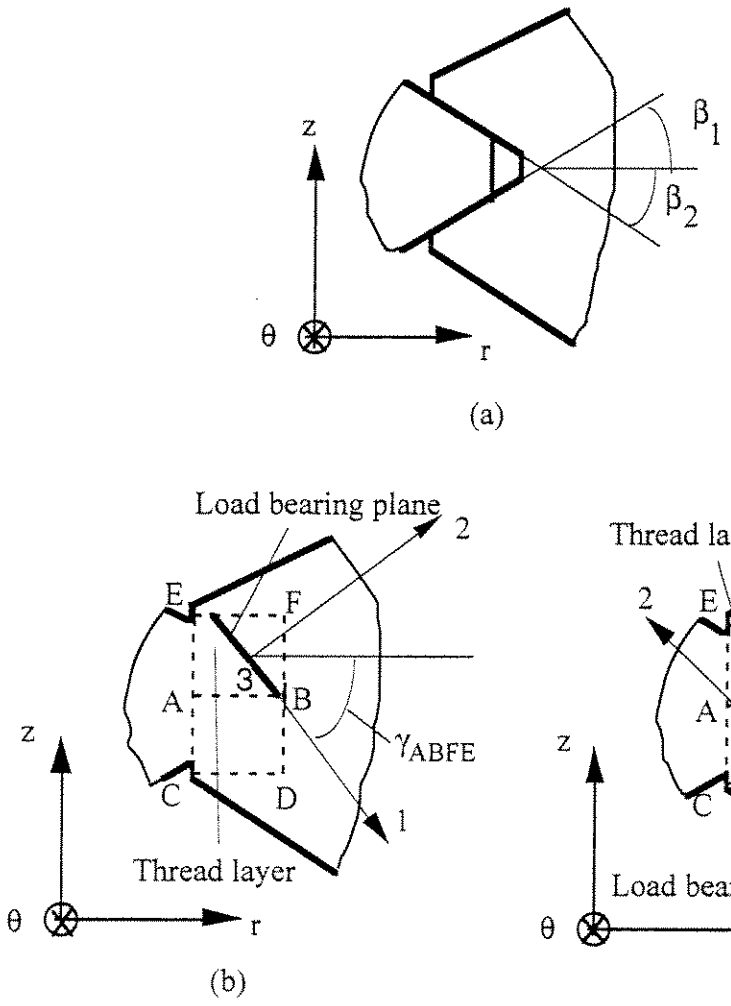

Fig. 7-2 Load-bearing Plane of Equivalent Thread Layer; (a) Actual Local Thread Engagement, (b) Loading-bearing Plane in ABFE, and (c) Load-bearing Plane in ABDC

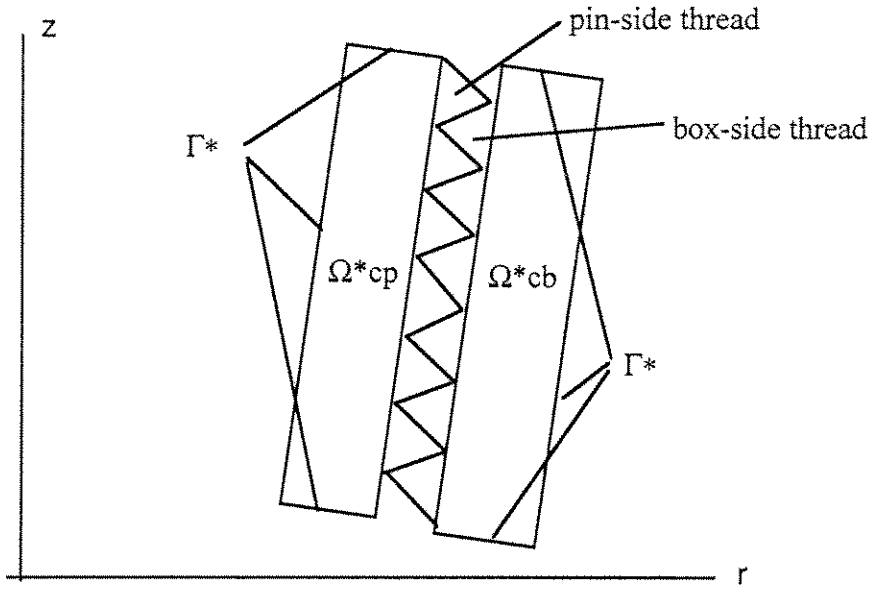

Fig. 7-3 Local Modeling of Tubular Composite Threaded Joint

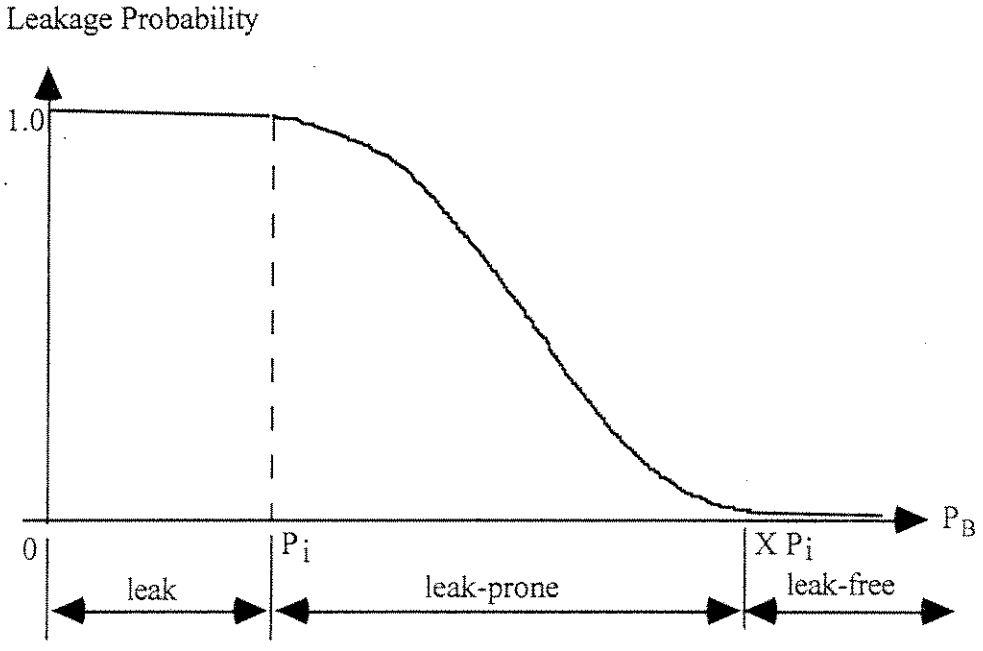

Fig. 8-1 Leakage Probability vs. Bearing Pressure for a Threaded Fiber-composite Tubular Joint

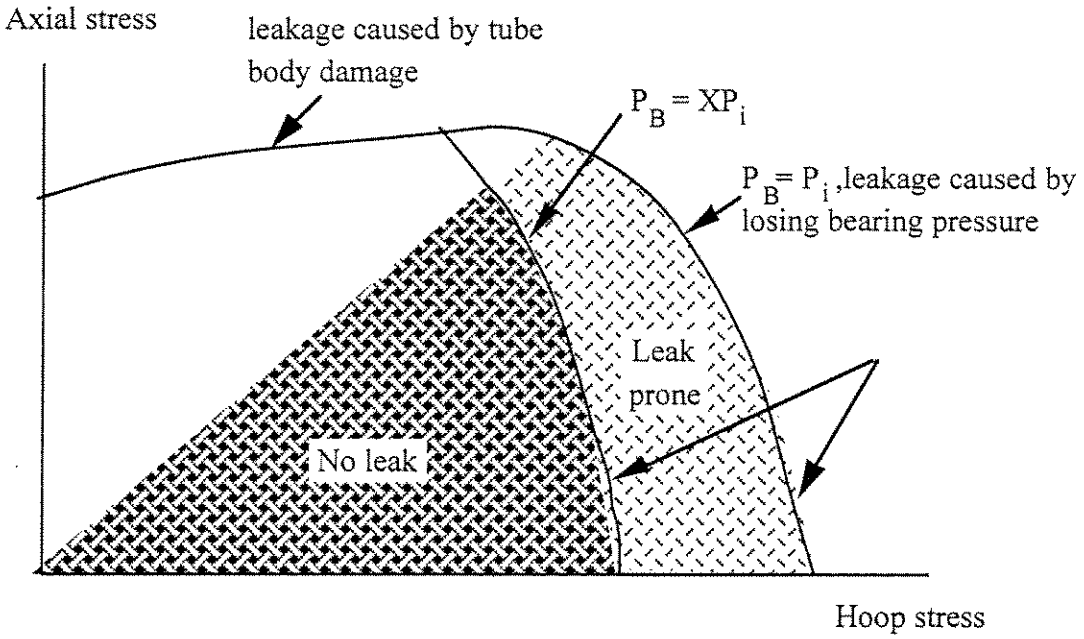

Fig. 8-2 Schematic Leakage Failure Envelope

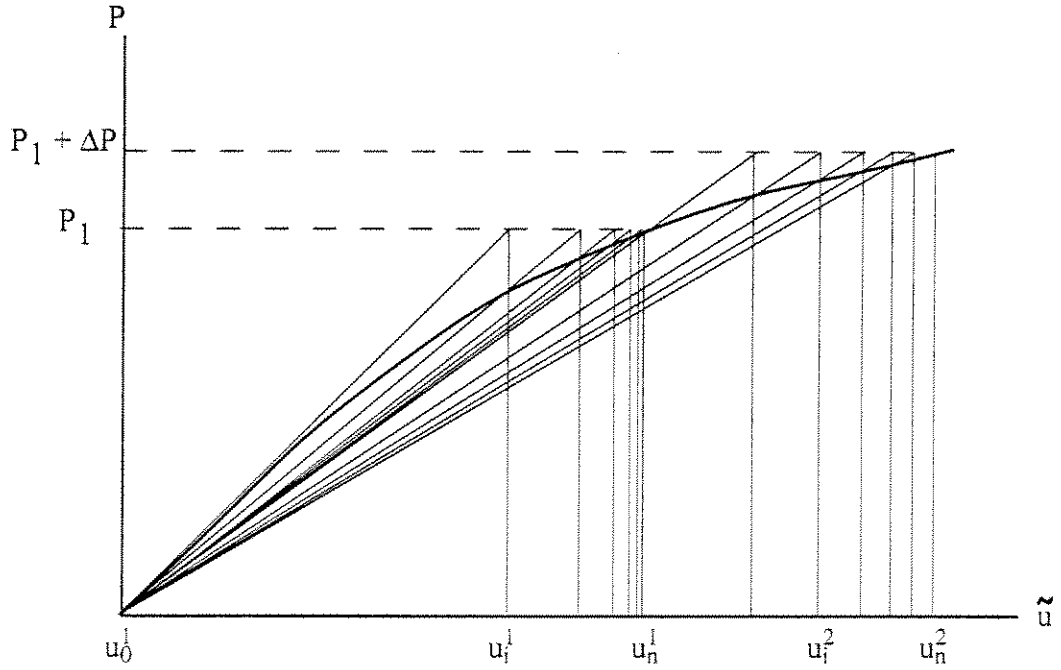

Fig. 9-1 Incremental-iterative Scheme for Material Nonlinearity in Finite-element Analysis

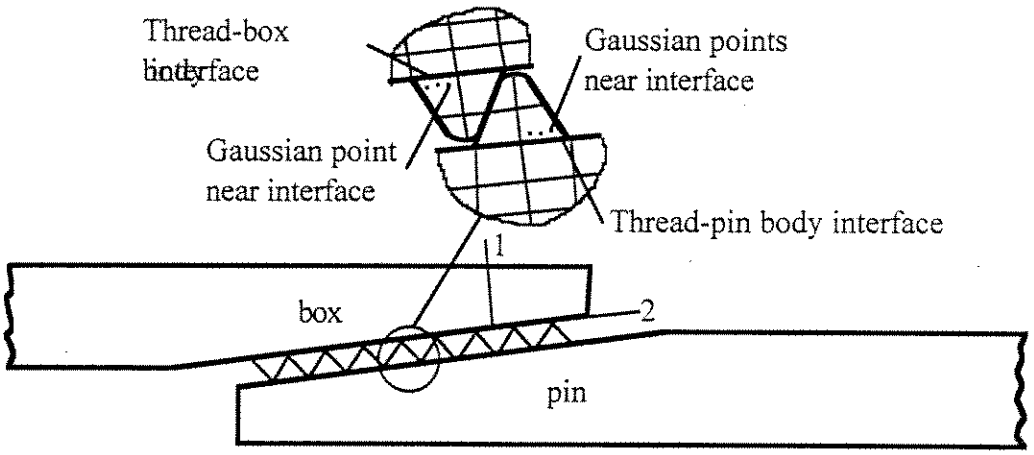

Fig. 9-2 Finite-Element Discretization and Associated Gaussian Points Near the Thread-Tube Body Interface

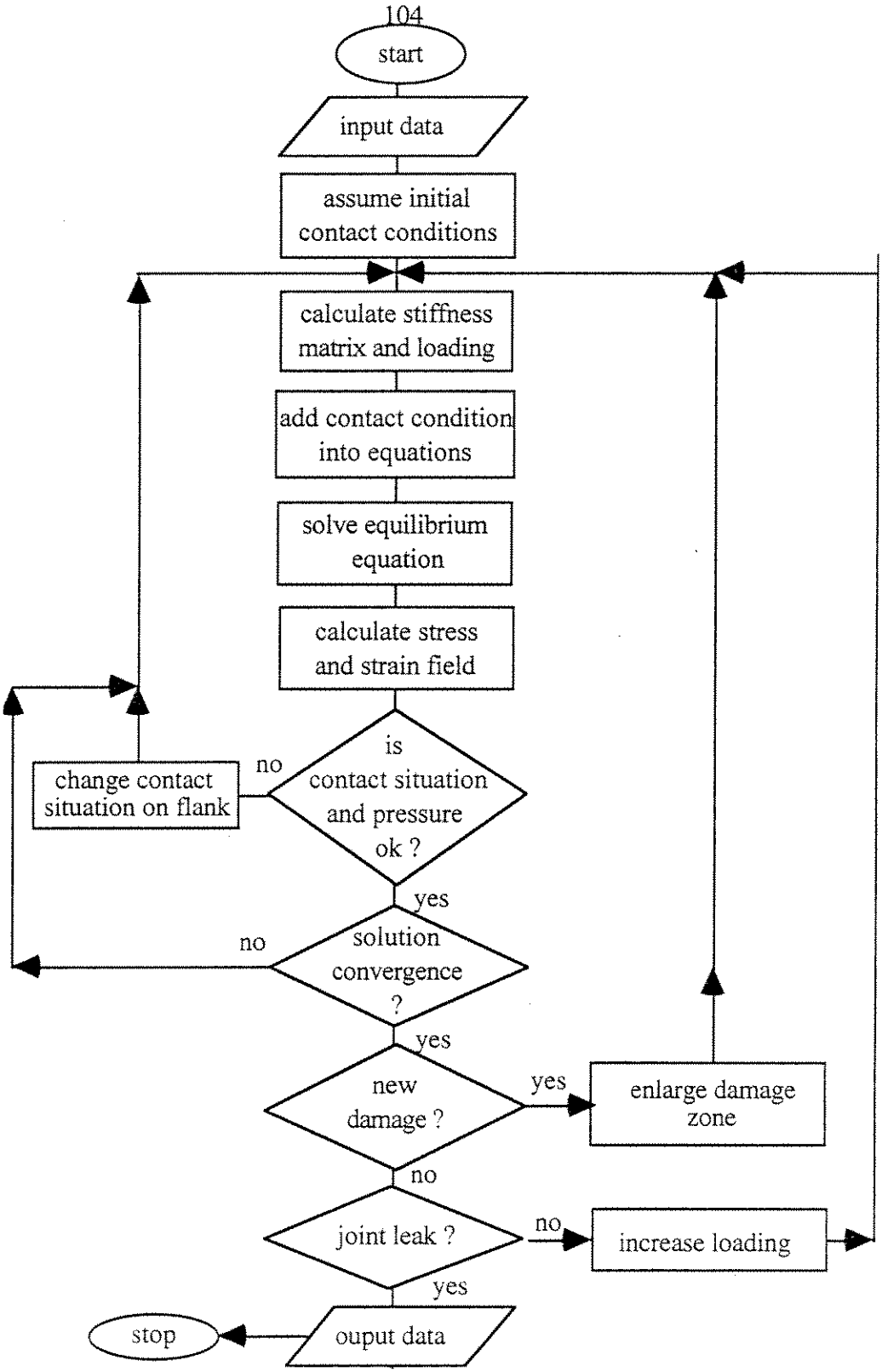

Fig. 9-3 Computational Algorithm and Incremental-iterative Solution Scheme for Analysis and Prediction of Composite Joint Leakage

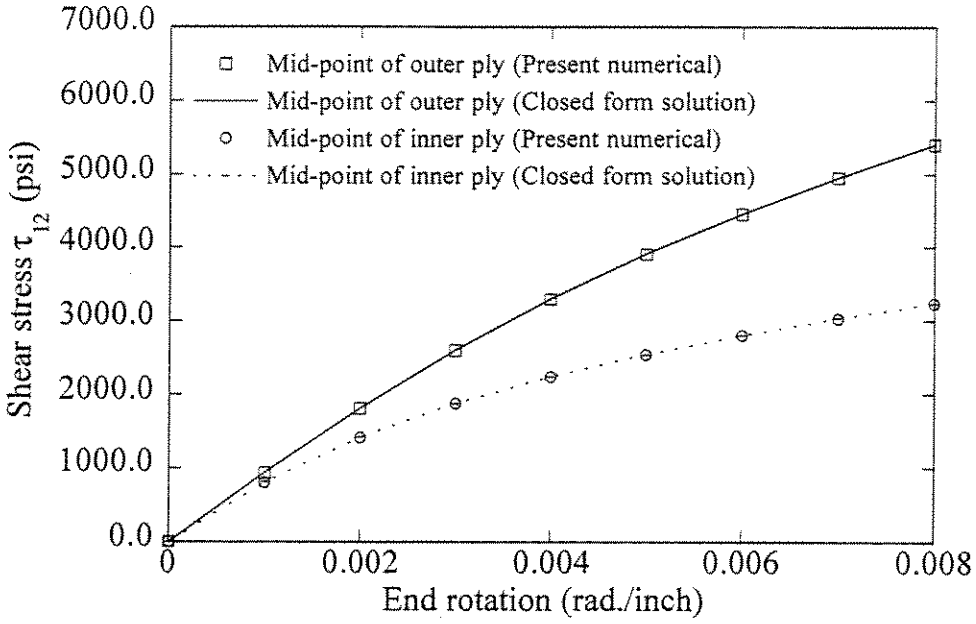

Fig. 9-4 Shear Stress in Two-layer, Long Composite Tube under End Torsion

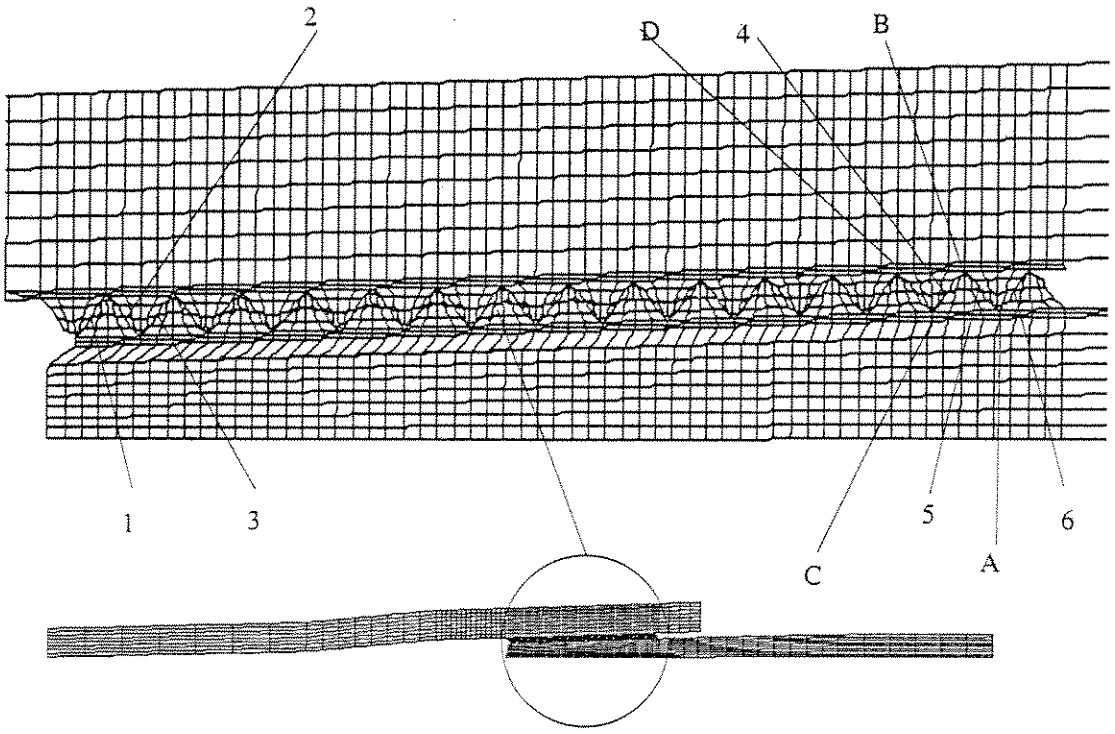

Fig. 9-5a Finite-element Discretization for Global Modeling of Threaded Composite Joint

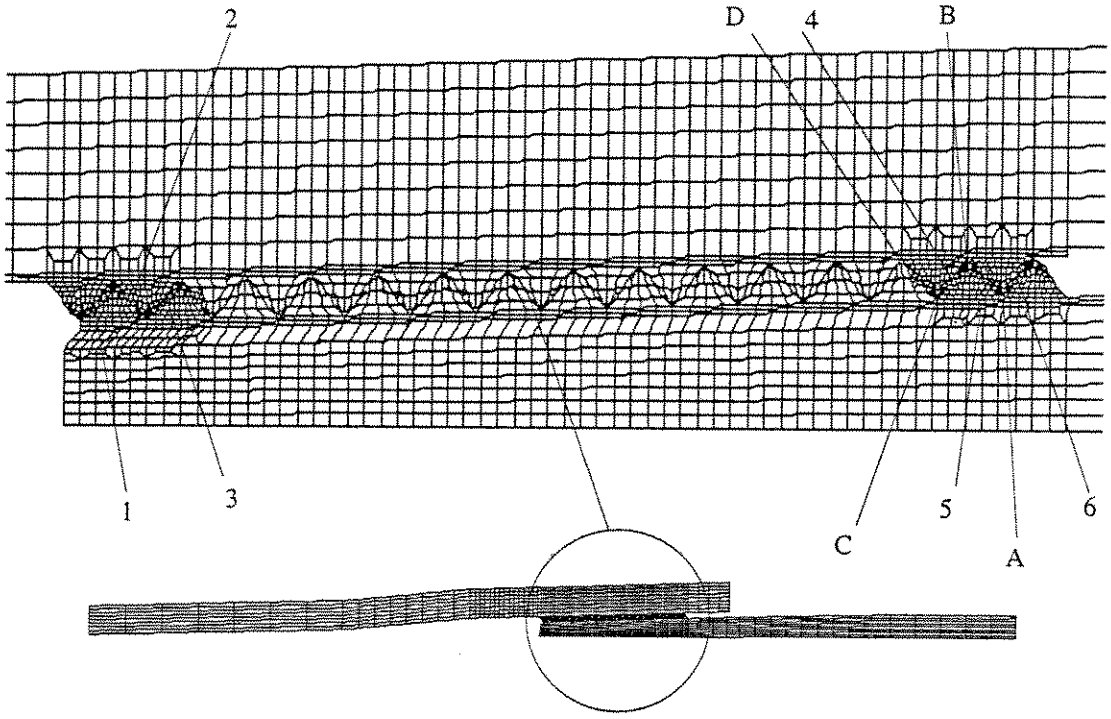

Fig. 9-5b Locally Enriched Mesh for Threaded Composite Joint

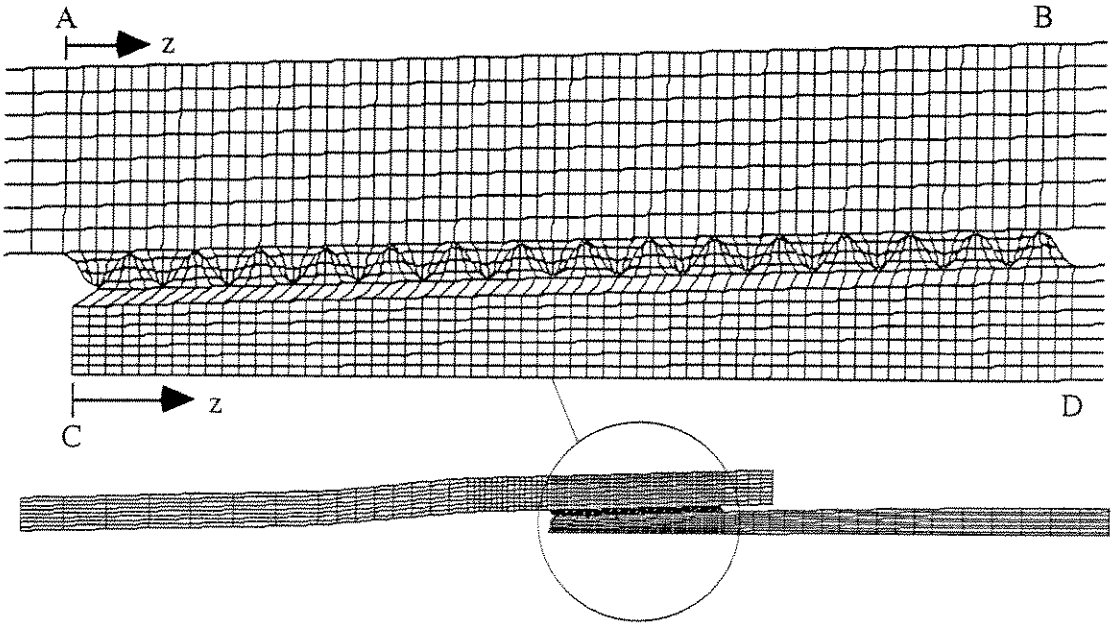

Fig. 9-6 Finite Element Mesh for Direct Full-Field Modeling

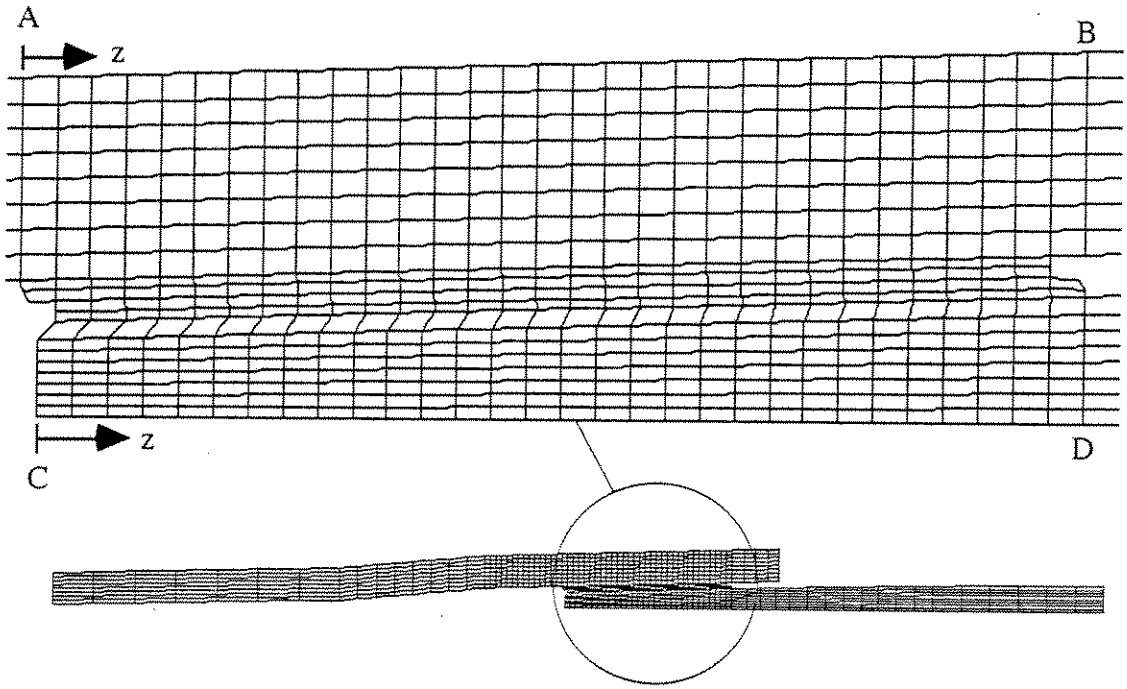

Fig. 9-7 Global Model for a Threaded Composite Tubular Joint with an Equivalent Thread Layer

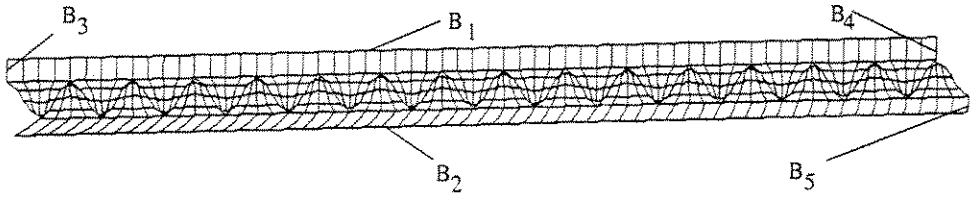

Fig. 9-8 Local Model for Individual Threads in a Composite Tubular Joint

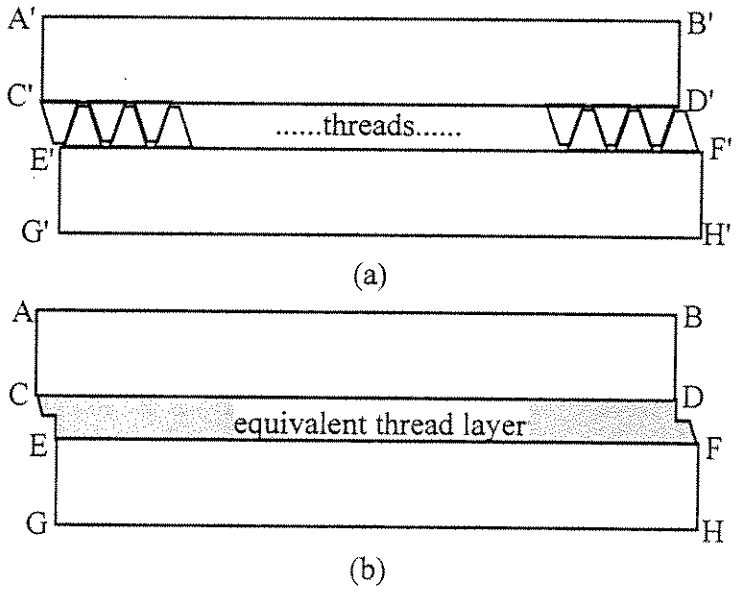

Fig. 9-9 Modeling Threads in Composite Joint; (a) Local-Scale Model, and (b) Global-Scale Model

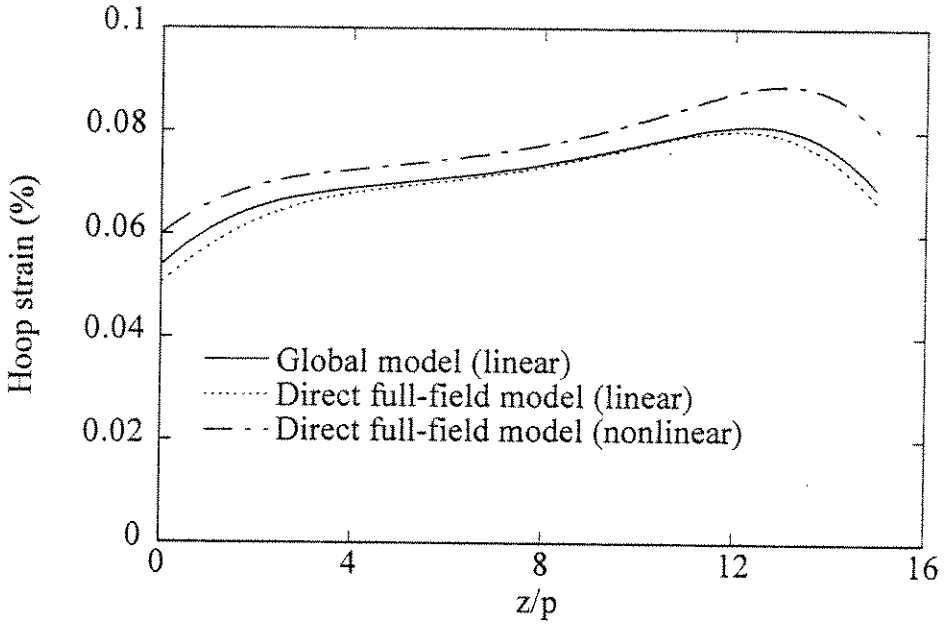

Fig. 9-10 Hoop Strain along External Surface AB of Box Section in Threaded Composite Joint with One-turn Make-up (p=0.125 inch)

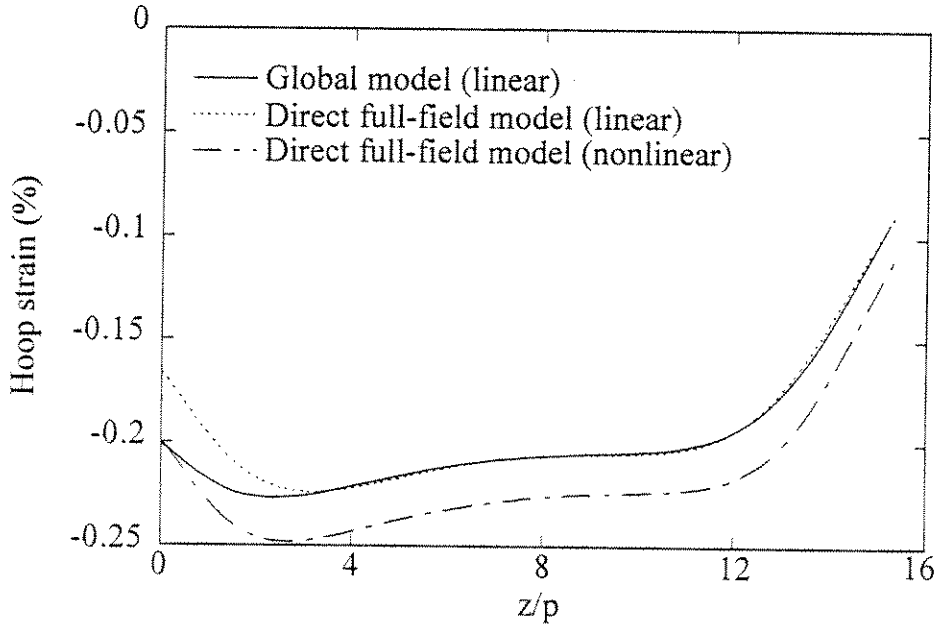

Fig. 9-11 Hoop Strain along Internal Surface CD of Pin Section in Threaded Composite Joint with One-turn Make-up (p=0.125 inch)

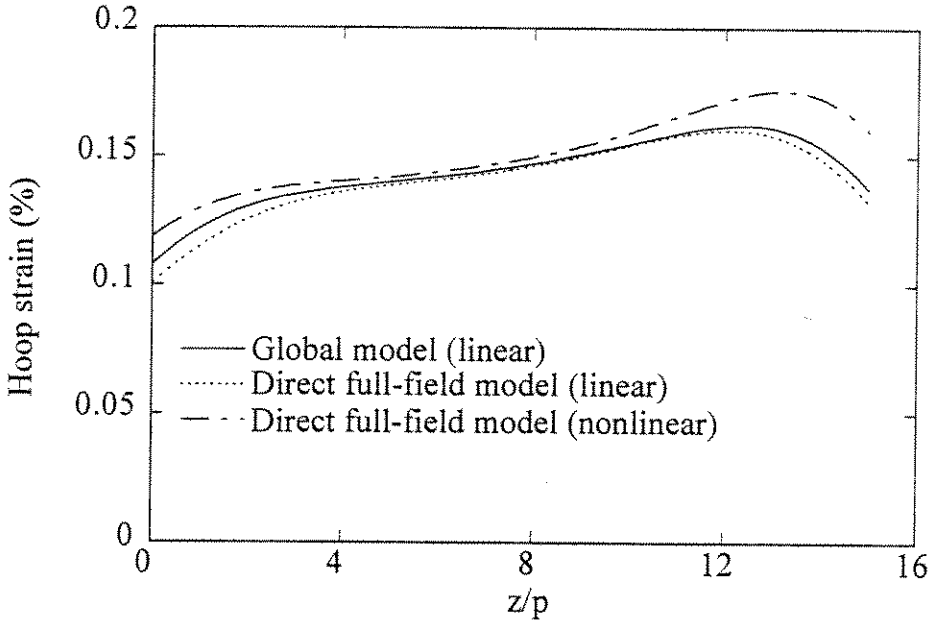

Fig. 9-12 Hoop Strain along External Surface AB of Box Section in Threaded Composite Joint with Two-turn Make-up (p=0.125 inch)

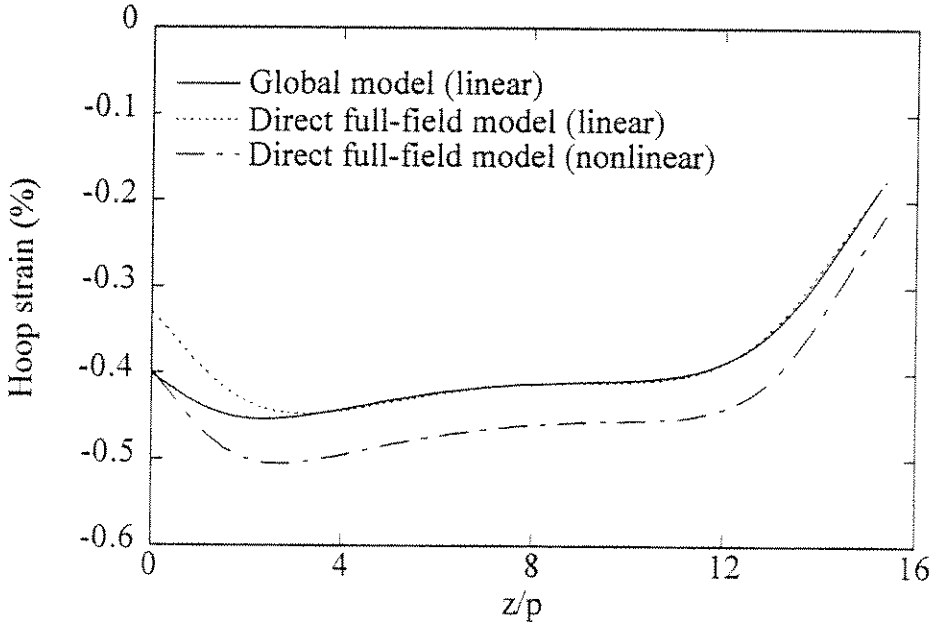

Fig. 9-13 Hoop Strain along Internal Surface CD of Pin Section in Threaded Composite Joint with Two-turn Make-up (p=0.125 inch)

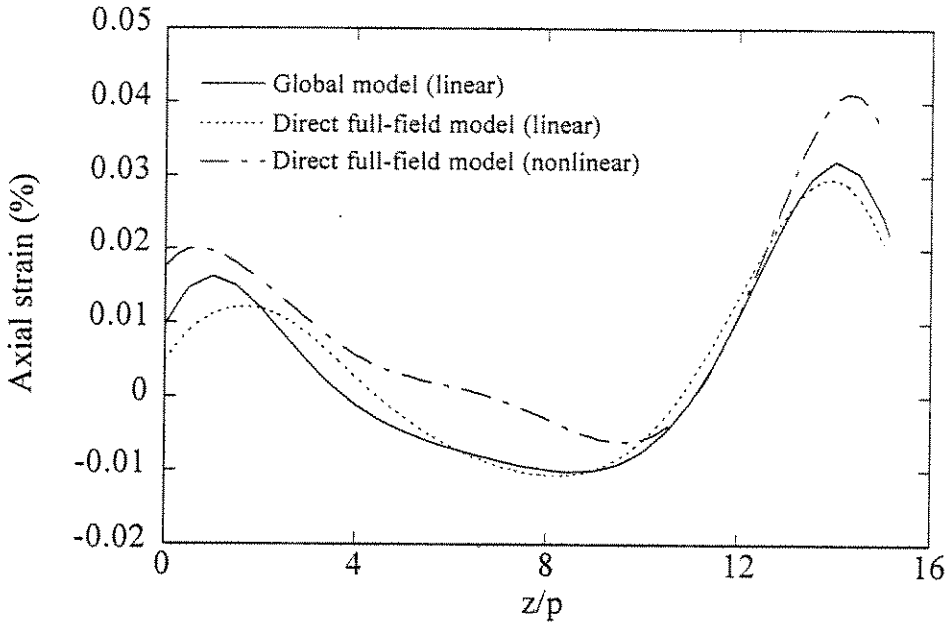

Fig. 9-14 Axial Strain along External Surface AB of Box Section in Threaded Composite Joint with One-turn Make-up (p=0.125 inch)

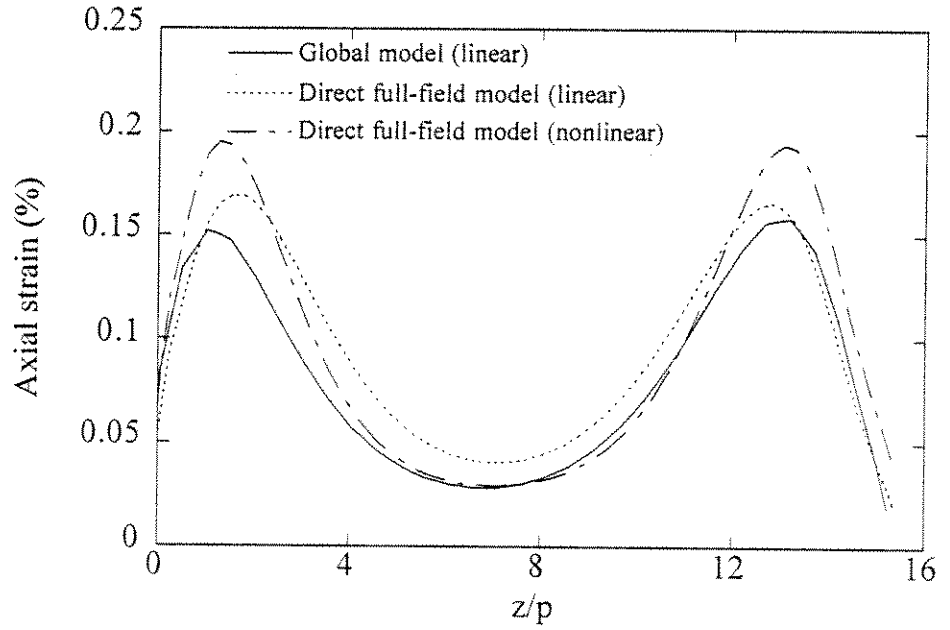

Fig. 9-15 Axial Strain along Internal Surface CD of Pin Section in Threaded Composite Joint with One-turn Make-up (p=0.125 inch)

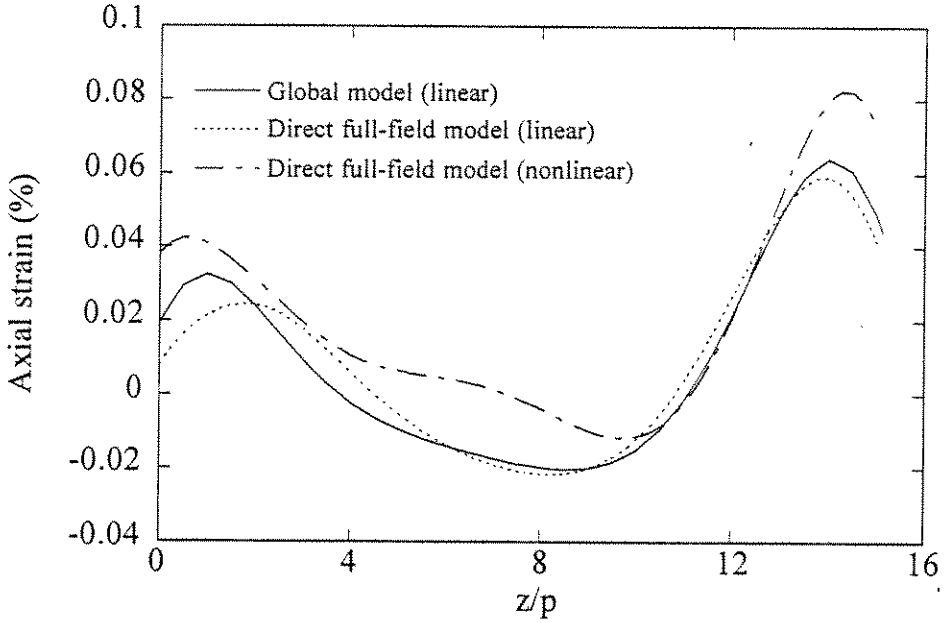

Fig. 9-16 Axial Strain along External Surface AB (or A'B') of Box Section in Threaded Composite Joint with Two-turn Make-up (p=0.125 inch)

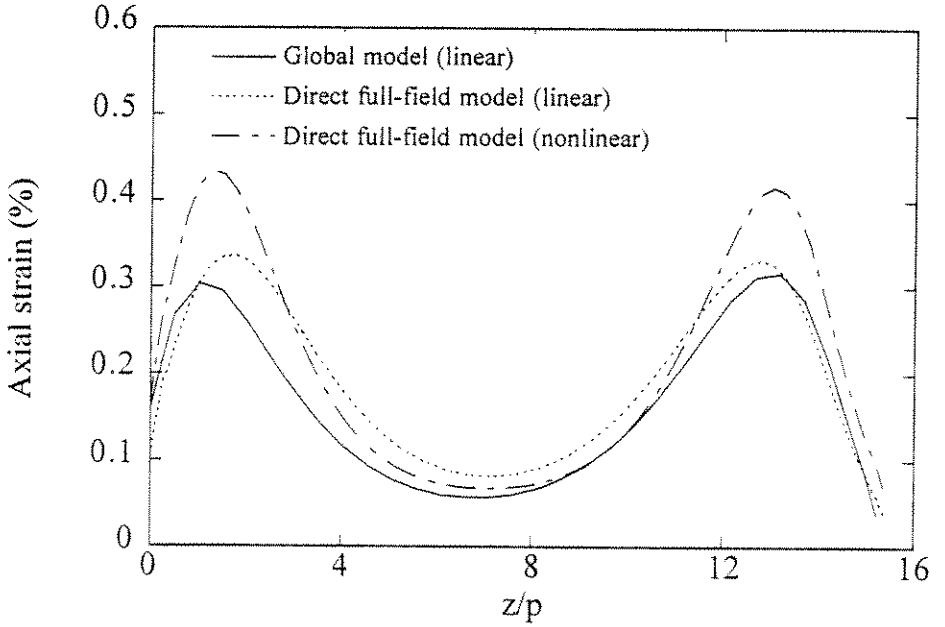

Fig. 9-17 Axial Strain along Internal Surface CD (or C'D') of Pin Section in Threaded Composite Joint with Two-turn Make-up (p=0.125 inch)

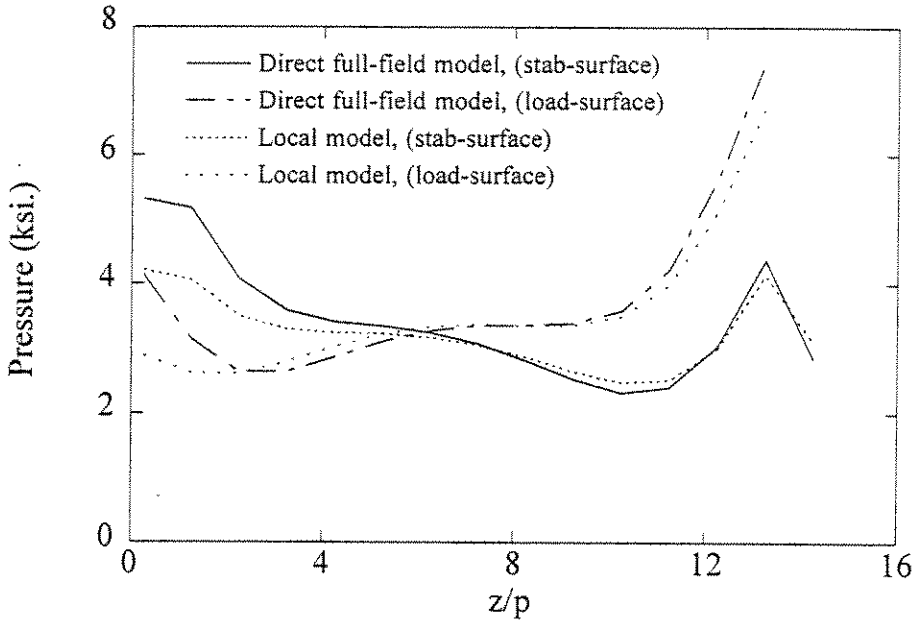

Fig. 9-18a Contact Pressure along Thread Surface of a Composite Joint with One-turn Make-up (p=0.125 inch)

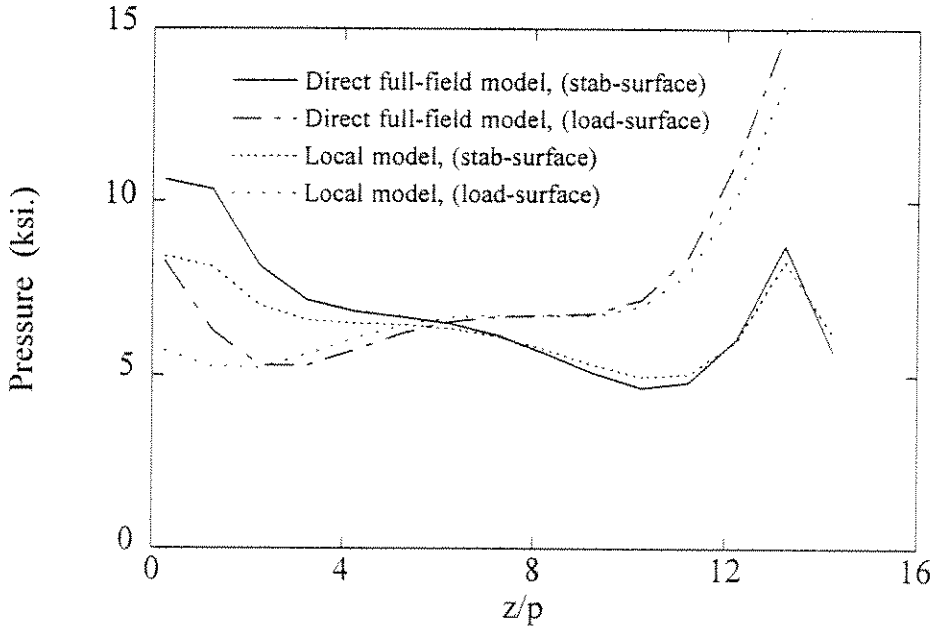

Fig. 9-18b Contact Pressure along Thread Surface of a Composite Joint with Two-turn Make-up (p=0.125 inch)

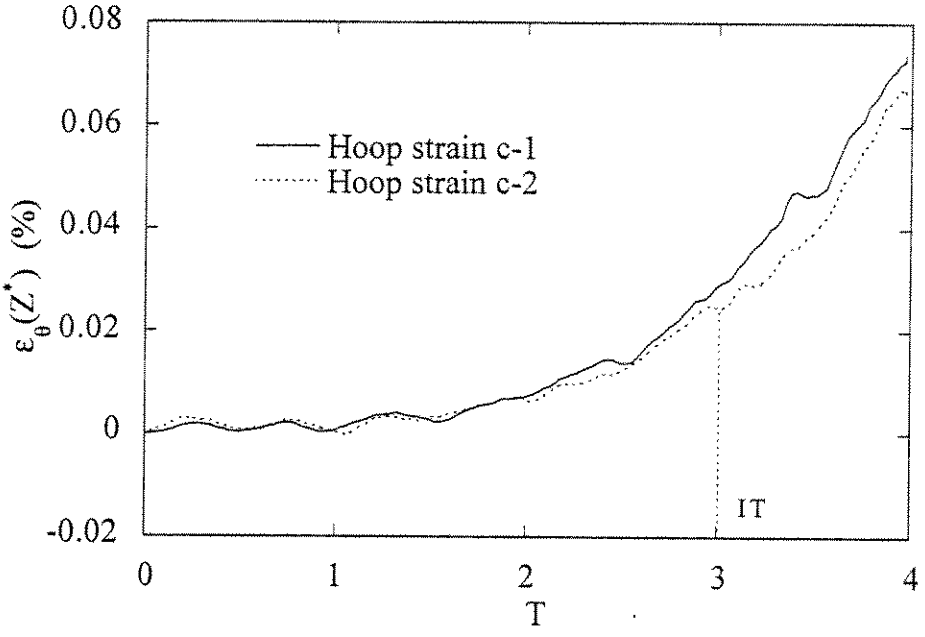

Fig. 10-1 Hoop Strains at Z^*=7.5 During One-turn Make-up of a Threaded Fiber Composite Tubular Joint (P_i=0; P_a=0) (with Thread Compound)

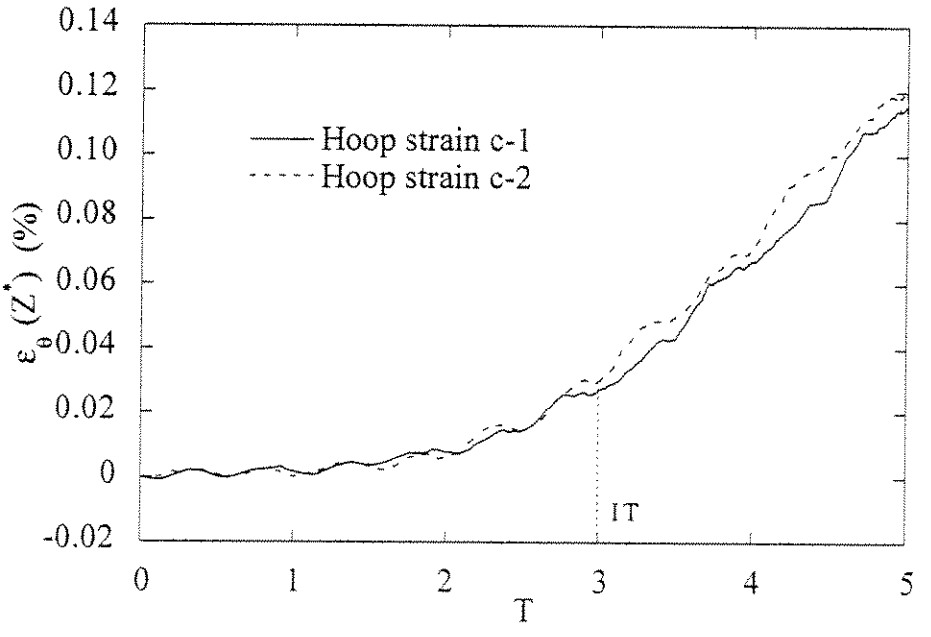

Fig. 10-2 Hoop Strains at Z^*=7.5 During Two-turn Make-up of a Threaded Fiber Composite Tubular Joint (P_i=0; P_a=0) (with Thread Compound)

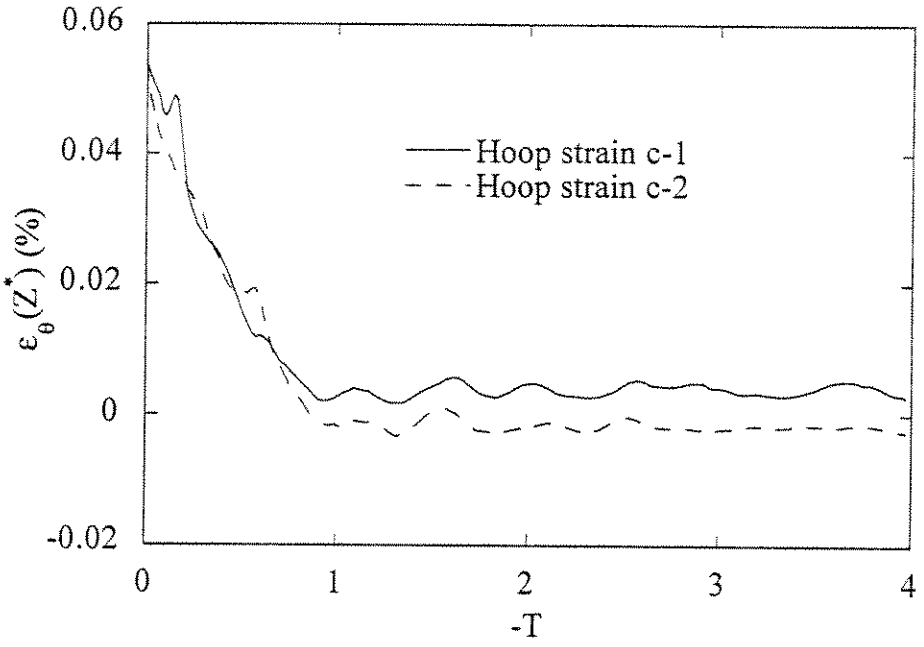

Fig. 10-3 Hoop Strains During Break Out of a Threaded Composite Joint (After One-turn Make-up; P_i=0; P_a=0)

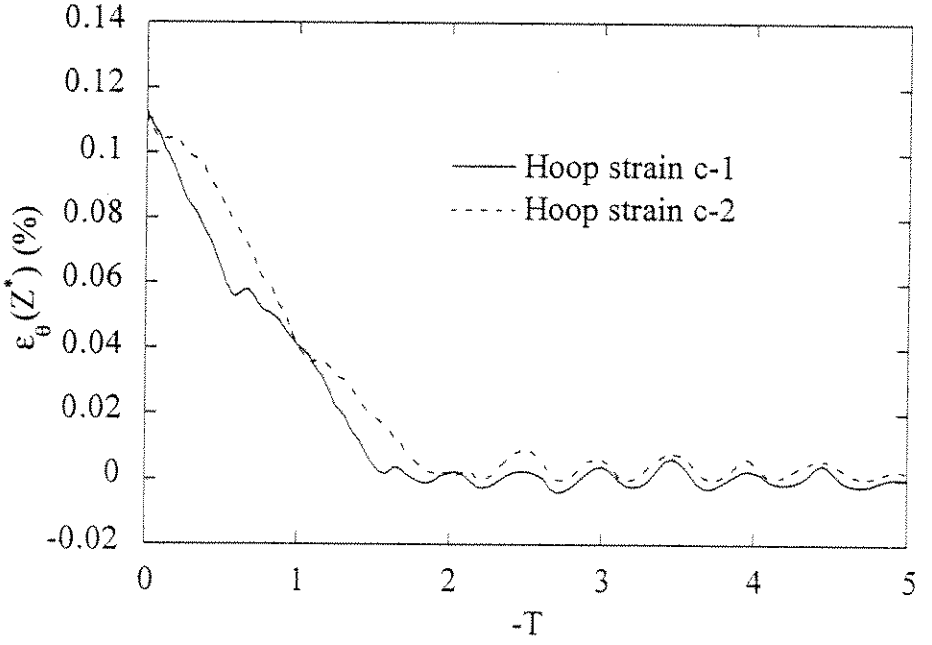

Fig. 10-4 Hoop Strains During Break Out of a Threaded Composite Joint (After Two-turn Make-up; P_i=0; P_a=0)

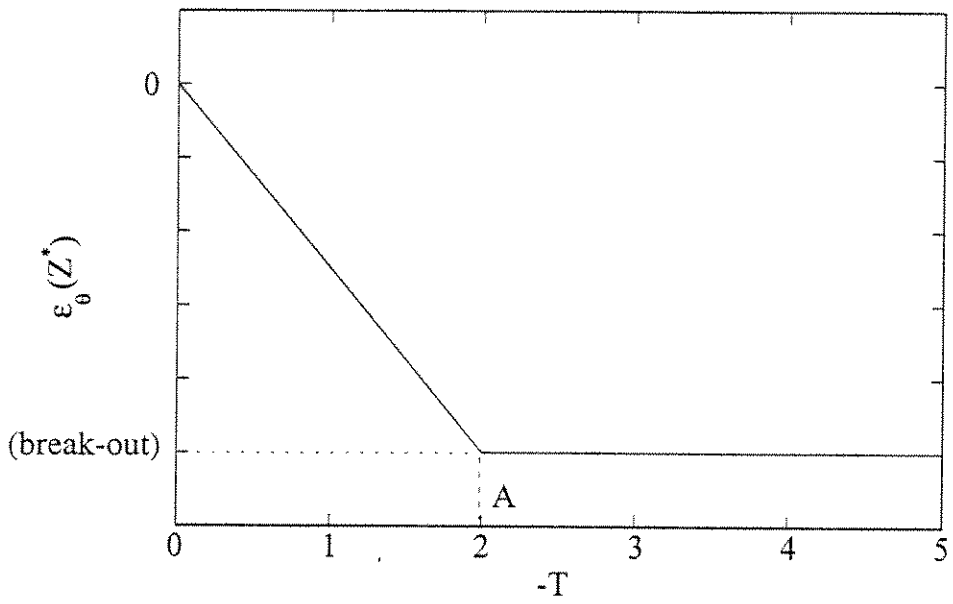

Fig. 10-5 Idealized Hoop Strain Development During Break Out of a Threaded Composite Joint (P_i=0; P_a=0)

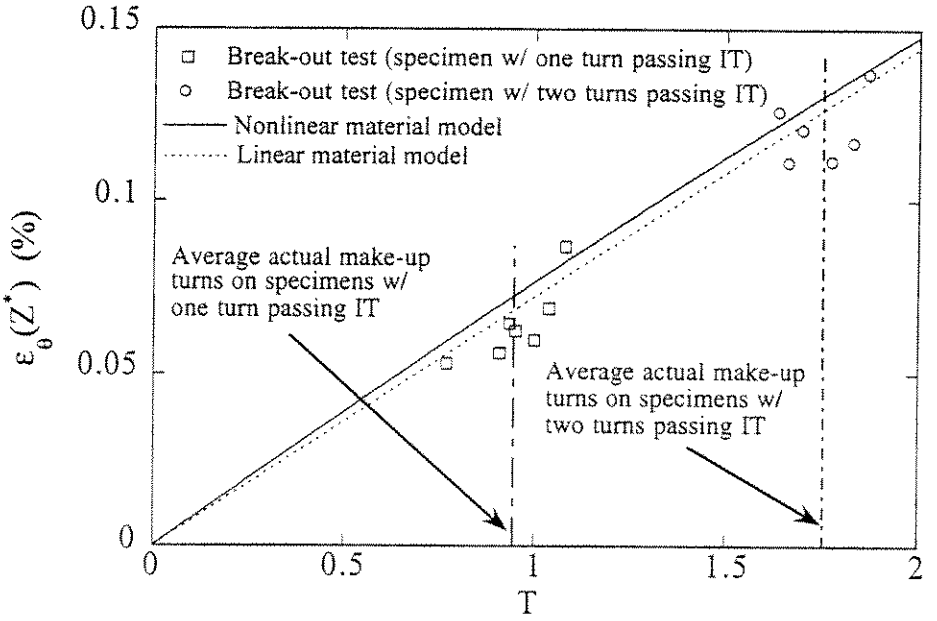

Fig. 10-6 Hoop Strains in Threaded Integral Composite Joint Under Increasing Make-up Loading (2-3/8-inch Integral Composite Joint; P_i=0; P_a=0)

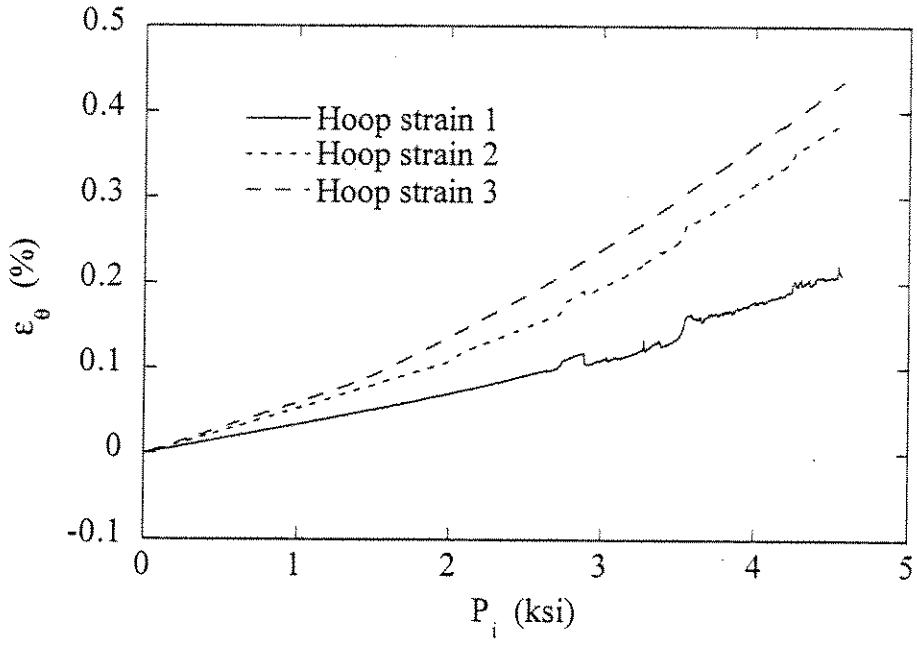

Fig. 10-7 Hoop Strains on External Surface of a Threaded Composite Joint Subjected to Increasing Internal Pressure P_i (P_a= 0; T=2)

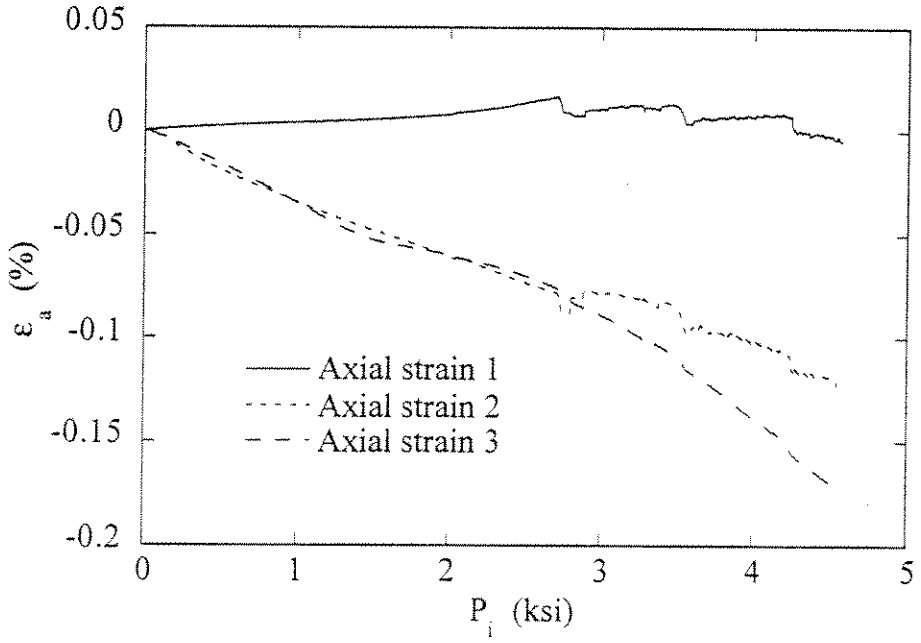

Fig. 10-8 Axial Strains on External Surface of a Threaded Composite Joint Subjected to Increasing Internal Pressure Pi, (P_a= 0; T=2)

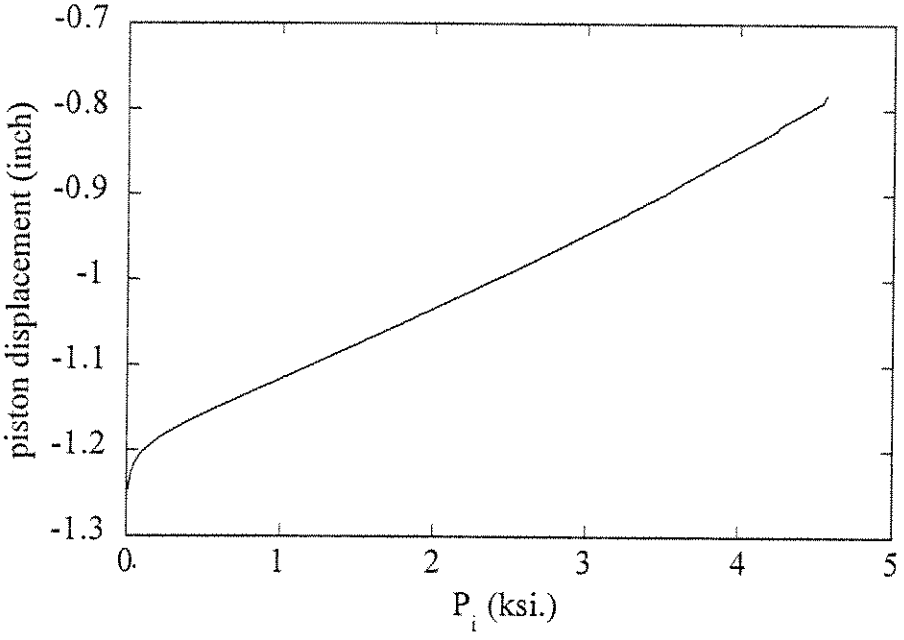

Fig. 10-9 Piston Displacement as a Function of Applied Pressure in a Leakage Failure Experiment of a Threaded Composite Joint (P_a= 0; T=2)

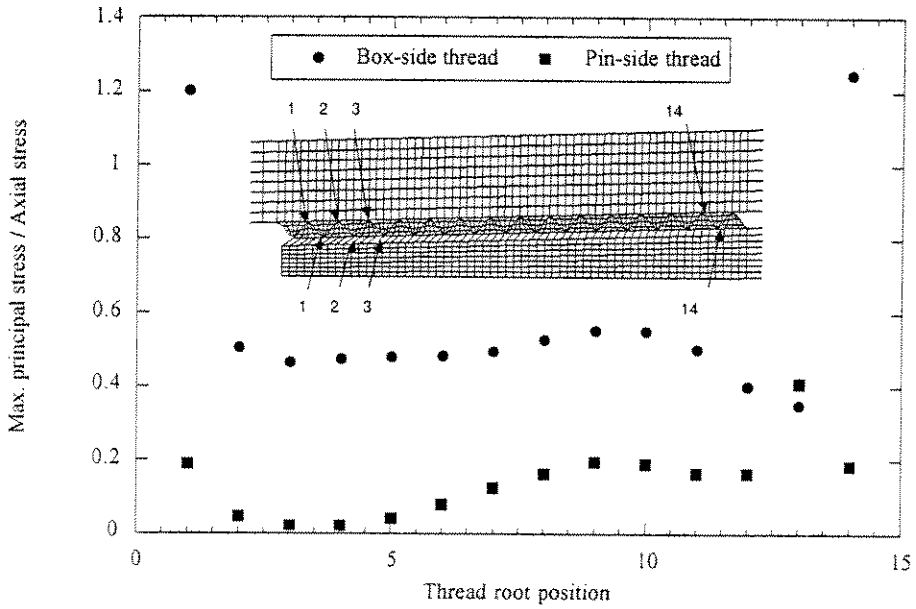

Fig. 10-10a Max. Principal Stress at Thread root of Composite Integral Joint under Two-Turn Makeup and 2:1 Loading (Internal Pressure = 2000 psi.)

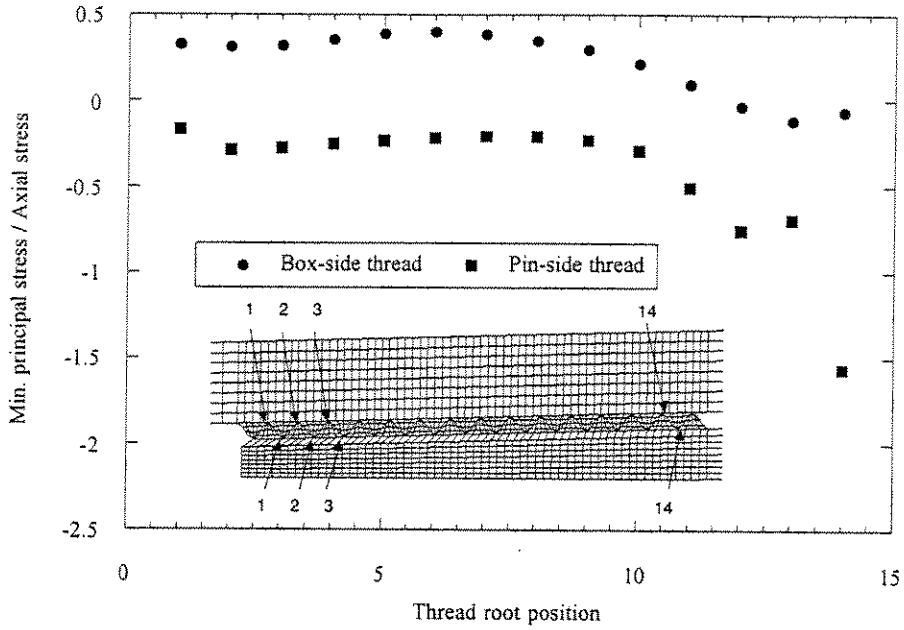

Fig. 10-10b Min. Principal Stress at Thread root of Composite Integral Joint under Two-Turn Makeup and 2:1 Loading (Internal Pressure = 2000 psi.)

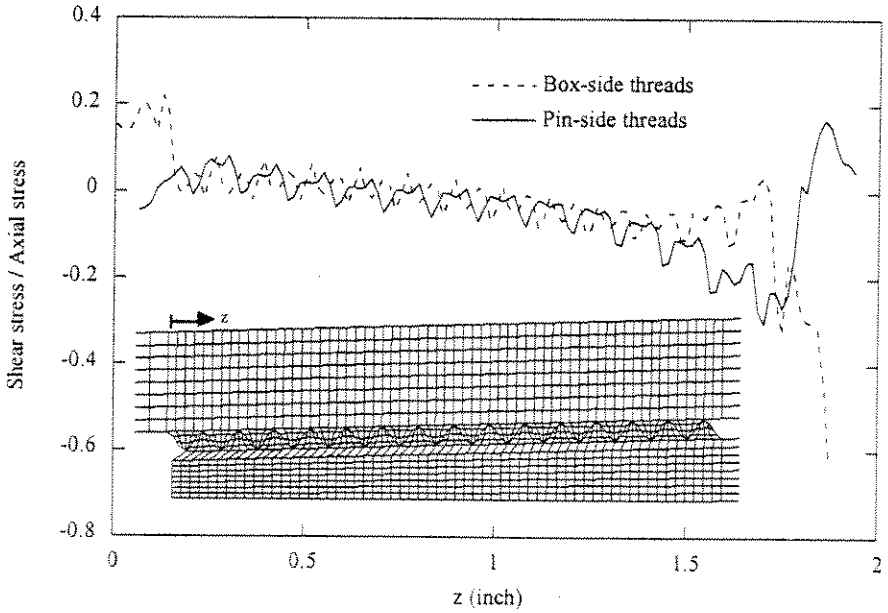

Interface shear stress between threads and bodies of composite integral joints under two-turn makeup and 2:1 loading (internal pressure=2000 psi.)

Fig. 10-11 Interface Shear Stress between Threads and Bodies of Composite Integral Joint under Two-Turn Makeup and 2:1 Loading (Internal Pressure = 2000 psi.)

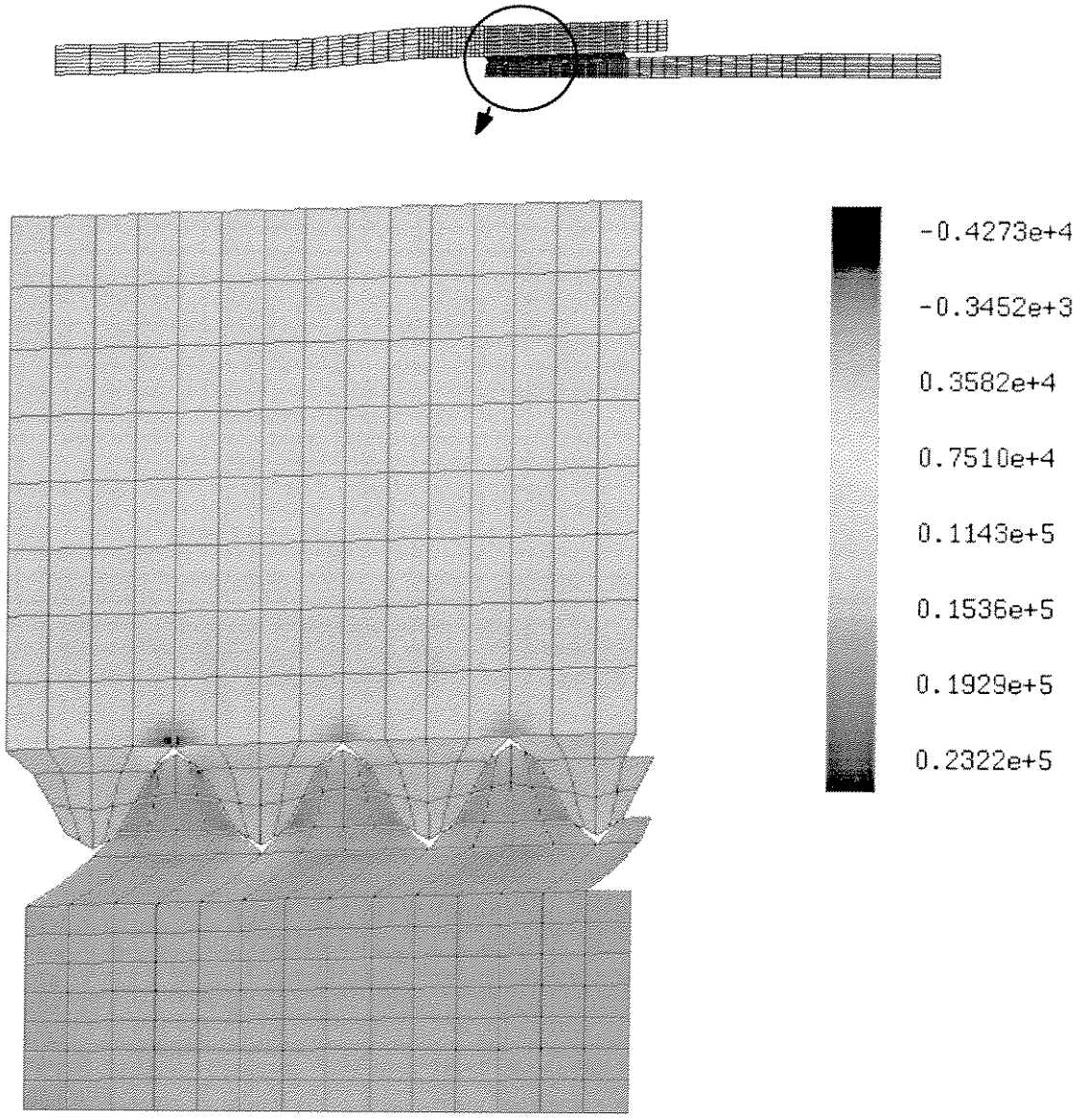

Fig. 12a Maximum principal stress of 2-3/8" composite integral joint under 2:1 loading with two-turn makeup and 2000 psi internal pressure

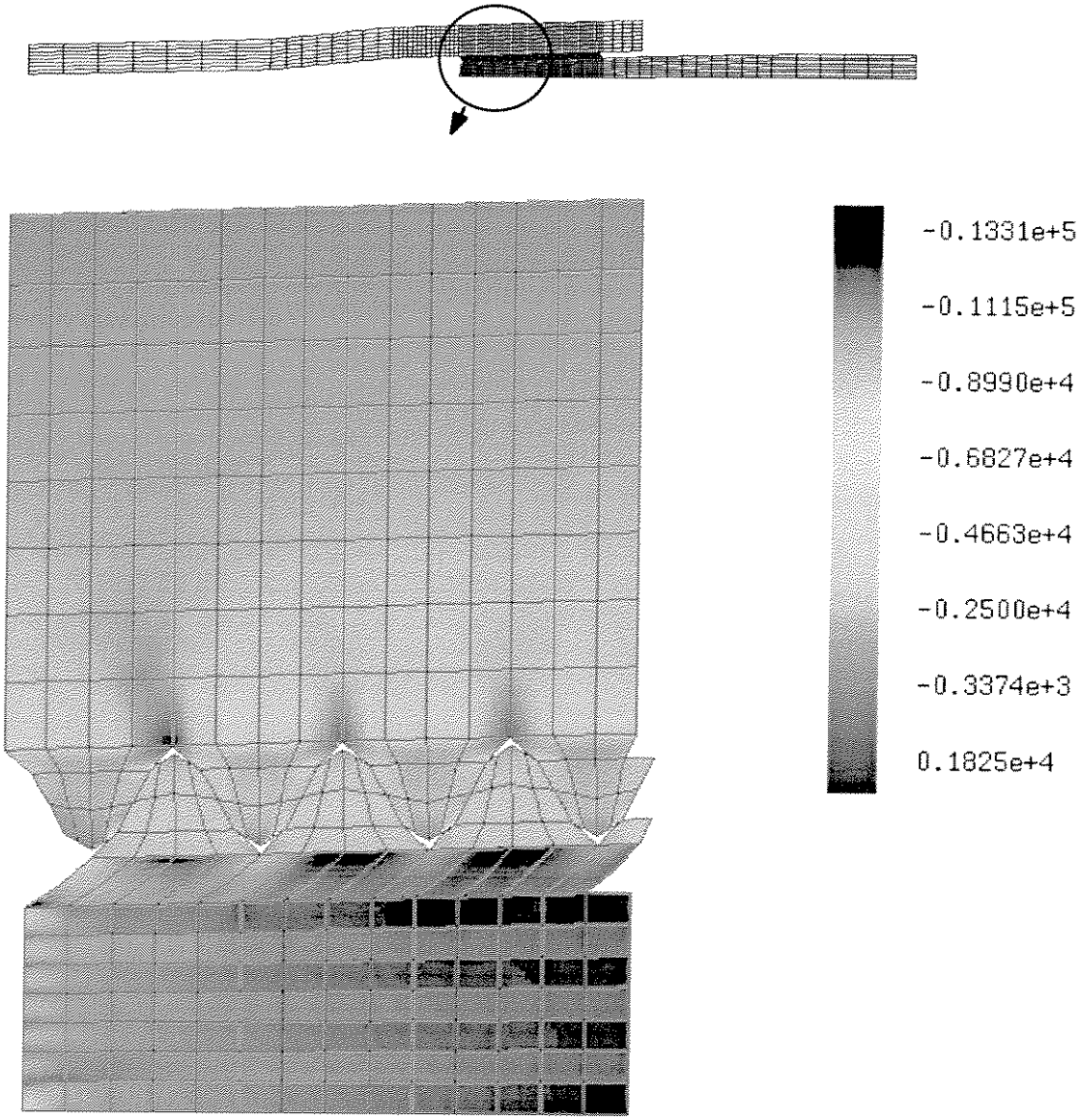

Fig. 12b Minimum principal stress of 2-3/8" composite integral joint under 2:1 loading with two-turn makeup and 2000 psi internal pressure

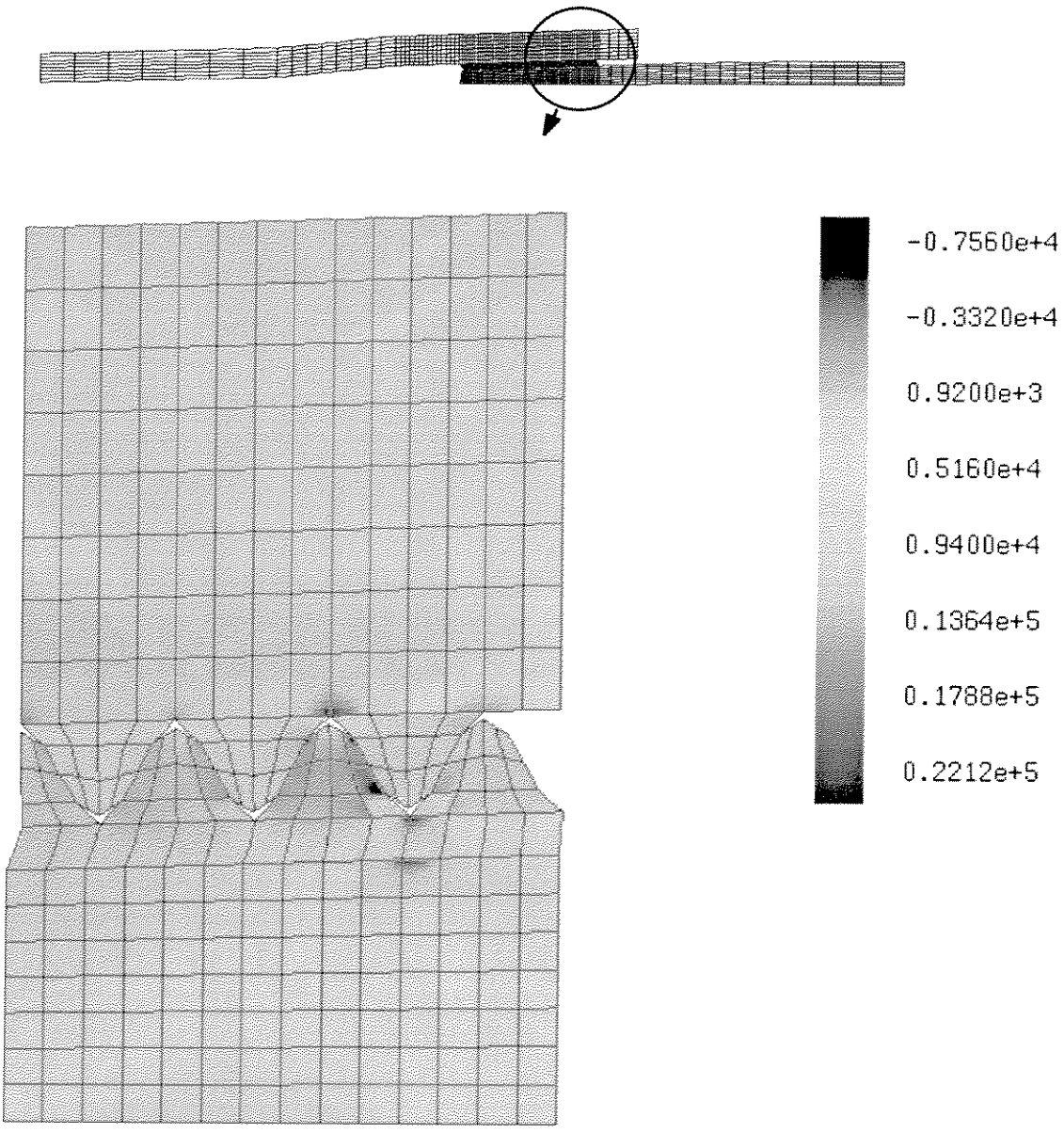

Fig. 12c Maximum principal stress of 2-3/8" composite integral joint under 2:1 loading with two-turn makeup and 2000 psi internal pressure

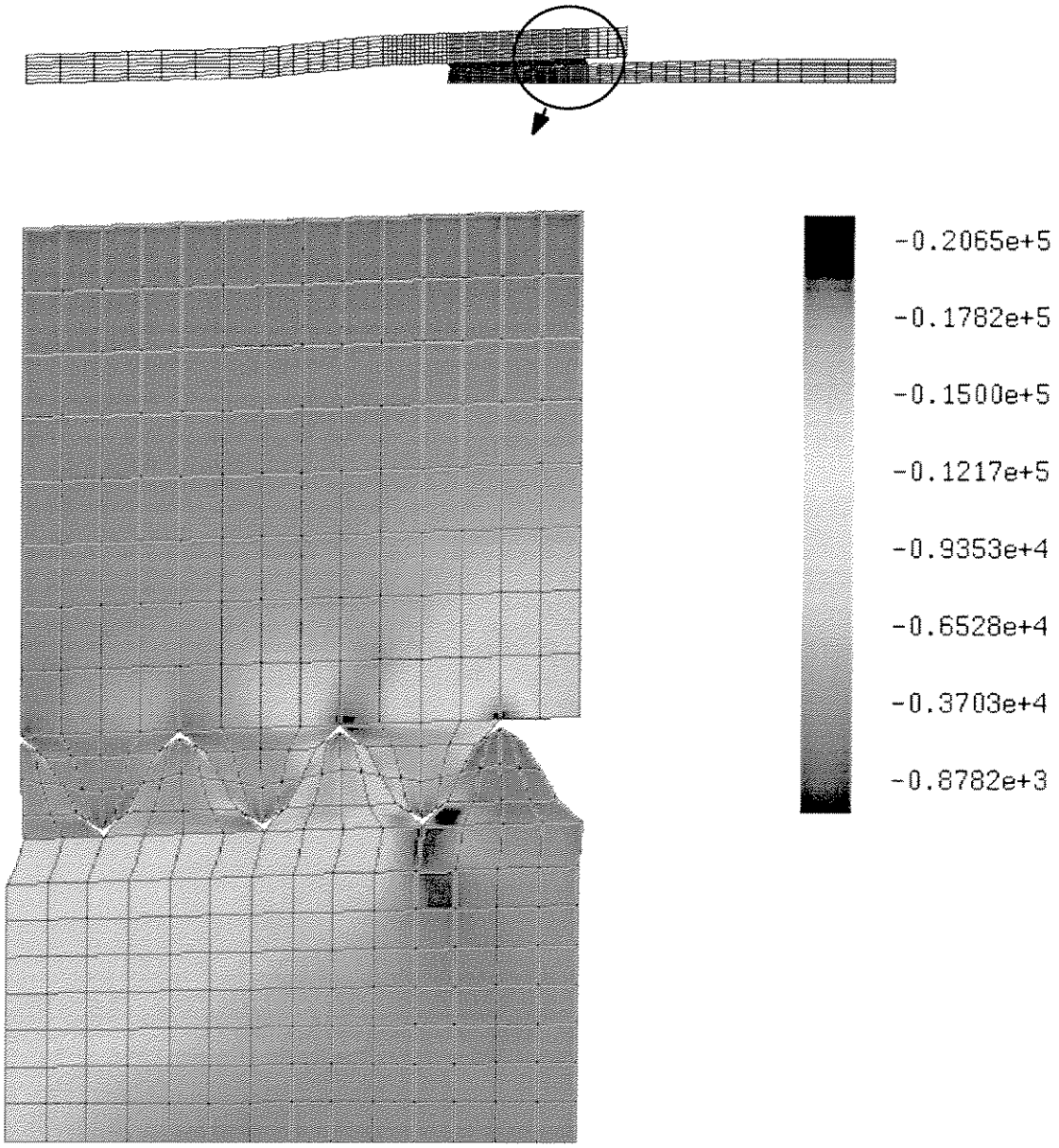

Fig. 12d Minimum principal stress of 2-3/8" composite integral joint under 2:1 loading with two-turn makeup and 2000 psi internal pressure

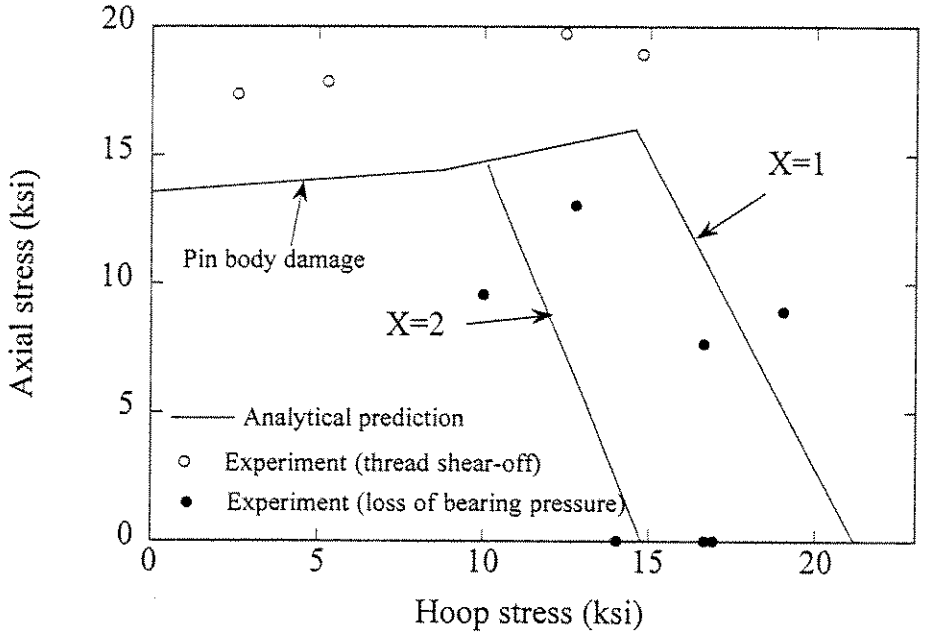

Fig. 10-13 Leakage Failure Envelope of a Threaded Composite Joint with One-turn Make-up (2-3/8-inch Integral Composite Joint), Subjected to Combined Axial Load and Internal Pressure

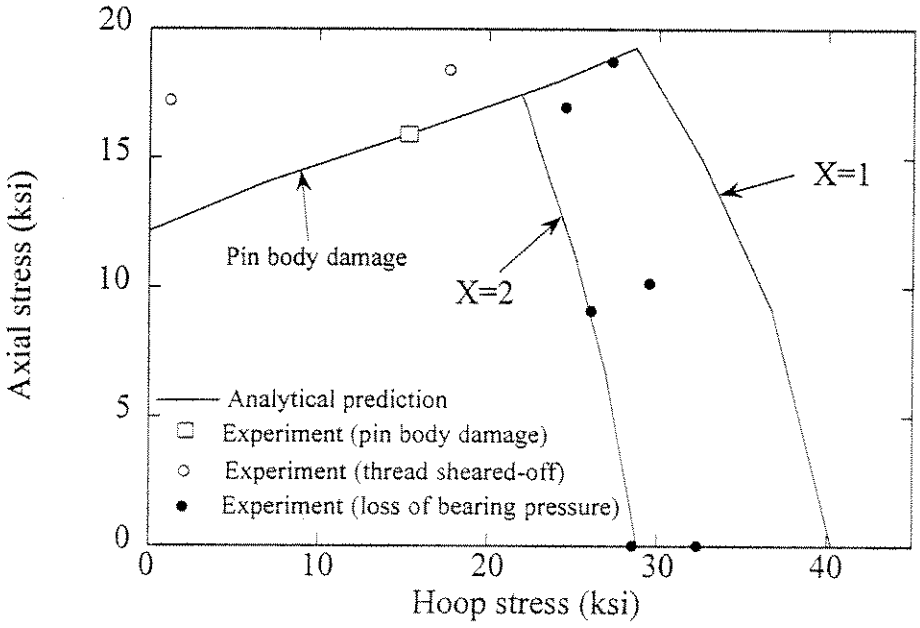

Fig. 10-14 Leakage Failure Envelope of a Threaded Composite Joint with Two-turn Make-up (2-3/8-inch Integral Composite Joint) Subjected to Combined Axial Load and Internal Pressure

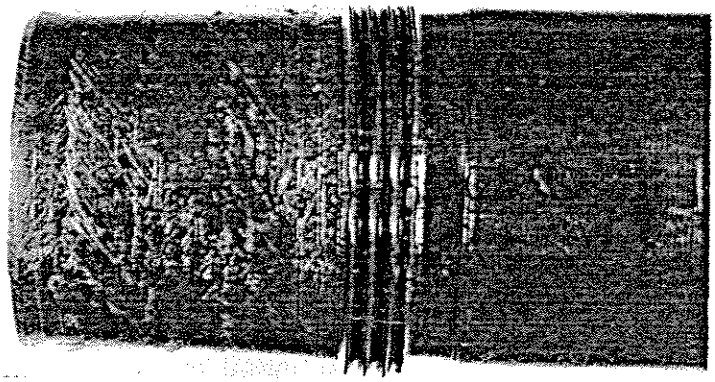

Fig. 10-15 Damaged Pin Section of Threaded Composite Joint [Threaded Composite Joint Leaked at P_i=3 ksi and P_a=21 kips with T=2]

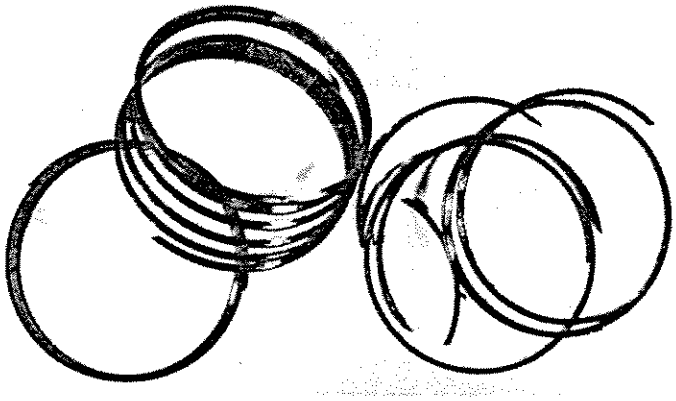

Fig. 10-16 Sheared-off Threads [Threaded Composite Joint Leaked at P_i=3 ksi and P_a=21 kips with T=2]

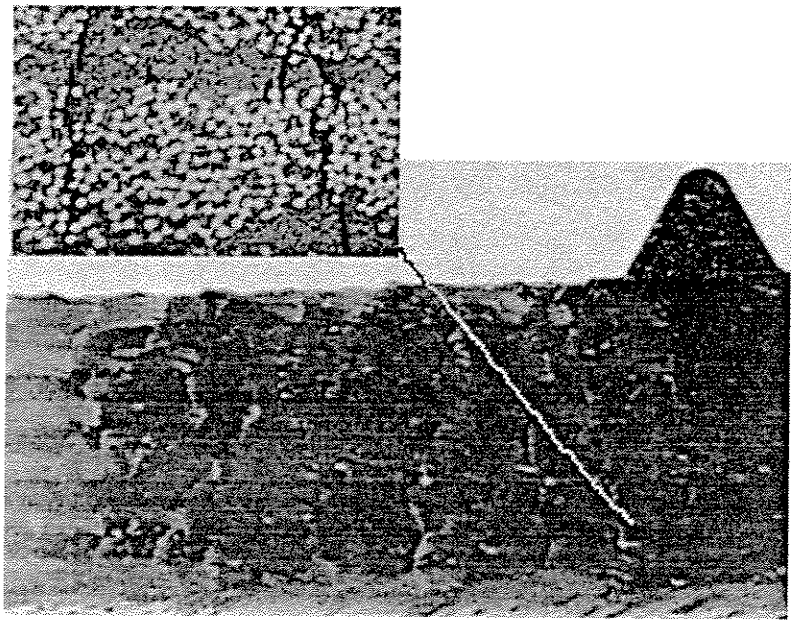

Fig. 10-17 Optical Micrographs of Damaged Pin Body [Threaded Composite Joint Leaked at P_i=0.9 ksi and P_a=20.5 kips with T=1]

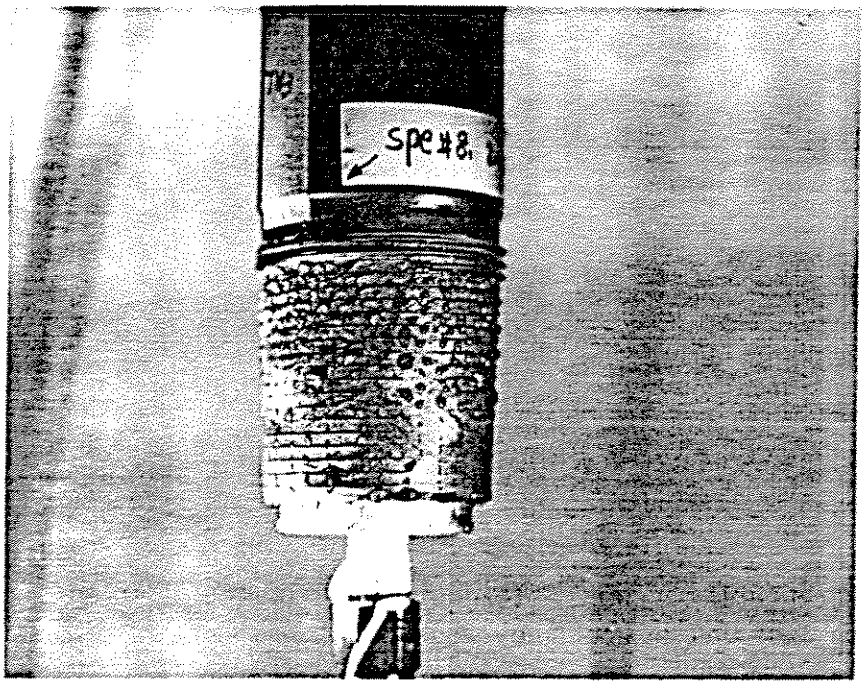

Fig. 10-18 Leakage Test of Damaged (Pin Section) Tube Body [Threaded Composite Joint Failed at P_i=3 ksi and P_a=21 kips with T=2]

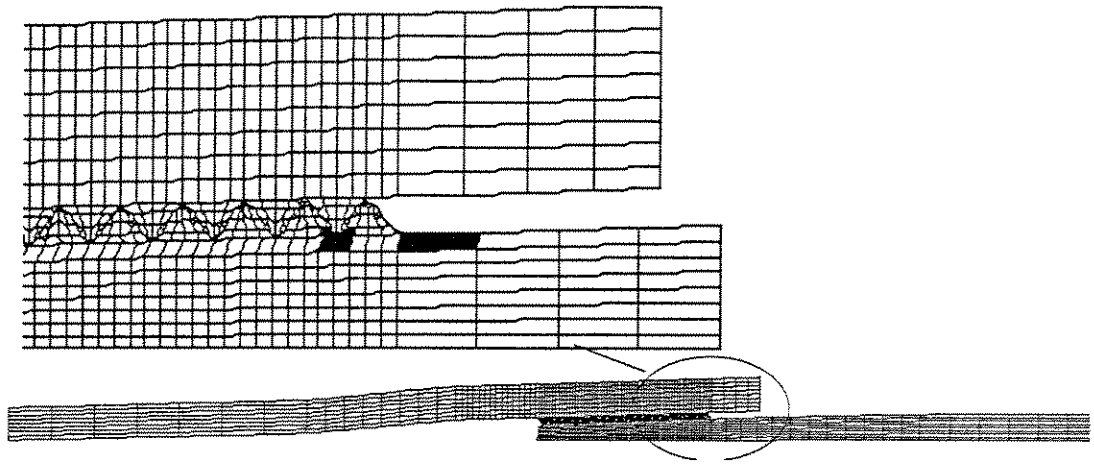

(a)

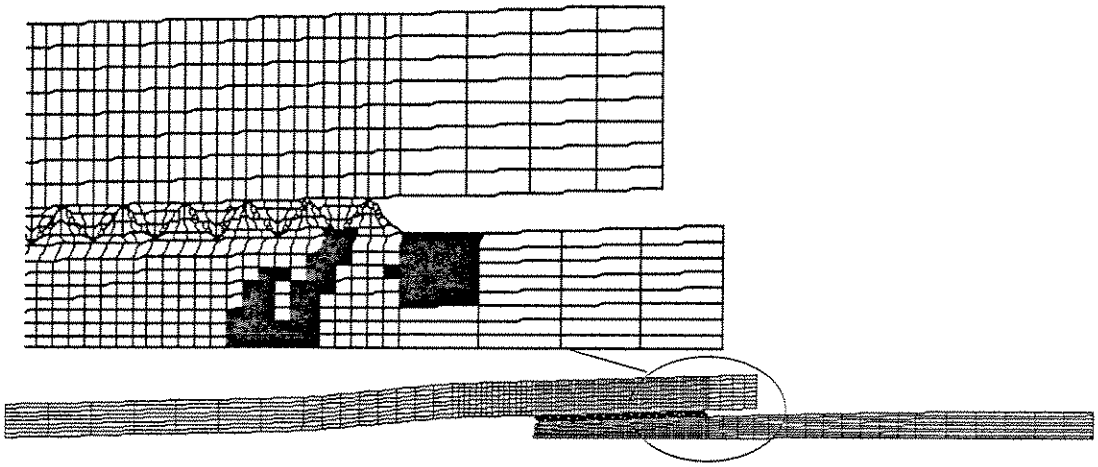

(b)

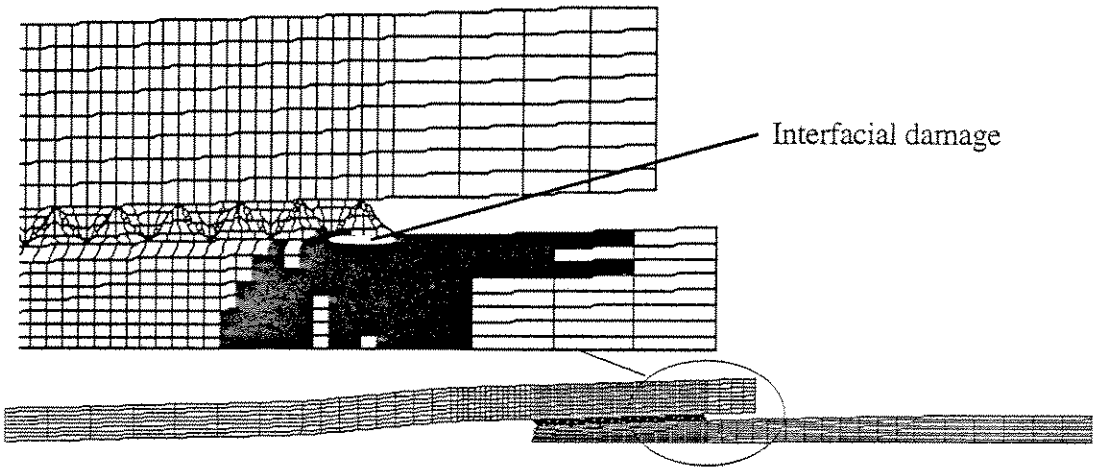

(c)

Fig. 10-19 Predictions of Tube-body Damage Growth and Leakage Failure of a 2-3/8-inch Threaded Composite Joint with a Make-up, T=2, Subjected to Combined Axial Loading and Internal Pressure; (a) Initiation (0.93 ksi / 5.6 kips) , (b) Growth (2.02 ksi / 12 kips), and (c) Leakage (2.71 ksi / 16 kips)

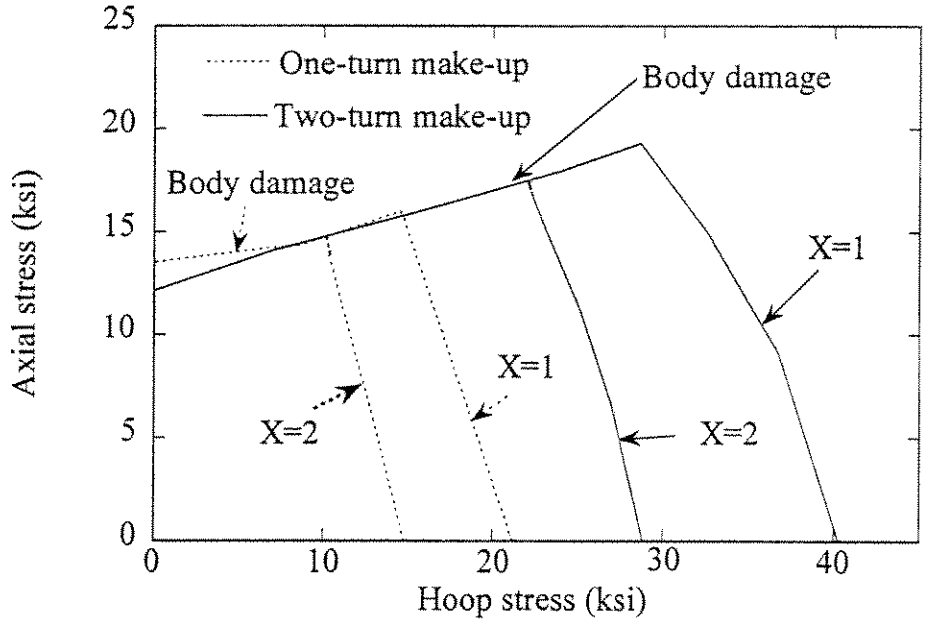

Fig. 10-20 Leakage Failure Envelopes of Threaded Composite Joint with One-turn and Two-turn Make-ups, Subjected to Combined Axial Loading and Internal Pressure (2-3/8-inch Composite Integral Joint)

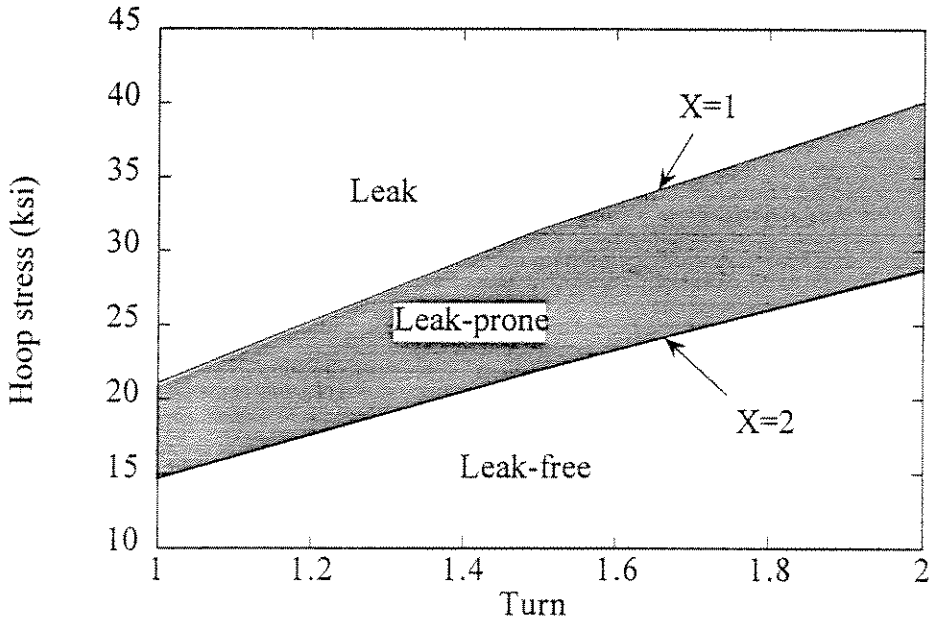

Fig. 10-21a Leakage Failure of Integral Composite Joint Subjected to Pure Internal Pressure and Make-up Interference

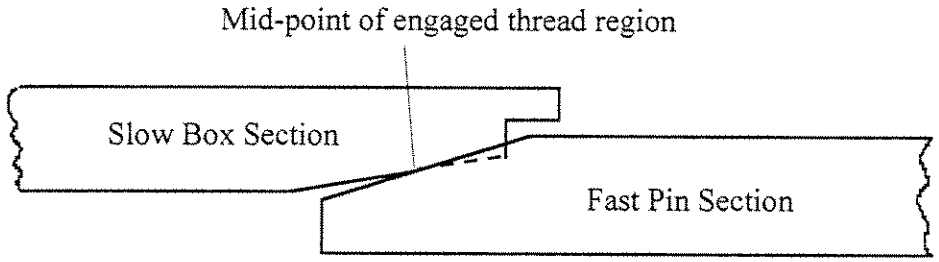

Fig. 10-22 Threaded Composite Joint with a "Fast-Pin-and-Slow-Box" Geometry

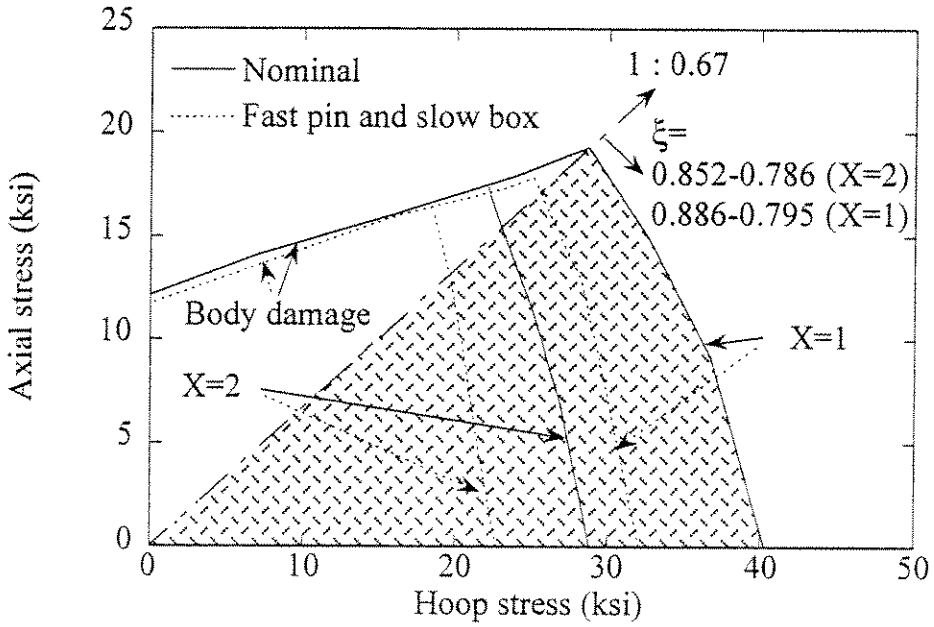

Fig. 10-23 Failure Envelopes of Threaded Composite Joints with Nominal and Nonnominal Thread Tapering (T=2)

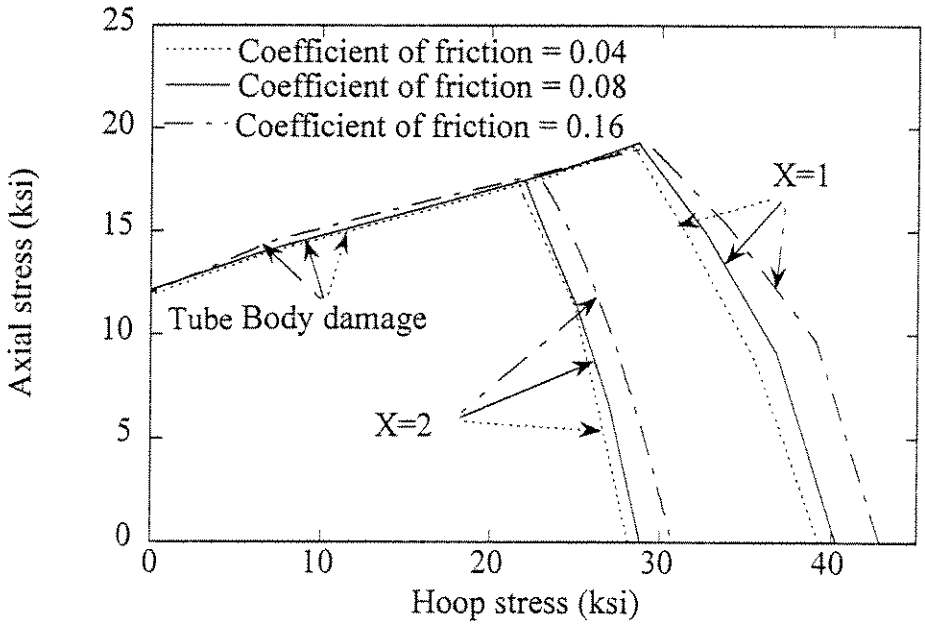

Fig. 10-24 Leakage Failure Envelopes of Threaded Integral Composite Joint with Different Frictional Coefficients (T=2) Subjected to Combined Axial Loading and Internal Pressure

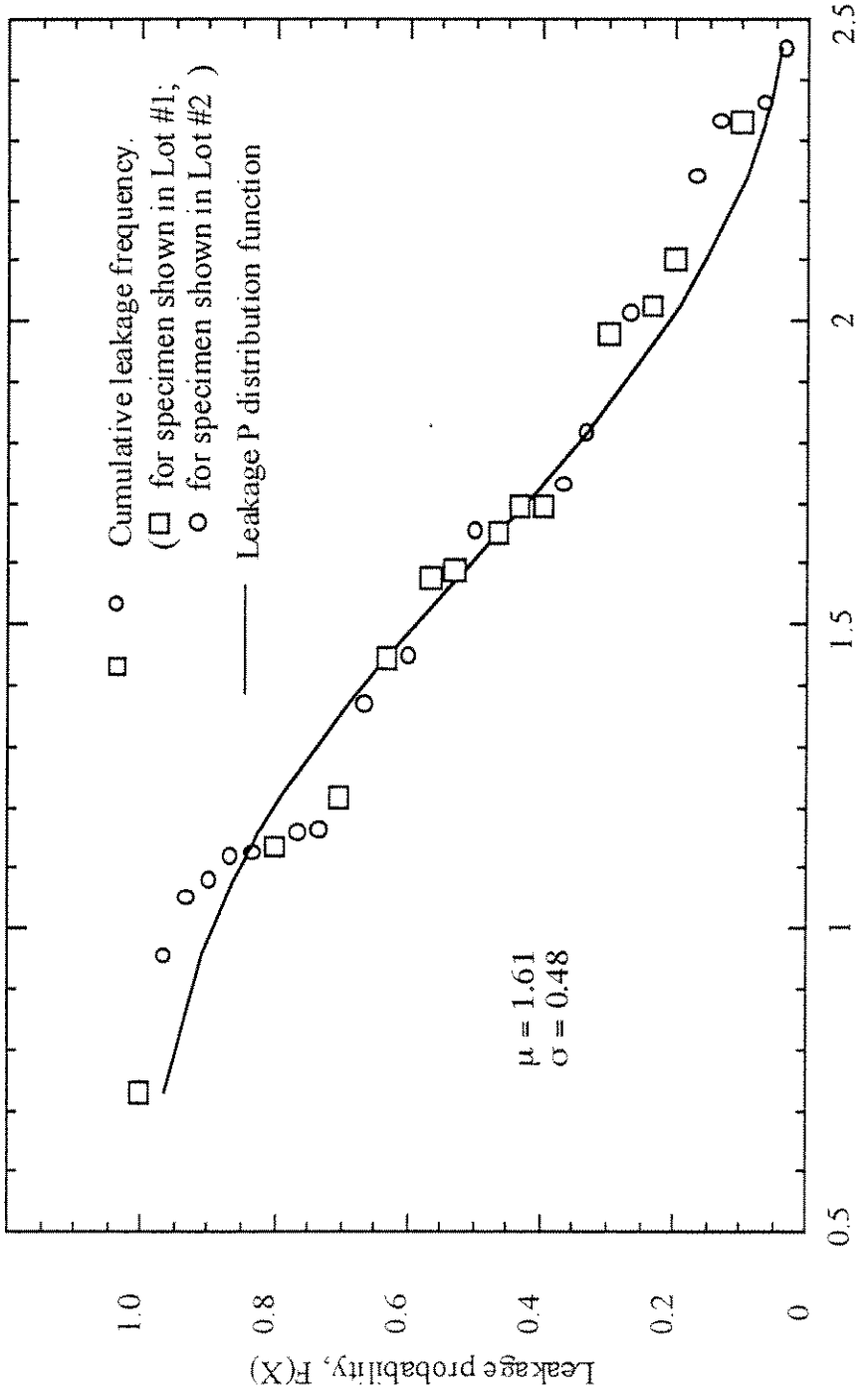

Fig. 10-25 Leakage Failure Probability of 2-3/8 inch Diameter Threaded Integral Composite Joint Subjected to Combined Internal Pressure, Axial Loading and Make-up with Loading Ratio between 1.0 to 1.0.67

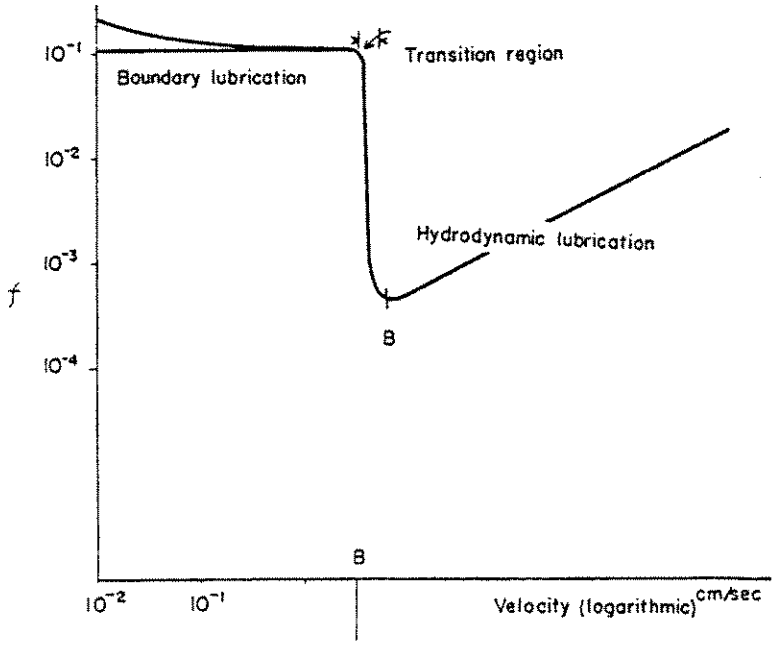

Fig. 10-26 Relationship between Velocity and Coefficient of Friction

14. TABLES

Table 5-1 Test Matrix of Threaded Composite Joints[1]

Test No.	Batch	Sample No.	Axial Loading	Internal Pressure	Make-up Turn
1	1	1	3.3P	P	1
2	1	2	0	P	1
3	1	2	0	P	1
4	1	2	0	P	1
5	1	3	P	2P	1
6	1	3	6.7P	P	2
7	1	4	P	P	1
8	1	5	P	0	1
9	1	6	1.5P	P	1
10	1	7	P	P	1
11	1	7	P	2P	1
12	1	7	1.3P	P	1
13	1	8	P	0	2
14	1	8	P	3P	2
15	1	8	P	1.4P	2
16	1	9	P	3P	2
17	1	9	0	P	2
18	1	9	P	P	2
19	1	9	P	P	2
20	1	10	P	1.4P	2
21	2	1	0	P	2
22	2	1	0	P	2
23	2	1	P	4P	2
24	2	2	0	P	2
25	2	2	P	4P	2
26	2	2	P	2P	2
27	2	3	0	P	2
28	2	3	P	4P	2
29	2	3	P	2P	2
30	2	4	0	P	2
31	2	4	P	4P	2
32	2	4	P	2P	2
33	2	5	0	P	2
34	2	5	P	4P	2
35	2	5	P	2P	2
36	2	9	0	P	2
37	2	9	P	4P	2

[1] All loading are proportional.

Table 9-1 Comparisons between Current and Reference Solutions for a Composite Tubular Subjected Internal Pressure

	Reference solution [52]		Current numerical solution	
r (inch)	σ_r (psi.)	σ_θ (psi.)	σ_r (psi.)	σ_θ (psi.)
1.05	-69.79	525.0	-68.67	529.4
1.10	-43.32	495.0	-42.30	497.2
1.15	-20.48	468.0	-19.52	469.4

Table 9-2 Maximum Principal Stress at Thread Root in Composite Joint

Thread root	Uniform mesh (psi)	Locally enriched mesh (psi)
A	9312	9258
B	5347	4391
C	2661	2315
D	2789	2669

Table 9-3 Average Contact Pressure on Thread Surface in Composite Joint

Thread surface	Uniform mesh[1] (psi)	Locally enriched mesh[2] (psi)
1	9989	9927
2	7009	6954
3	9596	9574
4	7750	7725
5	13910	13800
6	4959	4918

[1] Shown in Fig. 9-5a; with 6598 nodes and 2010 elements.
[2] Shown in Fig. 9-5b; with 8027 nodes and 2455 elements.

Table 10-1 Tightening Safety Factor of Threaded Integral Composite Joint (2-3/8 inches Diameter) Subjected to Combined Internal Pressure, Axial Load and Make-up Interference[1]

Sealing Confidence (%)	Tightening Safety Factor	Length of Pipe Line / Leakage
~10	1.0	30 ft
~80	2.0	150 ft
90	2.224	300 ft
95	2.399	600 ft
99	2.726	0.568 mile
99.9	3.093	5.68 mile
99.99	3.395	56.8 mile

[1] For a line pipe application.

APPENDIX A
GEOMETRY OF THREADED INTEGRAL COMPOSITE JOINT

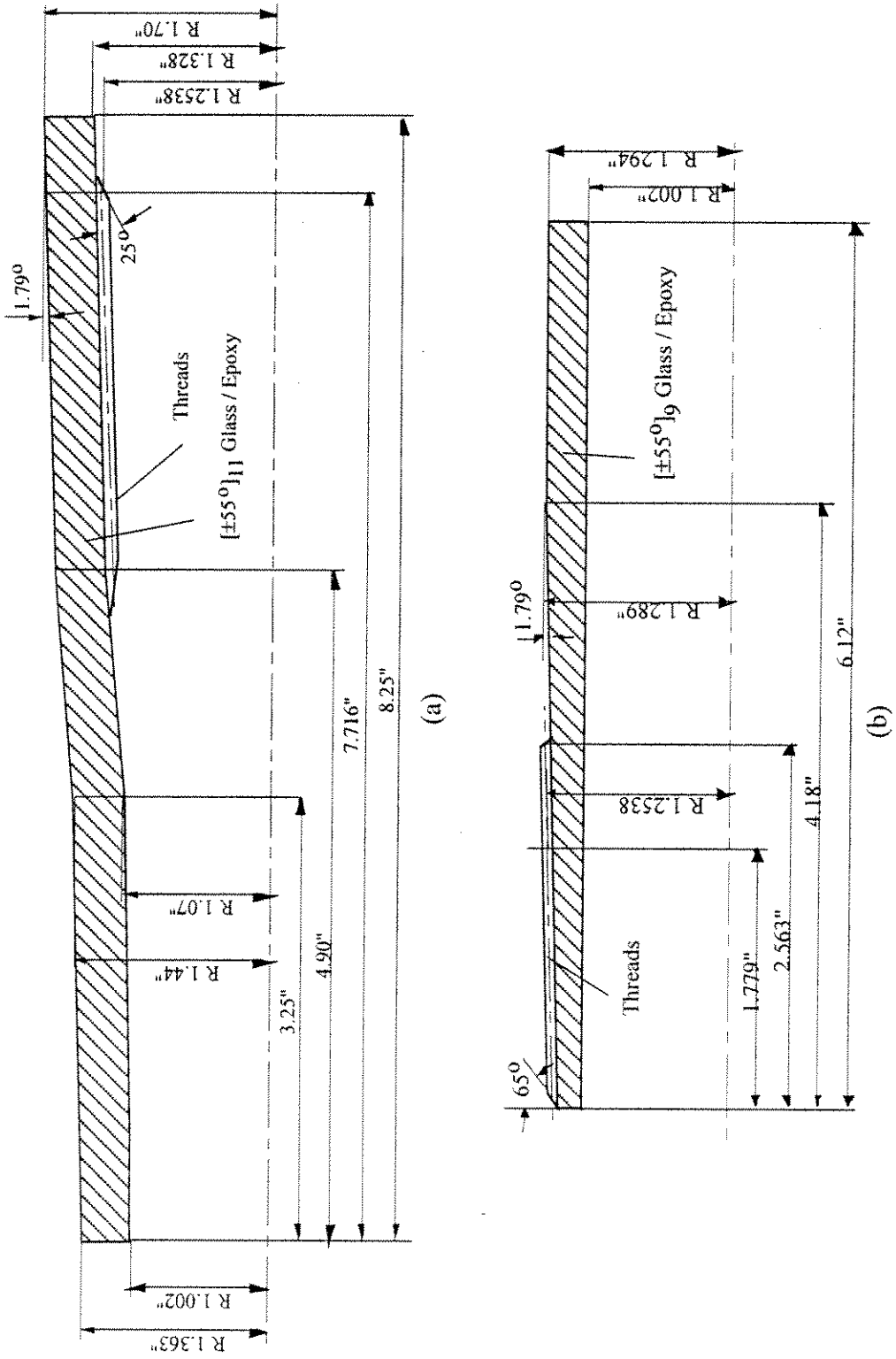

Fig. A-1 Threaded Integral Composite Joint, (a) Mill End and (b) Field End

APPENDIX B
API THREAD CONFIGURATIONS

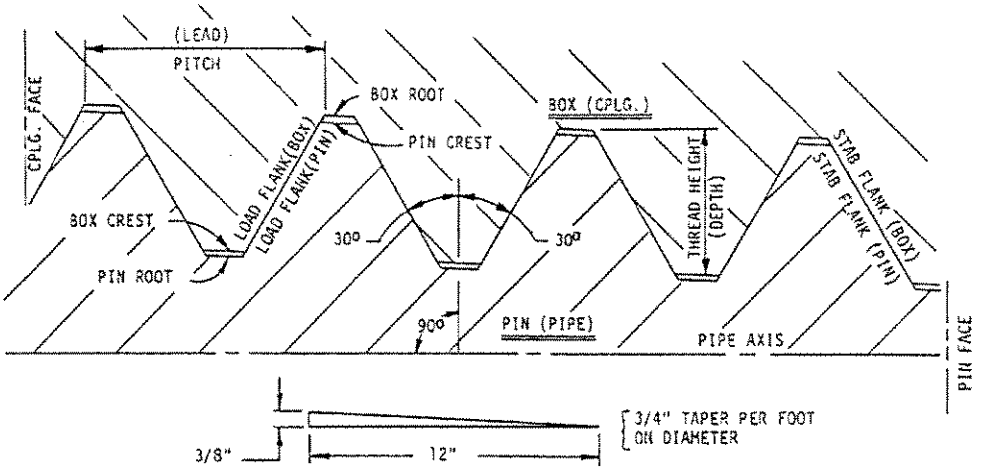

Fig. B-1 Thread Configurations [38,39], Line-pipe Threads

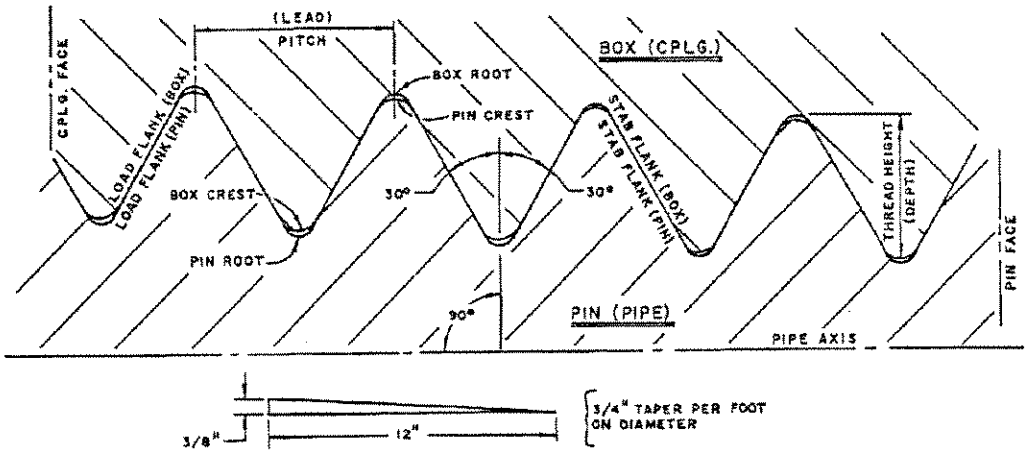

Fig. B-2 Thread Configurations [38,39], Round Threads

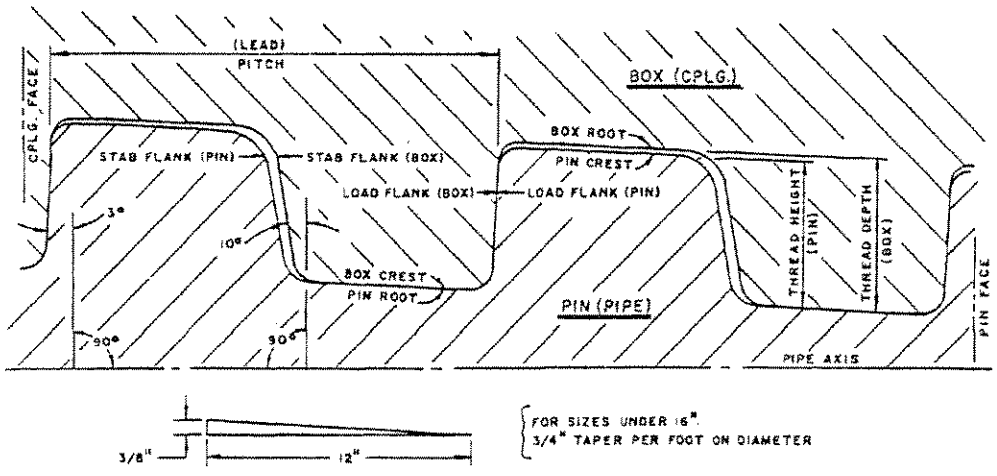

Fig. B-3 Thread Configurations [38,39], Buttress Threads

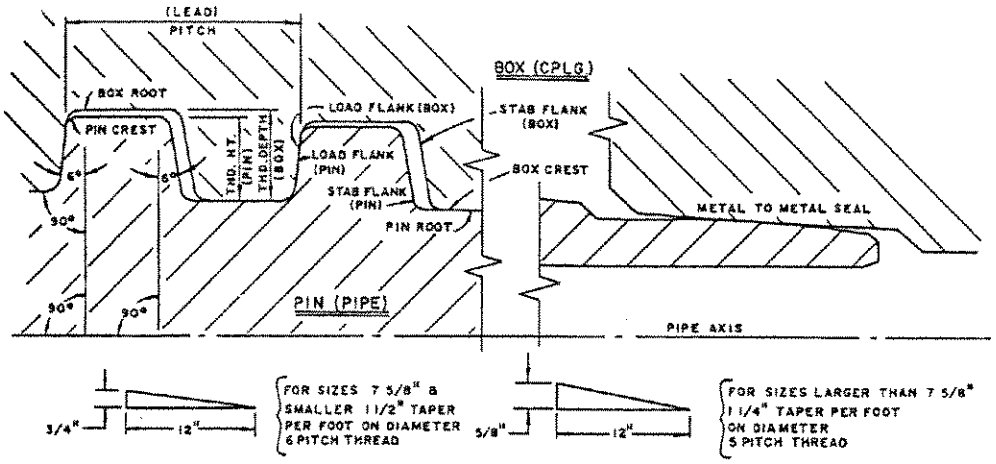

Fig. B-4 Thread Configuration [38,39], Extreme-line Casing Threads

APPENDIX C
THREAD TAPERING OF INTEGRAL COMPOSITE TUBULAR JOINTS

To determine the thread tapering, each joint has to be gaged individually. The thread gaging requires special gauges made by a licensed manufacturer and needs a special service in petroleum E&P operations. The specimens of integral fiber-composite joints used in the experimental investigation were gaged by a local pipe inspection company[1]. In Tables C-1 and C-2, results of the thread tapering in the composite joints used are shown. Values in the Tables were the measurements made at four locations along the axis of the joints (Fig. C-1, from right to left) as suggested by API [39].

It is obvious that the tapering of threads in the joint was not a constant (Tables C-1 and C-2). Also, taperings of pin-side threads and box-side threads were usually not identical. To achieve reliable sealing, the pin and the box sections of the joint should be chosen such that the difference in thread tapering between the pin-side threads and box-side threads is minimal.

Table C-1 Tapering of Mill End in Composite Joints
(% in diameter)

Box No.	Tapering 1	Tapering 2	Tapering 3	Tapering 4
1	6.4	6.4	6.2	6.4
2	6.4	6.2	6.2	6.2
3	6.2	6.2	6.4	6.2
4	6.4	6.2	6.2	6.4
5	6.0	6.0	6.2	6.4
6	6.2	6.2	6.2	6.2
7	6.0	6.0	6.2	6.2
8	6.2	6.2	6.4	6.2
9	6.0	6.0	6.2	6.2

Table C-2 Tapering of Field End in Composite Joints
(% in diameter)

Pin No.	Tapering 1	Tapering 2	Tapering 3	Tapering 4
1	6.2	6.4	6.4	6.2
2	6.4	6.2	6.2	6.0
3	6.4	6.4	6.2	6.2
4	6.4	6.2	6.2	6.2
5	6.4	6.2	6.4	6.0
6	6.2	6.2	6.2	6.0
7	6.4	6.4	6.2	6.0
8	6.2	6.2	6.2	6.0
9	6.4	6.4	6.2	6.0

[1] American Pipe Inspection, Inc., Houston, TX

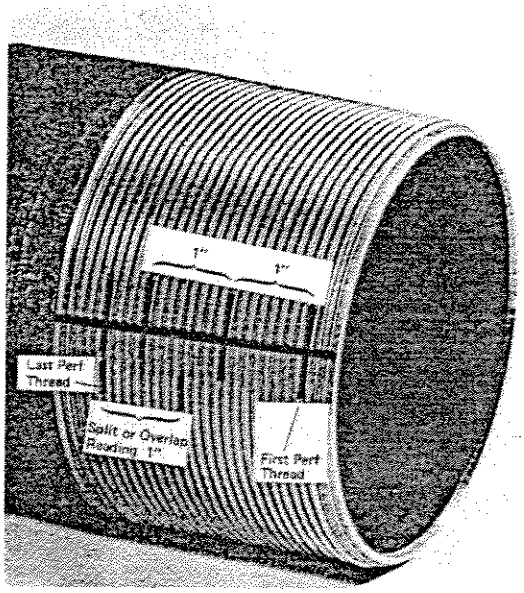

Fig. C-1 Thread Gaging Locations

APPENDIX D
FEATURES OF DATA ACQUISITION SYSTEM USED IN EXPERIMENTAL SETUP

A typical plug-in data acquisition board usually had only one A/D converter, which could transfer a single channel of analog signals to a digital one. In a multiple-channel data acquisition, a multiplexer (MUX) was used to scan all the channels available and digitized the analog inputs one by one, as illustrated in Fig. D-1. The scan frequency depended on a user-chosen resolution. In a given data acquisition board, an increase in the scan frequency would result in a decrease in the converted resolution and consequently, an increase in the digital noise. In order to achieve a high resolution in an A/D converter with a low noise level, a time delay between two channels should be set long and the board should be calibrated frequently during tests, especially when a test last long. All these contributed to a reduction in the scanning frequency of the data acquisition. The scanning frequency of the data acquisition board for eight channels was approximately one Hz in low noise and high resolution modes. The scanning frequency was also affected when the data was logged during an acquisition loop.

The sophisticated data acquisition system in a digital controller enabled a computer to acquire the data through the GPIB board in two modes. One of the modes permitted a user to request the data one by one through the GPIB board. The other allowed the user to send data into the controller buffer with a prescribed acquisition frequency and read the data from the buffer when it was full. The acquisition frequency in this case would not be changed during the data transfer.

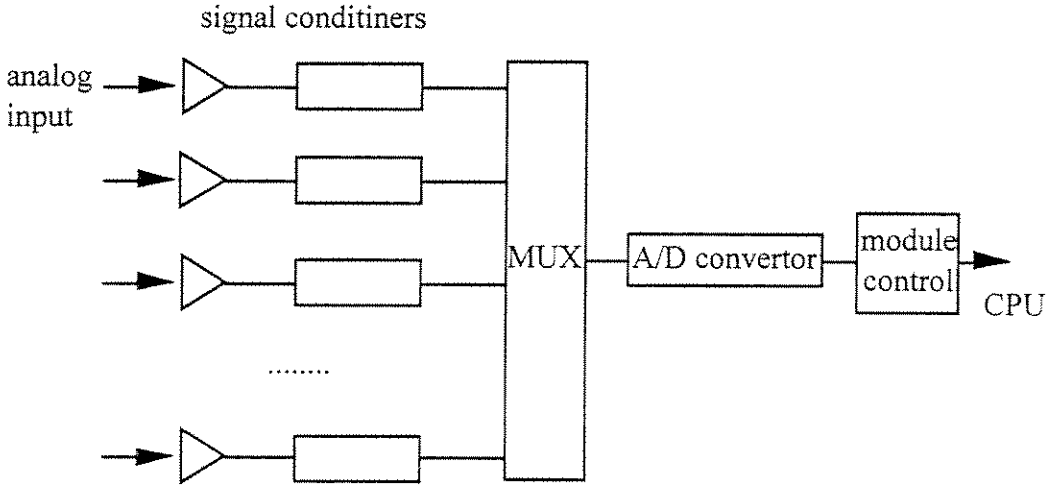

Fig. D-1 Typical Plug-in Data Acquisition System

APPENDIX E
THREAD HELICAL ANGLE OF THREADED JOINTS

The thread helical angle of threads in a joint depends on the joint diameter and pitch dimensions. For an API round thread, the thread pitch is usually between 6 to 10 threads/inch [38]. The thread helical angles of typical API round threaded joints are shown in Table E-1.

Table E-1 Helical Angles in Commonly Used Threaded Joints

	Tube Diameter		
Pitch(thread/inch)	1.5 inches	2.0 inches	2.5 inches
6	2.03°	1.52°	1.22°
8	1.52°	1.14°	0.91°
10	1.22°	0.91°	0.73°

APPENDIX F
STRAIN ENERGY FUNCTION OF AN ELASTIC BODY WITH IN-PLANE SHEAR NONLINEARITY

The complementary energy density function of an elastic body with in-plane shear nonlinearity is given as

$$W^* = \int \varepsilon_{ij}\, d\sigma_{ij} = \frac{1}{2} S_{ijmn}\, \sigma_{ij}\, \sigma_{mn} + \frac{1}{4} S^h_{66}\, \sigma^4_{12}, \tag{F-1}$$

where S_{ijmn} are linear elastic compliances and S^h_{66} is a high-order compliance described in Section 5.

From Eq. (F-1), it is easy to obtain

$$\varepsilon_{ij} = \frac{\partial W^*}{\partial \sigma_{ij}}. \tag{F-2}$$

The existence of a unique inverse of Eq. (F-2) is guaranteed by the condition,

$$\det\left(\frac{\partial^2 W^*}{\partial \sigma_i \partial \sigma_j}\right) \neq 0, \tag{F-3}$$

where σ_i and σ_j are stresses in contracted notation as described in Section 6.

Based on the fact that W^* is positive-definiteness, Eq. (F-3) yields

$$\bar{S}_{66} + 3\bar{S}^h_{66}\sigma^2_{12} \neq 0. \tag{F-3}$$

The strain energy density of the body can be expressed as

$$\begin{aligned} W &= \int \sigma_{ij}\, d\varepsilon_{ij} = \varepsilon_{ij}\, \sigma_{ij} - W^*, \\ &= \varepsilon_{ij}\, \sigma_{ij} - \frac{1}{2} \bar{S}_{ijmn}\, \sigma_{ij}\, \sigma_{mn} - \frac{1}{4} \bar{S}^h_{66}\, \sigma^4_{12}. \end{aligned} \tag{F-4}$$

The derivatives of the strain energy density W with respect to strain component give the corresponding stress components:

$$\frac{\partial W}{\partial \varepsilon_{ij}} = \sigma_{ij} + \frac{d\sigma_{mn}}{\partial \varepsilon_{ij}}\, \varepsilon_{mn} - \bar{S}_{stmn} \frac{d\sigma_{mn}}{\partial \varepsilon_{ij}}\, \sigma_{st} - \bar{S}^h_{66}\sigma^3_{12} \frac{d\sigma_{12}}{\partial \varepsilon_{ij}}$$

$$= \sigma_{ij} + \frac{d\sigma_{mn}}{\partial \varepsilon_{ij}}\, \varepsilon_{mn} - \bar{S}_{stmn} \frac{d\sigma_{mn}}{\partial \varepsilon_{ij}}\, \sigma_{st} - \frac{1}{2}\bar{S}^h_{66}\sigma^3_{12} \frac{d\sigma_{mn}}{\partial \varepsilon_{ij}} (\delta_{m1}\delta_{n2} + \delta_{m2}\delta_{n1})$$

$$= \sigma_{ij} + [\, \varepsilon^{*}_{mn} - \bar{S}_{mnst}\, \sigma_{st} - \frac{1}{2}\bar{S}^{h}_{66}\sigma^{3}_{12}(\delta_{m1}\delta_{n2} + \delta_{m2}\delta_{n1})] \, \frac{\partial \sigma_{mn}}{\partial \varepsilon_{ij}}. \qquad \text{(F-5)}$$

As shown in Eq. (6-19), the terms in the bracket in Eq. (F-5) vanish. Therefore, one has

$$\sigma_{ij} = \frac{\partial W}{\partial \varepsilon_{ij}}. \qquad \text{(F-6)}$$

APPENDIX G
TORSION OF A TWO-PLY COMPOSITE CYLINDER HAVING IN-PLANE SHEAR NONLINEARITY

Consider an infinitely long two-layer composite cylinder twisted by a torque. It is assumed that the inner diameter of the tube is 2a, and the thickness of the inner ply and the outer ply are t_1 and t_2, respectively. The solution for a single layer cylinder can be obtained by introducing nonlinear constitutive equations into the well-known Lekhnitskii's formulation [49] as

$$\sigma_r^{(i)} = \sigma_\theta^{(i)} = \sigma_z^{(i)} = \sigma_{r\theta}^{(i)} = \sigma_{rz}^{(i)} = 0, \quad u_r^{(i)} = 0, \tag{G-1a}$$

$$u_\theta^{(i)} = \Theta^{(i)} r z + \omega_3^{(i)}, \tag{G-1b}$$

$$u_z^{(i)} = u_{z0}^{(i)}, \tag{G-1c}$$

$$r\Theta^{(i)} = (S_{66}^{(i)} + S_{66}^{(i)h} \tau_{\theta z}^{(i)2}) \tau_{\theta z}^{(i)}, \tag{G-1d}$$

where the superscript i (i=1,2) denotes the i-th ply; $\Theta^{(i)}$ is the angle of twist per unit length, and $\omega_3^{(i)}$ and $u_{z0}^{(i)}$ are constants for rigid body motions.

The continuity conditions along the ply interface ($r = a+t_1$) may be expressed as

$$\Theta^{(1)} = \Theta^{(2)} = \Theta, \quad u_{z0}^{(1)} = u_{z0}^{(2)} = u_{z0}, \text{ and } \omega_3^{(1)} = \omega_3^{(2)} = \omega_3. \tag{G-2}$$

By properly constraining the rigid body motion, one has

$$u_\theta^{(i)} = \Theta r z, \text{ and } u_z^{(i)} = 0. \tag{G-3}$$

From Eq. (G-1d), one can obtain the shear stress caused by the twist as

$$\tau_{\theta z}^{(i)} = \sqrt[3]{\frac{\Theta r}{2S_{66}^{(i)h}} + \sqrt{\left(\frac{\Theta r}{2S_{66}^{(i)h}}\right)^2 + \left(\frac{S_{66}^{(i)}}{3S_{66}^{(i)h}}\right)^3}} + \sqrt[3]{\frac{\Theta r}{2S_{66}^{(i)h}} - \sqrt{\left(\frac{\Theta r}{2S_{66}^{(i)h}}\right)^2 + \left(\frac{S_{66}^{(i)}}{3S_{66}^{(i)h}}\right)^3}}. \tag{G-4}$$

Consequently, the torque can be determined as

$$T = \int_a^{a+t_1+t_2} r \tau_{\theta z} \, dr = \int_a^{a+t_1} r \tau_{\theta z}^{(1)} \, dr + \int_{t_1}^{t_2} r \tau_{\theta z}^{(2)} \, dr. \tag{G-5}$$

APPENDIX H
NORMALIZATION SCHEME FOR LEAKAGE LOAD

Based on the aforementioned joint sealing characteristics, one may show that leakage through threads may be initiated when the bearing pressure on a thread contact surface reaches a critical level, $\tilde{X}\ P_i$, where P_i is the internal pressure and $\tilde{X}$ is a leakage tightening factor to be determined. The bearing pressure is related to the applied loading on the joint, i.e., the make-up interference, internal pressure, and axial loading.

As a first-order approximation, a linear relationship is proposed between the loading and the bearing pressure. Thus, the initial condition for the joint leakage may be expressed as

$$P_{makeup} + \alpha P_i + \beta P_a \approx \tilde{X} P_i , \qquad \text{(H-1)}$$

where P_{makeup} is an average bearing pressure caused by a make-up interference; P_i is the internal pressure, and P_a, is the axial load. The α and β in Eq. (H-1) are constants related to the stiffness and the geometry of the composite joint, respectively.

The bearing pressure on the threads of the joint, caused by the make-up interference, may be expressed as

$$P_{makeup} \approx KT , \qquad \text{(H-2)}$$

where K is a constant and T is the number of make-up turns.

Substituting Eq. (H-2) into (H-1), one obtains

$$\frac{P_i}{T} \approx \frac{K}{\tilde{X} - \alpha - \beta \dfrac{P_a}{P_i}} . \qquad \text{(H-3)}$$

From Eq. (H-3), along a proportional loading path, i.e., P_a / P_i = constant, the ratio of internal pressure to make-up turn is constant in the case of leakage caused by the loss of bearing pressure. Using Eq. (H-3), one may normalize the experimentally determined leakage loading with a make-up interference to construct a leakage failure envelope. In the case of leakage caused by body damage, results are shown without normalization because the leakage load of a joint is not sensitive to the make-up interference, based on the experimental observations and the analytical solutions.

APPENDIX I
THREADED COMPOSITE JOINT USED IN PROBABILISTIC LEAKAGE FAILURE STUDY

As mentioned in Section 10, two sets of threaded integral composite tubular joints were used in the probabilistic study of joint leakage failure. The geometry and dimensions of the first set of joints are shown in Fig. A-1, the other ones are shown in Fig. I-1. The pin-section geometry and dimensions of the two lots of joints are identical. However, box-section dimensions and geometry of the two lots of joints are different. The leakage failure envelope for the second set of joint under two-turn make-up is shown in Fig. I-2 and a comparison between analytical prediction and experimental results is also given in the figure.

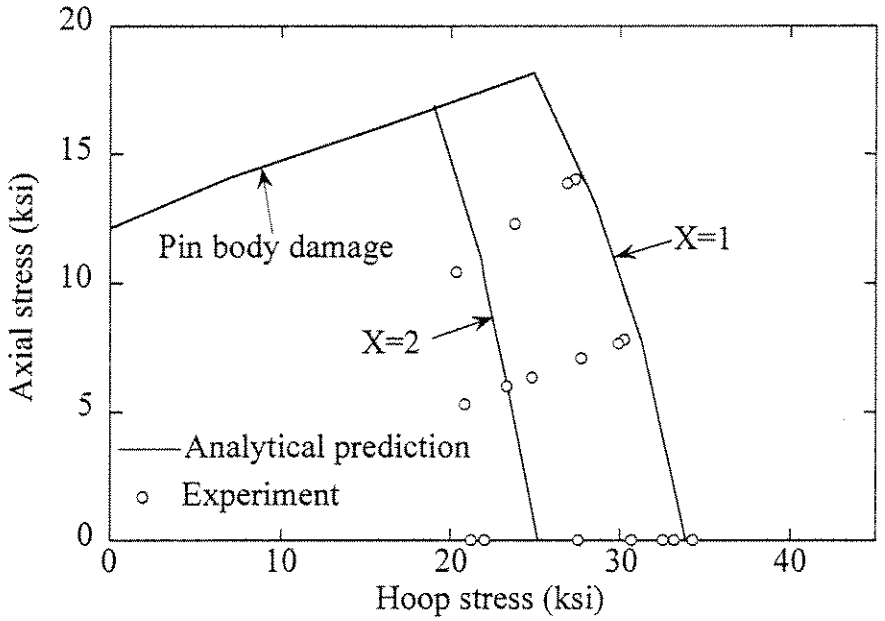

Fig. I-2 Leakage Failure Envelope of a Threaded Composite Joint with Two-turn Make-up (2-3/8-inch Integral Composite Joint Shown in Fig. I-1)